U.S. Department
of Transportation
National Highway
Traffic Safety
Administration

NHTSA

DOT HS 813 540d

May 2024

Restraint Design for Obese Occupants: GHBMC Obesity Model Modifications

Page intentionally left blank.

DISCLAIMER

This publication is distributed by the U.S. Department of Transportation, National Highway Traffic Safety Administration, in the interest of information exchange. The opinions, findings, and conclusions expressed in this publication are those of the authors and not necessarily those of the Department of Transportation or the National Highway Traffic Safety Administration. The United States Government assumes no liability for its contents or use thereof. If trade or manufacturers' names or products are mentioned, it is because they are considered essential to the object of the publication and should not be construed as an endorsement. The United States Government does not endorse products or manufacturers.

NOTE: This report is published in the interest of advancing motor vehicle safety research. While the report may provide results from research or tests using specifically identified motor vehicle models, it is not intended to make conclusions about the safety performance or safety compliance of those motor vehicles, and no such conclusions should be drawn.

Suggested APA Format Citation:

Kerrigan, J. R., Forman, J., Gepner, B., Joodaki, H., & Sun, Z. (2024, May). *Restraint design for obese occupants: GHBMC obesity model modifications* (Fourth of four parts. Report No. DOT HS 813 540d). National Highway Traffic Safety Administration.

The other three parts of this series:

Joodaki, H., Gepner, B., & Kerrigan, J. R. (2024, May). *Restraint design for obese occupants* (First of four parts. Report No. DOT HS 813 540a). National Highway Traffic Safety Administration.

Kerrigan, J. R., Joodaki, H., Sun, Z., & Gepner, B. (2024, May). *Restraint design for obese occupants: Rear-seat simulations* (Second of four parts. Report No. DOT HS 813 540b). National Highway Traffic Safety Administration.

Sun, Z., Kerrigan, J. R., Joodaki, H., and & Gepner, B. (2024, May). *Restraint design for obese occupants: Belt pull test simulations error effects modeling* (Third of four parts. Report No. DOT HS 813 540c). National Highway Traffic Safety Administration.

Page intentionally left blank.

Technical Report Documentation Page

1. Report No.	2. Government Accession No.	3. Recipient's Catalog No.
DOT HS 813 540d		

4. Title and Subtitle	5. Report Date
Restraint Design for Obese Occupants: Obese GHBMC Model Modifications (Fourth of four parts)	May 2024
	6. Performing Organization Code

7. Authors	8. Performing Organization Report No.
Zhaonan Sun, Bronek Gepner, Jason R. Kerrigan	

9. Performing Organization Name and Address	10. Work Unit No. (TRAIS)
University of Virginia Center of Applied Biomechanics 4040 Lewis and Clark Dr. Charlottesville, VA 22911	11. Contract or Grant No. DTNH2215D00022

12. Sponsoring Agency Name and Address	13. Type of Report and Period Covered
National Highway Traffic Safety Administration 1200 New Jersey Avenue SE Washington, DC 20590	14. Sponsoring Agency Code

15. Supplementary Notes

16. Abstract

Fourth of four parts. The objective of this study was to modify the Global Human Body Models Consortium obesity models to improve their response relative to the obese postmortem human surrogates in a series of tabletop belt tests. This study found that submarining could be modeled by breaking boundary condition or large shear deformation in flesh; detaching connection between the pelvis and surrounding flesh could release the boundary condition and therefore allow for submarining; pulling hard with a denser mesh in the flesh could break the boundary between flesh and pelvis, therefore leading to submarining; large shear deformation can be realized through using SPG particle-to-particle bond failure criteria; tuned smooth particle Galerkin parameters worked well in the belt pull test simulation, recreating similar kinematics in the GHBMC obesity model to the PMHS; and the same set of tuned SPG parameter did not enable the GHBMC obesity model submarining in the rear seat sled test simulation.

17. Key Words	18. Distribution Statement
smooth particle Galerkin, post mortem surrogate, belt test, GHBMC, Global Human Body Models Consortium, obesity model, submarining	This document is available to the public from the DOT, BTS, National Transportation Library, Repository & Open Science Access Portal, https://rosap.ntl.bts.gov.

19. Security Classif. (of this report)	20. Security Classif. (of this page)	21. No. of Pages	22. Price
Unclassified	Unclassified	104	

Form DOT F 1700.7 (8-72) Reproduction of completed page authorized

Page intentionally left blank.

Table of Contents

List of Figures

List of Tables

Executive Summary

The objective of this study was to modify the Global Human Body Models Consortium (GHBMC) obesity models to improve their response relative to the obese postmortem human surrogates (PMHS) in a series of table-top belt pull tests previously performed at the University of Virginia's Center for Applied Biomechanics. In task 1 of this study, we concluded that the GHBMC obesity model could not replicate submarining (belt motion over the iliac wings into the abdomen) in any loading conditions simulated (sled test and belt pull). However, changing the material properties as well as the formulation could potentially lead to a stable model capable of replicating occupant submarining. For this task, the simulation results of the GHBMC obese male model that had a stature of 1,750 mm, a weight of 86 kg and a body mass index (BMI) of 30 were compared to the response of the female PMHS subject with a BMI of 31.0, height of 1,650 mm and weight of 84.4 kg.

Next, we investigated the modeling modifications that could lead the GHBMC obesity model to show kinematics like that of the PMHS. To start, we created a simplified version of the GHBMC obesity model to investigate parameters influencing occupant submarining and achieve quick debugging and shorter run times. A series of studies was performed on this simplified prototype including effects of the contact and constraint definition, input and boundary conditions, spatial discretization, material model of the flesh, element formulation of the flesh and various parameters within the new formulation, smooth particle Galerkin (SPG) method. Then, we performed additional studies on the full GHBMC obesity models.

Three types of modeling modifications, that could facilitate the mechanism of submarining belt response, were identified for the belt pull test simulation. The first modification enabled tissue sliding relative to the pelvis by detaching the constraints between the pelvis and surrounding tissue. The second modification was obtained through remeshing the pelvic flesh, which facilitated yielding of the iliac wings, and failing the connection between the pelvis and surrounding tissue. The third modification was obtained using the SPG formulation, enabling large shear deformation within the abdominal flesh tissue.

The new SPG formulation that allowed submarining was identified as the solution to model modification and similar implementations were performed for the rear seat sled test and for selected GHBMC certification suite simulations. The results showed consistent submarining in the belt pull test and that the amount of shear deformation within the flesh can be controlled using SPG parameters. However, the same implementation did not show stable results in the rear seat sled test. Additionally, we performed GHBMC certification suite abdominal bar impacts that allowed for reliable assessment of model stability.

SPG showed promising results in enabling the GHBMC obesity model to replicate the abdominal tissue deformation observed during submarining motion. However, potential contact and stability issues still exists and need to be evaluated. The results of this task led to the decision of using Lagrangian finite elements in the restraint optimization study since the potential issues with SPG could halt the progress of the optimization.

Page intentionally left blank.

Summary of Findings

1. Submarining could be modeled by breaking boundary condition or large shear deformation in flesh.
2. Detaching the connection between the pelvis and surrounding flesh could release the boundary condition and therefore allow for submarining.
3. Pulling hard with a denser mesh in the flesh could break the boundary between flesh and pelvis therefore leading to submarining.
4. Large shear deformation can be realized through using SPG particle-to-particle bond failure criteria.
5. Tuned SPG parameters worked well in the belt pull test simulation, recreating similar kinematics in the GHBMC obesity model to the PMHS.
6. The same set of tuned SPG parameter did not enable the GHBMC obesity model submarining in the rear seat sled test simulation.

Page intentionally left blank.

Introduction

Obesity is associated with increased fatality risk and altered distribution of occupant injuries relative to lower BMI occupants in automotive collisions (Mock et al., 2002; Zhu et al., 2006; Viano et al., 2008; Jehle et al., 2012). Obesity affects the occupant-restraint interaction. Restraining obese occupants is a challenge due to increased body mass, unfavorable belt placement (Reed et al., 2012), and increased forward excursion within the occupant compartment (Forman et al., 2009; Kent et al., 2010). An increased depth of abdominal soft tissue, results in delayed and limited engagement of the lap belt with the pelvis and increases the risk of pelvis submarining under lap belt, exposing occupant's abdomen to belt loading (Kent et al., 2010).

Several experimental studies have been performed to research the challenges obesity poses on restraints during motor vehicle collisions (MVC). Forman et al. (2009), Kent et al. (2010), Gepner et al. (2018), and Forman et al. (2018) performed rear-seat sled tests on both obese male PMHS and 50th percentile PMHS. It was found that obese occupants exhibited backward torso rotation (pelvis forward of shoulders) at the time of maximum forward excursion, whereas non-obese occupants did not. Kent et al. (2010) pointed out that obese PMHS in frontal-impact sled tests exhibited submarining behavior, which is defined as the properly placed belt slid over the iliac crests and penetrated the abdomen without engaging the pelvis (Gepner et al., 2018). The authors suggested that submarining resulted in increased forward excursion and decreased forward torso pitch, which may be related to increased risk of lower extremity and thoracic injuries in obese occupants.

Human body models (HBMs) with varied stature, age and BMI levels were generated using University of Michigan Transportation Research Institute's (UMTRI) rapid mesh morphing tools based on statistical models of external body contour and ribcage geometry. Obese versions of both total human model for safety (THUMS) (Shi et al., 2015; Wang et al., 2015) and GHBMC (Hu et al., 2016) were generated. While these HBMs are available to study occupant kinematics, simulations illustrating HBM responses like PMHS kinematics are not available in the literature. Kitagawa et al. (2017) performed a series of obese THUMS simulations. Greater forward excursion was observed in frontal impact simulation, but no submarining was observed. Similar efforts have been carried out by Gepner et al. (2018) with the GHBMC obesity models. In the belt pull test simulations performed by Gepner et al. (2018), the model did not exhibit submarining behavior as observed in the PMHS test. Also, the lap belt pull simulations failed to reproduce the belt/abdomen interaction seen in the PMHS. It was also found that the material model used to represent the HBM flesh was found to be approximately one order of magnitude stiffer than human abdominal subcutaneous adipose tissue. This study shows that improved modeling of the belt-flesh-pelvis interaction should be required to obtain biofidelic response.

Experiments have suggested that adipose tissue is able to undergo substantially large shear deformations (Sommer et al., 2013). Such large deformations challenge Lagrangian finite element approaches to modeling since such large deformations can result in instabilities and collapsing elements. Previous work has shown the potential to model these large deformations using meshfree methods, which offer advantages in simulating large deformation over conventional finite element methods (Li & Liu, 2002). The earliest developed meshfree method is the smoothed particle hydrodynamics (SPH) method (Wu et al., 2014). However, this method suffers from tension instability, lack of consistency and other numerical artifacts if it is applied to solid analyses directly (Libersky et al., 1993; Wu et al., 2014). Recently, a robust and accurate

meshfree method, was developed by Livermore Software Technology Corporation,[1] referred to as the SPG method. The formulation is based on a smoothed displacement field within the meshfree Galerkin variational framework. It could provide stable and accurate solution for solid mechanics problems (Wu et al., 2014). This method has been applied to manufacturing problems including drilling and metal milling. However, no previous study using this method for biological material can be found.

Since improved modeling of belt-flesh-pelvis interaction in existing HBMs is needed, and work in task 1 showed potential in a new method for large deformation modelling. The goal of this study is to apply new approaches to model belt-flesh-pelvis interaction to the obese HBMs and evaluate their ability to replicate submarining in the belt pull test.

[1] In 2019 Livermore Software Technology Corporation, of Livermore, California, was acquired by Ansys, Inc., Canonsburg, PA.

Theorized Mechanism of Submarining

In Task 1 we observed that throughout the belt pull test simulation, the belt remained engaged with the iliac wings and it remained anterior to the pelvis. The GHBMC obesity model failed to replicate the belt trajectory observed during the experiments, where it slid over the iliac crest and into the abdomen. Even with the increased belt pull force the belt remained constrained in the proximity of the anterior superior iliac spine (ASIS). It should be noted, however, that in both PMHS experiments no belt slippage relative to the occupant skin/flesh was observed, and consequently, the motion of the belt up and over the ASIS and into the abdomen was the result of shearing deformation of the pelvic/abdominal flesh. As a result, we concluded that the difference in the occupant response is likely associated with the abdominal flesh formulation.

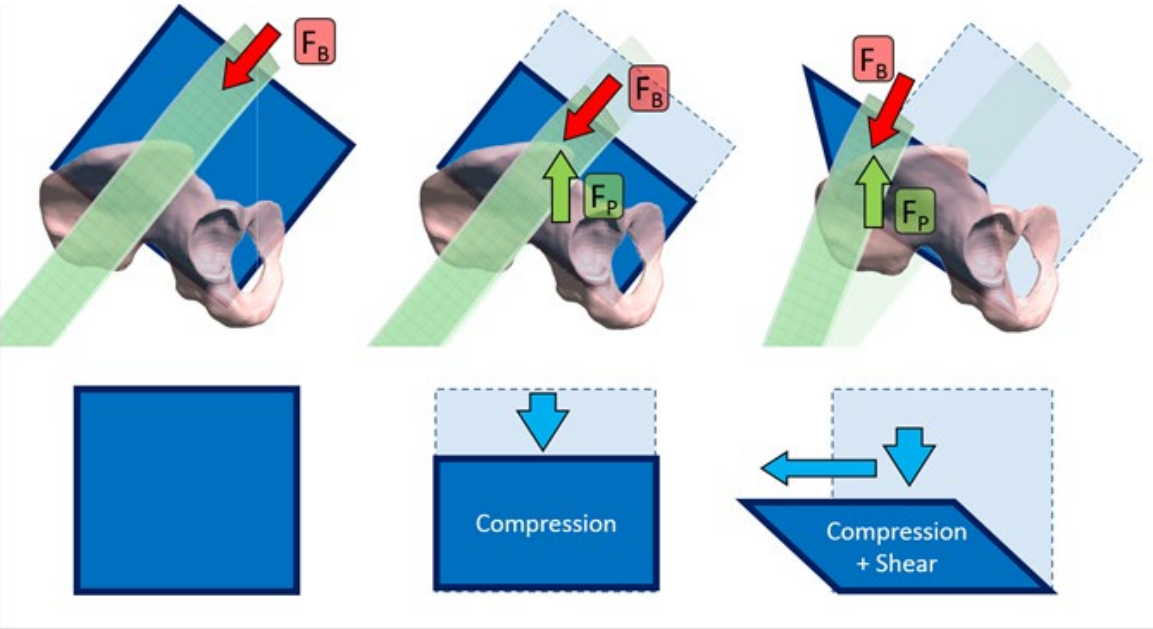

Figure 1. Mechanism of belt motion in belt pull tests, FB – force from the belt, FP – reaction force from the pelvis; (a) initial belt positioning with undeformed abdominal flesh, (b) compression of the abdominal flesh over the pelvis, c) compression and shearing (Gepner et al., 2018)

With these observations in mind, it was theorized that the GHBMC flesh material model along with the current mesh formulation results in the overly stiff response when used to represent human adipose tissue. A belt pull test serves as a good explanation for this hypothesis (Figure 1). When the belt is initially pulled with a force FB it compresses the adipose tissue over the pelvis (Figure 1). Next the belt encounters the boney structure of the pelvis which provides a reaction force FP (Figure 1). If, at this point, the belt is superior to the ASIS, the result of these two forces will guide the belt over the iliac crest and into the abdomen (Figure 1). However, if the flesh model is overly stiff in shear, then the result of the belt and pelvis forces could be carried by the flesh and prevent the belt from sliding over the iliac wing.

Page intentionally left blank.

Data Presentation

Figure 2 shows a typical graph used to present results from the belt pull test simulations throughout the report. The top left shows the left side view of the belt kinematics, where the yellow square marks the position of the left ASIS. The coordinates of the belt midline in the simulation are visualized using green dots while the blue dots show the corresponding experimental results. The bottom left figure adapted the same format but with a right-side view, where the yellow dot marks the position of the right ASIS. The top right figure shows the force time history in the experiment and the simulation. The bottom right figure shows the belt displacement time history in the experiment and the simulation. Belt displacement data was recorded at the pulley in both experiment and simulation.

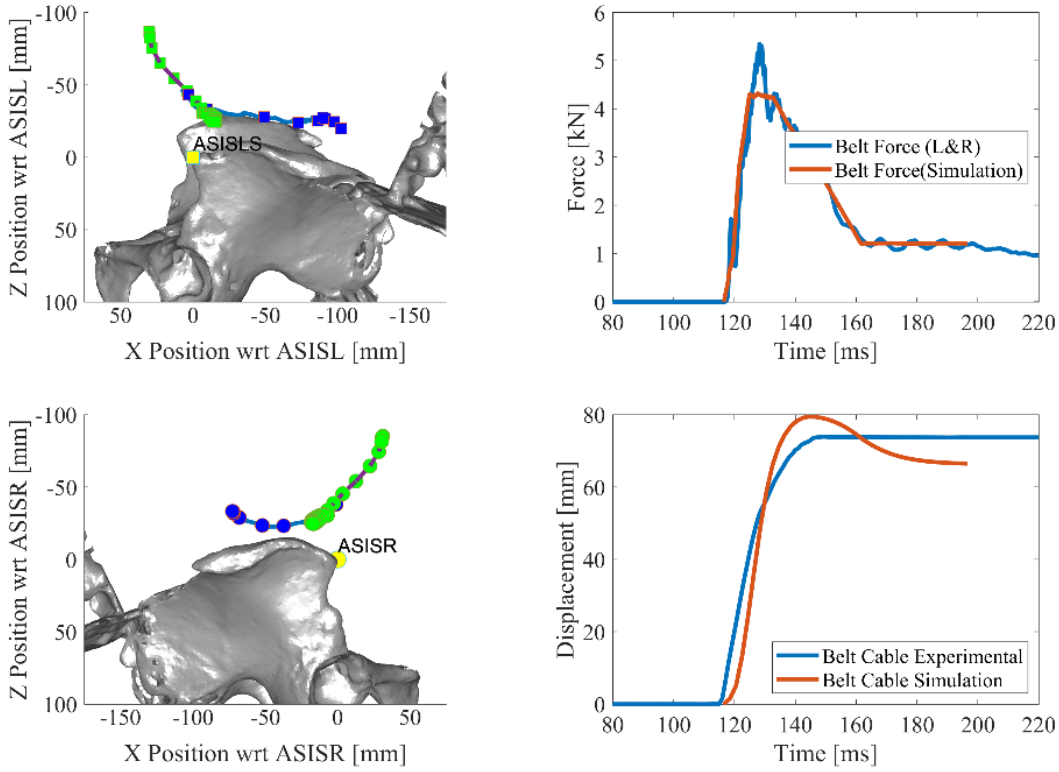

Figure 2. A sample of data presentation in the belt pull test simulations

Page intentionally left blank.

Type I Submarining

At the completion of Task 1 of this project, we concluded that the GHBMC obesity models failed to replicate the submarining behavior. Also, the GHBMC obesity models failed to replicate the belt trajectory observed in the PMHS belt pull tests. It was also found that the GHBMC flesh material model exhibits a much stiffer stress/strain response in shear.

Previous studies have shown that the 50th percentile male GHBMC model could submarine in a reclined seating position (Forman et al., 2018; Lin et al., 2017) with the seat belt initially positioned below the iliac wings but then move towards the iliac wings, change direction of motion, and move into the abdomen. Since we theorized that the key to submarining is the large shear motion, we decided to detach the constraints between the pelvis and the surrounding flesh (Figure 3) and explore whether this would enable large shear motion.

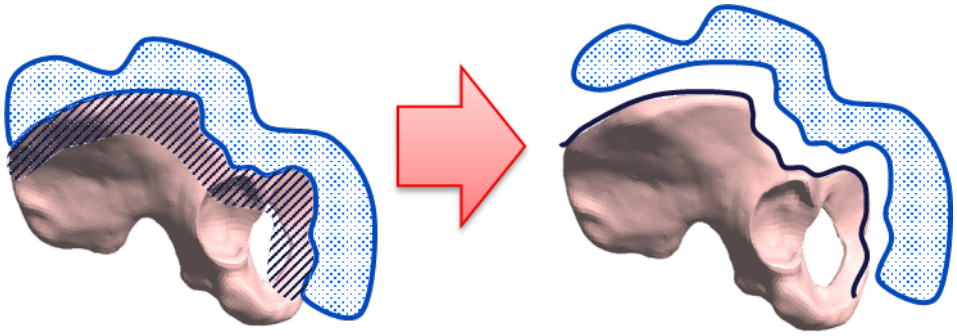

Figure 3. Schematic of detaching the surrounding soft tissue from the pelvis

In the GHBMC obesity model, the pelvic wings are connected to surrounding tissue through tied contact and shared nodes (Figure 4). Negative volume element problem occurred in task 1 simulations when the belt pulling force was increased from the baseline, preventing the simulation from normal termination. This could potentially prevent the large shear motion within the elements of surrounding soft tissue since some elements always have to be connected to the bony pelvis. We released the tied contacts and shared nodes relationship between the parts and ran the belt pull test simulation with four different input pulses. Four simulations were performed to investigate the effect of releasing the contact under different loading conditions.

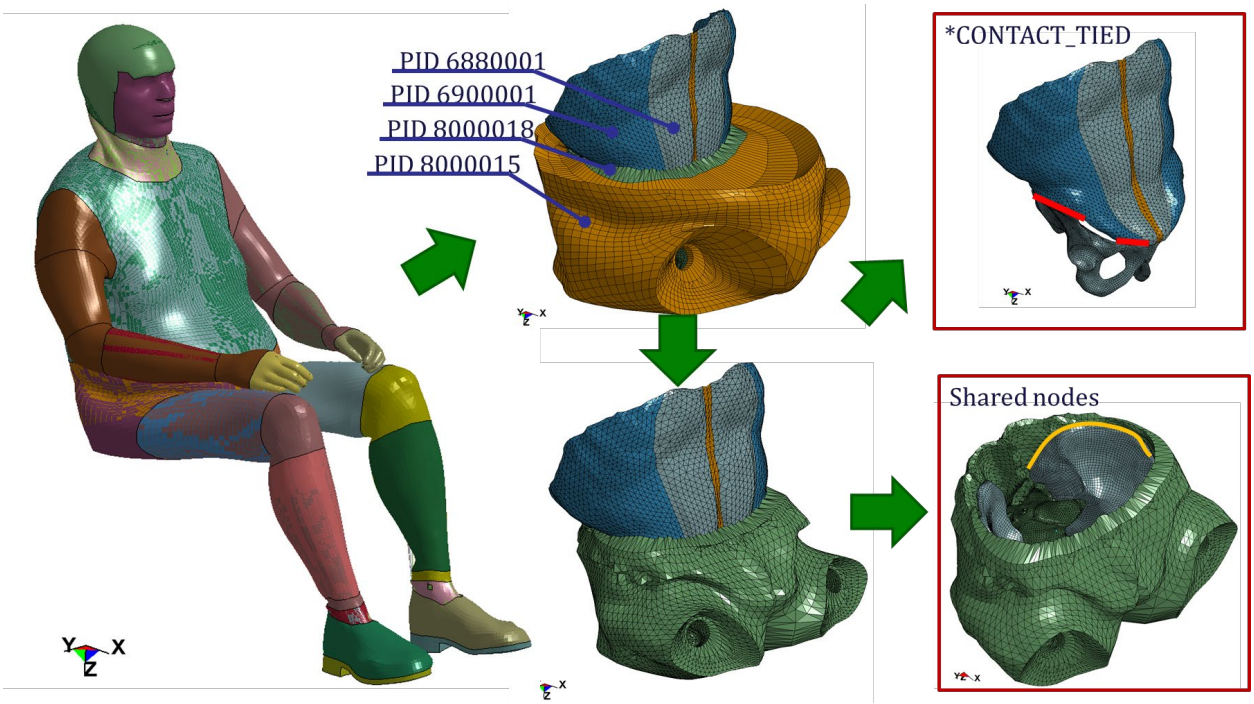

Figure 4. Connections between the pelvis and surrounding tissue in the GHBMC obesity model

When the detached model was pulled with the baseline force fit to the time history from the experiment, no submarining was observed (Figure 5). The belt went straight towards the pelvis without showing trend for direction change. We recognized this might be due to insufficient energy input to the whole system for three reasons. First, the peak force was held for less than 20 ms, leaving not enough time for belt movement. Second, the obese GHBMC in the simulation is an overall larger person than the PMHS, therefore requiring more energy to achieve the same amount of deformation. Third, in task 1, we concluded that abdominal flesh in the GHBMC obesity model appeared to be orders of magnitude stiffer in shear compared to subcutaneous adipose tissue. This would affect the pulling force required to reach desired deformation.

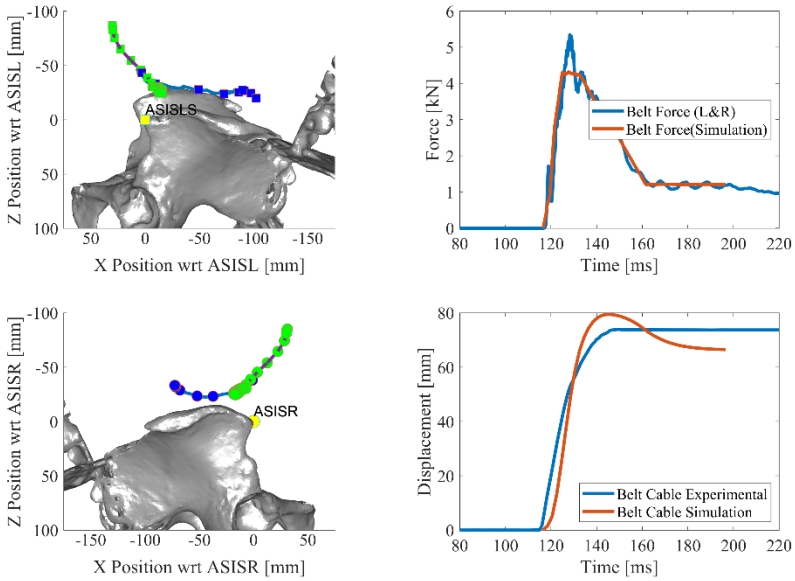

Figure 5. Detached pelvis with a fit-to-experiment input pulse

With the above reasons for insufficient energy, we then increased the duration of the peak force, effectively putting more energy into the system. The result did not show submarining behavior either, but higher belt displacement was observed (Figure 6).

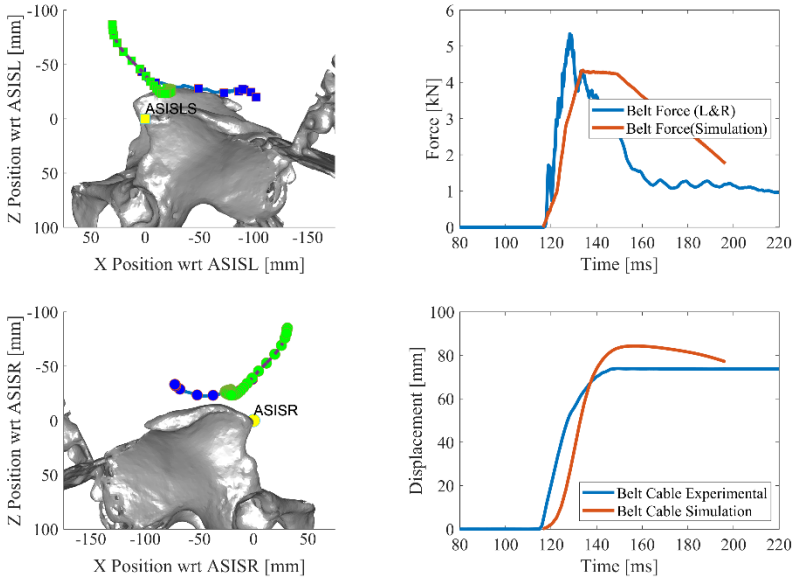

Figure 6. Detached pelvis with added energy input

By further increasing the peak simulation pulling force to twice the peak experimental force, we observed the belt changing directions after initially moving towards the abdominal cavity (Figure 7). The belt started to move above the pelvic wings and compress the abdomen. However, since the peak force was held for less than 20 ms, the belt retracted when peak force was released. This simulation showed that by detaching the surrounding flesh towards the pelvis, global submarining motion could appear but keeping that motion would require sufficient energy to hold the force.

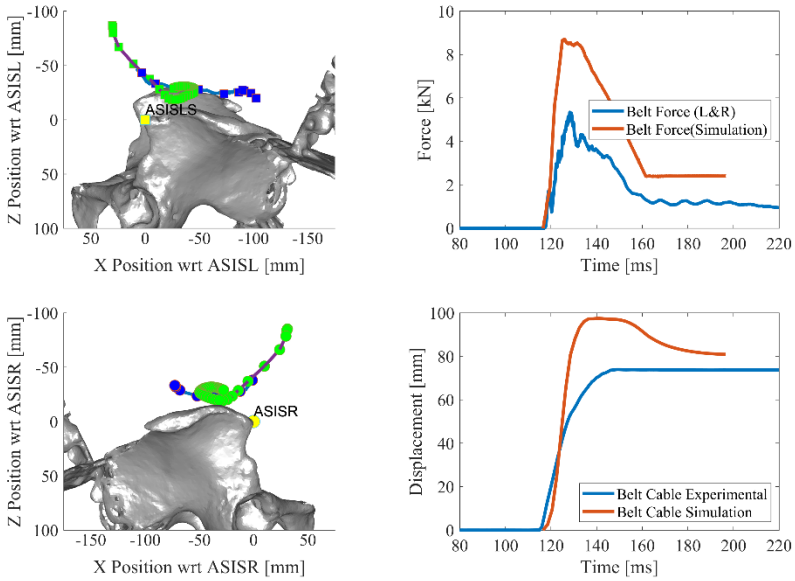

Figure 7. Detached pelvis with double peak input

Based on the results, we further increased the amount of energy input to the system by holding the peak force twice as long as the previous simulation. Highly matched belt trajectory with the experiment was observed (Figure 8). The belt first compressed the abdomen towards the pelvis, then under the influence of the reaction force from the pelvic wings, changed its direction and moved in to compress the abdominal cavity. Since the global belt kinematics matched with the belt pull test, for brevity we classified this model setup and subsequent model response as type I submarining. In this case, the original boundary condition of the belt pull test was modified by detaching surrounding tissue from the pelvis. However, this type of interconnectivity is not what is observed in the human body since surrounding muscles are attached to the pelvic wings. As a result, this method violates the continuity of pelvis-flesh interface and should be used with caution to modify the current GHBMC obesity models for further simulations.

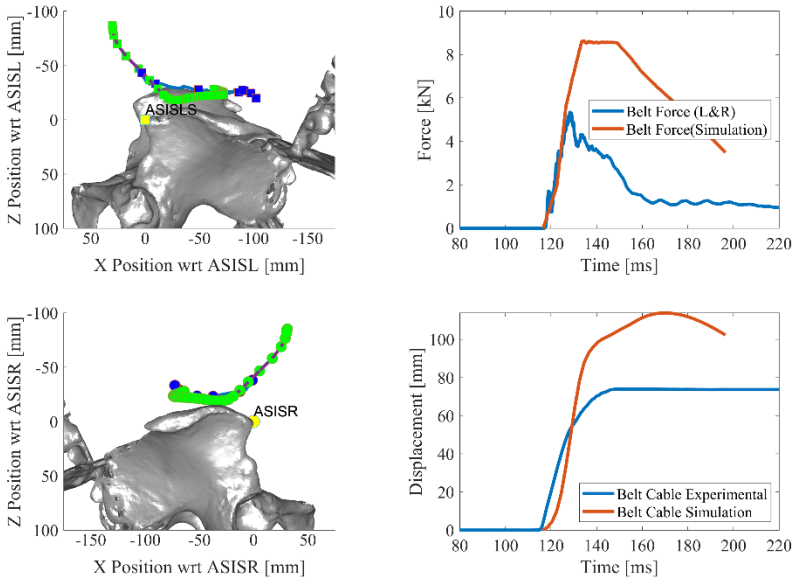

Figure 8. Detached pelvis with added energy double peak input

Smooth Particle Galerkin Method Introduction

Experiments have suggested that adipose tissue is able to undergo substantially large shear deformations (Sommer et al., 2013). Such large deformations challenge Lagrangian finite element approach for modeling soft tissues since such large deformations can result in instabilities and collapsing elements. Previous work has shown the potential to model these large deformations using meshfree methods, which offer advantages in simulating large deformation over conventional finite element methods (Li & Liu, 2002). The earliest developed meshfree method is the SPH method (Wu et al., 2014). However, this method suffers from tension instability, lack of consistency and other numerical artifacts if it is applied to solid analyses directly (Libersky et al., 1993; Wu et al., 2014). Recently, a robust and accurate meshfree method was developed by LSTC, referred to as the SPG method. The formulation is based on a smoothed displacement field within the meshfree Galerkin variational framework. It could provide a stable and accurate solution for solid mechanics problems (Wu et al., 2014). This method has been applied to manufacturing problems including drilling and metal milling. However, no previous study using this method for biological material can be found. To the best of our knowledge, the SPG method has not been applied to the field of soft tissue modelling yet.

Specifically, we proposed two methods of applying the SPG method. First, we propose to use the SPG method without particle-to-particle bond failure criteria. In theory, this would also enable material flow since mass advection could be realized by particles moving around. Alternatively, we propose to use the particle-to-particle bond failure criteria as a tool to control both the structural stiffness and the large shear deformation under lap belt loading. The particle-to-particle bond failure mechanism is explained in Figure 9.

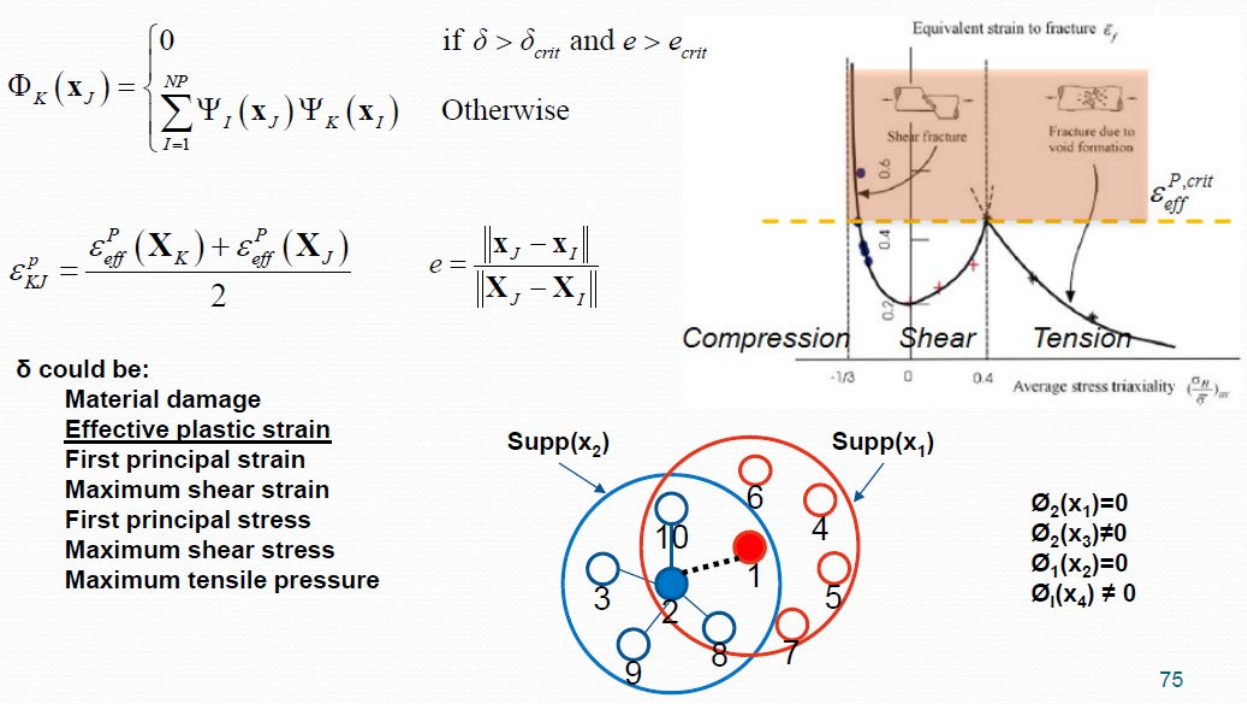

Figure 9. Particle-to-particle bond failure mechanism (slide adapted from LSTC)

In the rest of the report, SPG parameters will be mentioned along with SPG simulations. Meshfree kernels are the fundamental rule of neighbor searching in the deformed configuration.

In the current implementation, three types of kernels are defined: updated Lagrangian kernel, Eulerian kernel and pseudo-Lagrangian kernel (Figure 10). In this series of simulations, large shear deformation is the key, so we used critical shear strain criteria to define particle-to-particle bond failure. Both critical shear strain and critical stretch were defined. When either shear strain or stretch reached critical value, bond failure happened and released the connection.

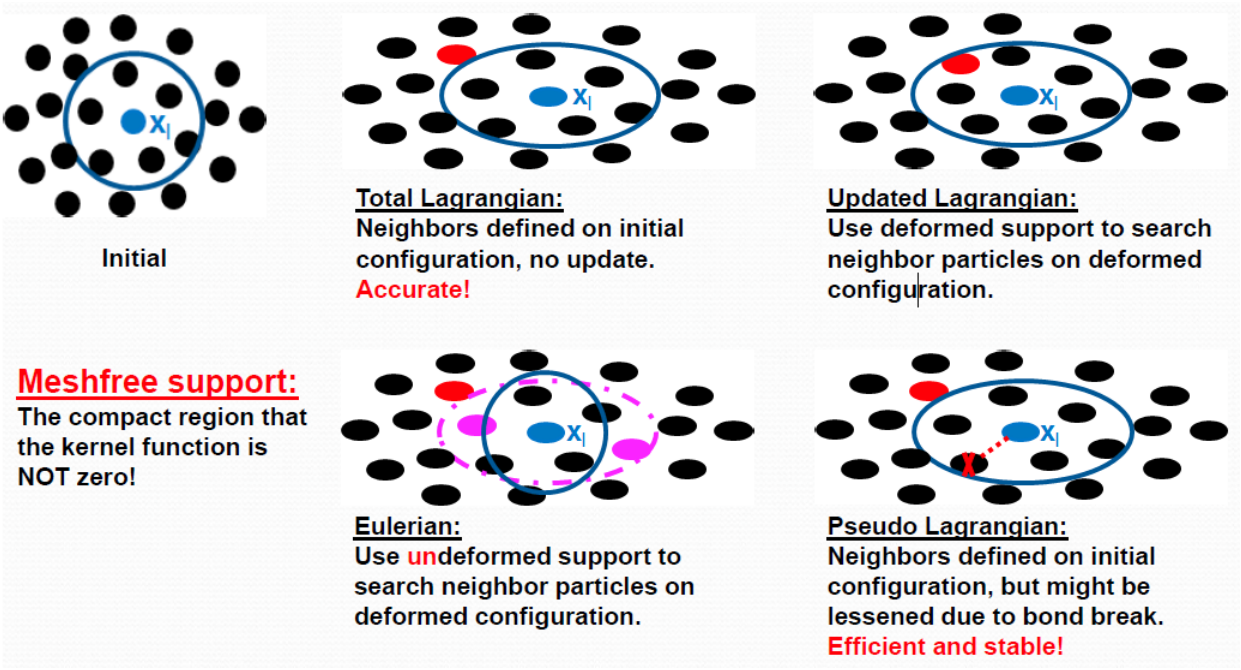

Figure 10. Meshfree kernels (adapted from LSTC)

Obese GHBMC Model Simplification and Remesh

To further investigate necessary model modifications, we created a simplified version of the GHBMC obesity model to isolate the large shear problem, reducing run time and making debugging easier. Also, since we identified SPG as the method for large deformation, we needed to explore various combinations of boundary condition, input pulse and SPG parameters to obtain some in-depth understanding of the method.

To explore the benefits of SPG, our goal was to create a model that is easy to adjust, computationally inexpensive but very similar to the yGHBMC obesity model. The purpose of this model is to understand the optimum way of modeling large shear deformation. The model was created based on the 1,750 mm and BMI 30 model used in the belt pull test with removed body parts. Specifically, the upper and lower extremities, vertebras, head, and internal organs were removed. All relevant contact definitions were removed as well (Figure 11).

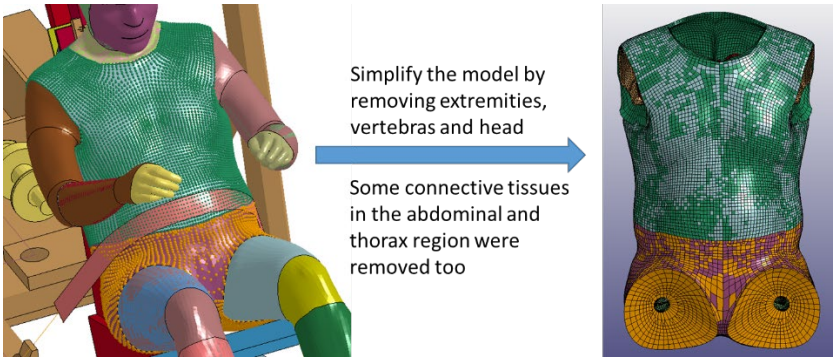

Figure 11. Creating the simplified model for SPG tuning

Although SPG is a meshless method by nature, the creation of SPG particles is mesh based. After creating the mesh, LS-DYNA solver turns each node in the selected SPG section into one smooth particle and discards the solid element connection between the particles (Figure 12).

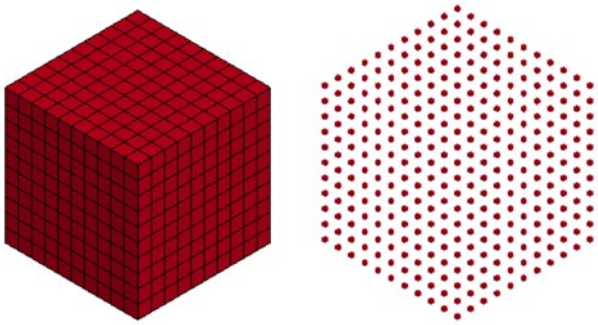

Figure 12. Generation of SPG particles from a solid mesh, with each node turned into one particle

Also, to apply the SPG method in the flesh of obese GHBMC, we needed to change the abdominal tissue mesh density. After discussion with LSTC we have concluded that at least four layers of particles in between the Lagrangian boundary is recommended. Since the obese GHBMC was created by morphing the AM50 GHBMC model, only nodal coordinates changed in this process. As shown in Figure 13, the obese GHBMC only used three elements across the

abdominal front wall, which turns into only two layers of smooth particles in between the Lagrangian boundaries. Additionally, since the morphing process was applied to the geometry of the non-obese occupant, resulting in substantially distorted obese mesh, and was characterized by non-homogenous mesh/node distribution. It was assumed that the homogeneous SPG particle distribution is essential for robust evaluation of the method.

Based on these requirements, we remeshed the abdominal and thoracic flesh with constant density tetrahedral elements. Although tetrahedral elements are inherently stiffer in shear due to shear locking mechanism, this was not a concern since we only use tetrahedral elements to generate the coordinates for the smooth particles. After remeshing, we increased the number of nodes by around five times.

After removing all relevant parts, remeshing was performed on two solid and two shell parts. Both solid parts were meshed with constant density tetrahedral elements. The number of elements increased from 11,526 to 63,185 after the remesh. The purpose of remeshing is to create grid space for SPG particles. To create SPG particles, we first need to create a solid Lagrangian mesh. Then, we could simply change the section definition from solid to solid_SPG with an element form 47. The SPG method requires at least three layers of particles in between the boundary to make the simulation stable and physical. However, the original GHBMC obesity model only had three elements across the abdominal wall thickness. The three elements are defined by four nodes, which is turned to four particles in SPG. Therefore, there are only two layers of particles in between the boundaries since the outer and inner boundary share nodes with other parts in contact. After remeshing, there are more than 15 layers of particles in between the boundaries.

After this simplification and remeshing, we created three models: Simplified model with original mesh in Lagrangian finite element, 2) Simplified model with remesh in Lagrangian finite element, and 3) is the simplified model with remesh in SPG and using different SPG paramenters. The purpose of creating the three models is to investigate the effect of spatial discretization in finite element analysis (FEA) and SPG formulation.

Figure 13. Remeshing the abdominal and thoracic flesh

A total of 23 simulations were performed with the simplified models (Table 1). For simplicity, results from 11 simulations are shown in Table 2 while the complete set of results can be found in Appendix A.

Table 1. Summary of simulations performed with simplified belt pull test model

Simplified Belt Pull Test Model				
Simulation #	Boundary Condition	**Formulation**	**Mesh**	SPG Parameters
27-29	Pelvis and centered flesh	FEA	Original	N/A
30-36	Pelvis and centered flesh	FEA	Remesh	N/A
37-49	Pelvis and centered flesh	SPG	Remesh	Adjusted kernels and failure criteria

Since we have removed the vertebrae in the simplification process, we could not use the same boundary condition as in the original belt pull test. Instead, we chose to constrain the nodes on the centerline of the back flesh to mimic the original boundary condition on the spine as well as the pelvic wings since our main goal is to study whether we could enable the belt to shear the flesh around the pelvic region. This set of boundary condition is shown in Figure 14.

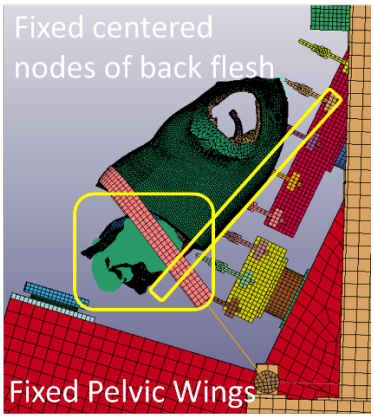

Figure 14. Boundary conditions of the simplified model belt pull test

Table 2. Summary of simulation results of the simplified belt pull test model

Simplified Belt Pull Test Model						
Simulation #	**Belt Pull Force**	**Formulation**	**Mesh**	**SPG Parameters**	**Belt Kinematics**	**Belt Displacement**
27	Baseline Flat	Lagrangian	Original	N/A	Belt over pelvic wings	90 mm
28	sfo3 Flat	Lagrangian	Original	N/A	Belt pulled towards pelvis, negative volume error termination	100 mm
30	Baseline Flat	Lagrangian	Tetra Remesh	N/A	Belt over pelvic wings	90 mm
33	sfo3sfa3 Flat	Lagrangian	Tetra Remesh	N/A	Belt over pelvic wings	160 mm
37	Baseline Flat	SPG	Tetra Remesh	K=2; No failure card	Belt over pelvic wings	75 mm
38	Baseline Flat	SPG	Tetra Remesh	K=2; IDAM=3; fs=0.85;s=1.85	Belt over pelvic wings	78 mm
39	sfo3 Flat	SPG	Tetra Remesh	K=2; No failure card	Belt over pelvic wings	140 mm
40	sfo3 Flat	SPG	Tetra Remesh	K=2; IDAM=3; fs=0.25;s=1.25	Belt over pelvic wings	140 mm
41	sfo3 Flat	SPG	Tetra Remesh	K=2; IDAM=3; fs=0.45;s=1.45	Belt over pelvic wings	155 mm
42	sfo3 Flat	SPG	Tetra Remesh	K=2; IDAM=3; fs=0.65;s=1.65	Belt pulled towards pelvis, negative volume error termination	90 mm
43	sfo3 Flat	SPG	Tetra Remesh	K=2; IDAM=3; fs=0.85;s=1.85	Belt over pelvic wings	140 mm

With this set of boundary condition, we first performed simulation on the Lagrangian element model with original mesh.

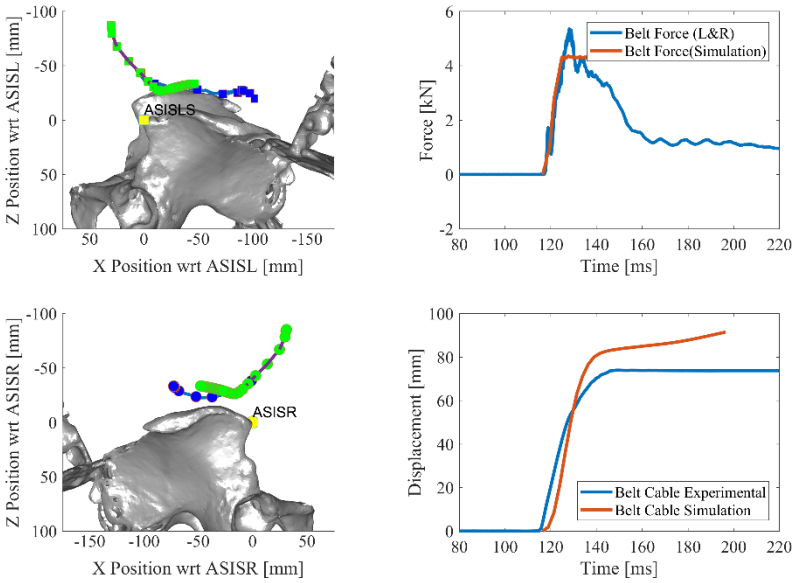

Figure 15. Baseline FEA simulation with original mesh and new boundary conditions #27

With the right set of boundary conditions, Figure 15 seems to show that Lagrangian elements can undergo large deformation since we see potential large shear here and the belt has passed the pelvic wings into the abdomen. However, this kinematics have never been shown in any complete GHBMC obesity models in task 1. This difference can be explained by the different mass, contact definition and boundary conditions between the simplified model and the full model. When the input is scaled up to three times, negative volume problem occurred (Figure 16). This problem remained when we further scaled up the input to 10 times.

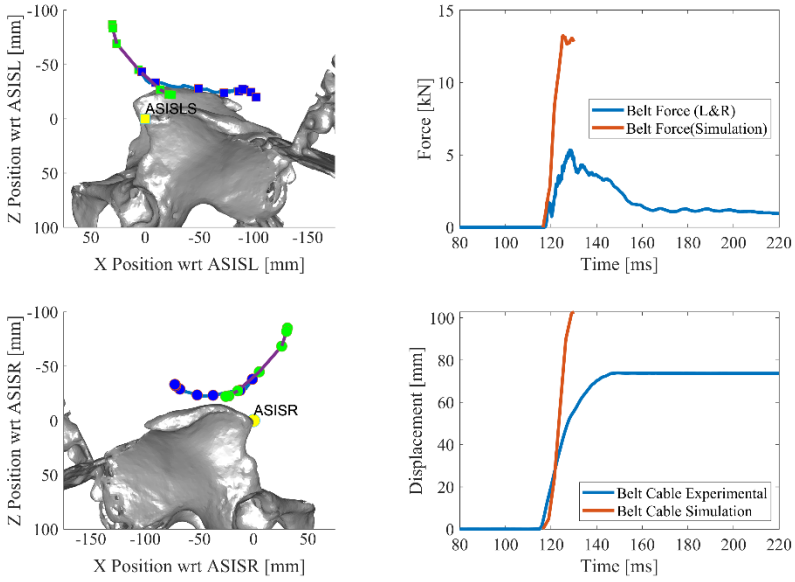

Figure 16. Three times baseline flat input simulation on simplified GHBMC obesity model with Lagrangian elements #28

Since we created this model to explore the benefits of SPG and that requires the new mesh, we performed simulations 29-35 on the remeshed Lagrangian model and 36-47 on the SPG model.

Now let's examine the remeshed model in all Lagrangian elements. The baseline simulation showed larger abdominal deformation than the original mesh as shown in Figure 17.

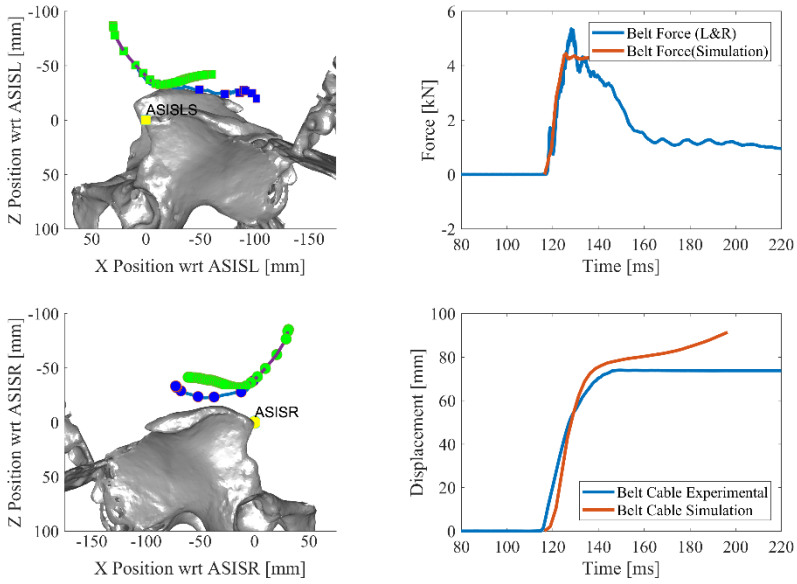

Figure 17. Baseline flat input simulation on simplified GHBMC obesity model with Lagrangian elements #30

The input was then scaled up to three times baseline and large abdominal deformation was observed. This simulation was then terminated due to a negative volume element in the armpit area. As a verification, we then performed an extreme case of simulation using scaling factor of 10. The negative volume problem occurred earlier than the three times baseline simulation. These two simulations showed that if the loading rate is high enough, we would still face negative volume problem even if we simplify the model and contact conditions.

Since some potential rate sensitive effect was observed, some supplement simulations were performed using different combinations of scaling factors to the input pulse. Larger deformation was observed with a lower pulling rate. Figure 18 showed the result of one of these simulations. With the remeshed model, sensitivity on loading rate is less. All simulations achieved large deformation.

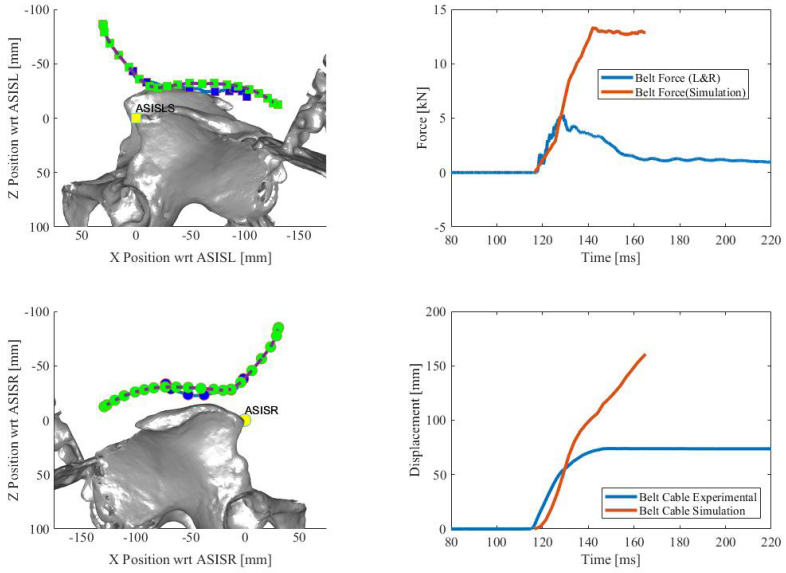

Figure 18. Three times peak force and rate flat input simulation on simplified GHBMC obesity model in Lagrangian formulation #33

Although the large deformation shown here is due to the model simplification, it has been shown that this model prototype could be used to explore the benefits of using the SPG method. SPG simulations were only performed based on the remeshed model since the purpose of remeshing is to generate smooth particles from corresponding nodal positions.

We first explored the possibility of using SPG without the failure criteria to simulate the large deformation. After discussion with LSTC, we chose to use the updated Lagrangian Kernel to perform the simulation. The baseline SPG simulation without particle-to-particle bond failure showed moderate amount of deformation (Figure 19). Slightly larger deformation can be seen in the SPG simulation with failure parameter implemented (Figure 20).

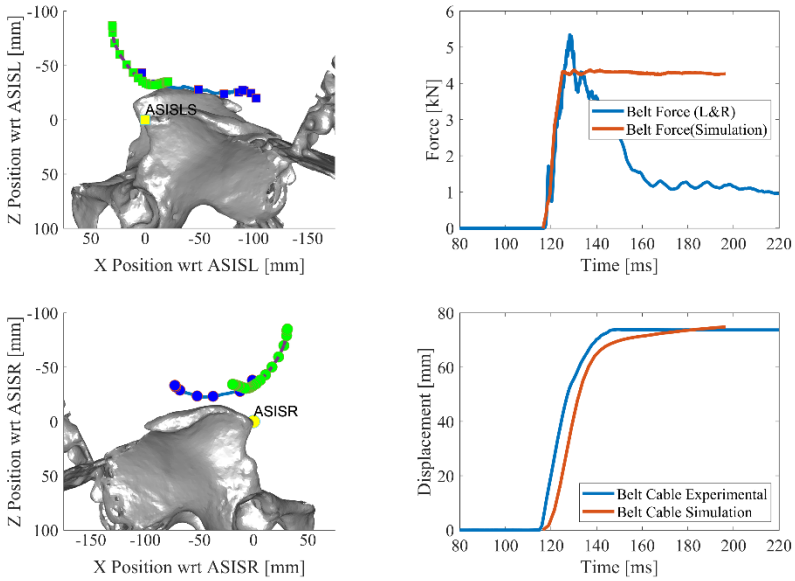

Figure 19. Baseline flat input simulation on simplified GHBMC obesity model with SPG formulation in updated Lagrangian kernel (kernel=2) with no particle-to-particle bond failure criteria #37

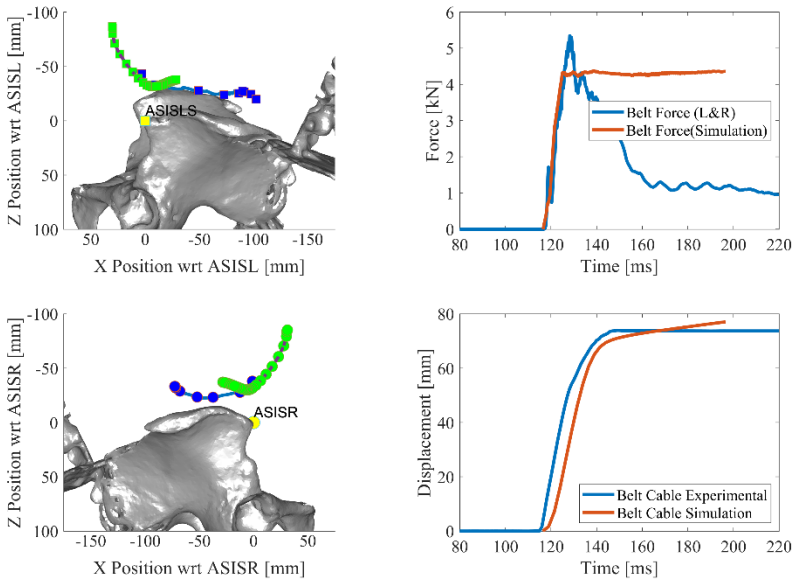

Figure 20. Baseline flat input simulation on simplified GHBMC obesity model with SPG formulation in updated Lagrangian kernel (kernel=2) with critcal shear strain particle-to-particle bond failure criteria (critical shear strain=0.85 and critical stretch=1.85) #38

Since both simulations terminated normally, it was determined that the energy input is not enough to make the model submarine. The focus then switched to using different energy input and the SPG method to make the model submarine. By applying a scaling factor of 3, we managed to make the model submarine using the SPG method.

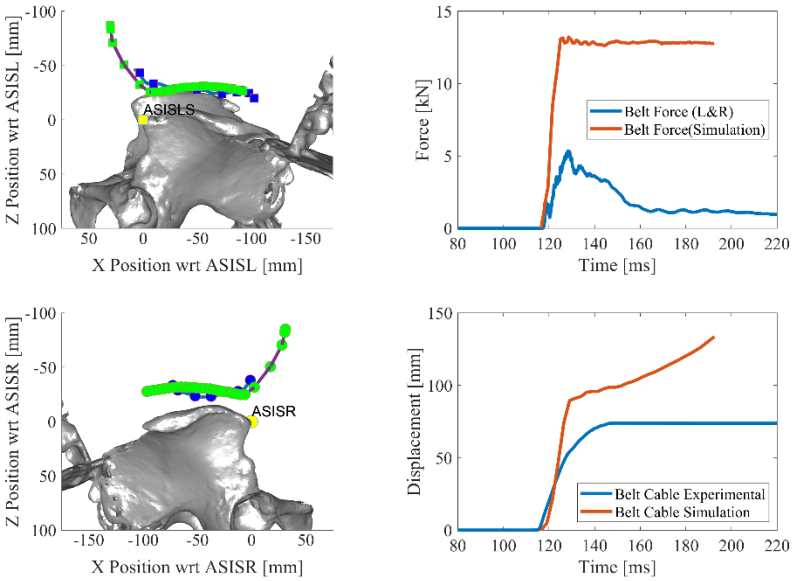

Figure 21. Three times baseline flat input simulation on simplified GHBMC obesity model with SPG formulation in updated Lagrangian kernel (kernel=2) with no particle-to-particle bond failure criteria #39

Now we start to explore the effect of failure parameters using this input setting. We used critical shear strain as a parameter and using different critical values ranging from 0.25 to 1.05. It was found that with a critical shear strain of 0.45, the largest amount of deformation was observed.

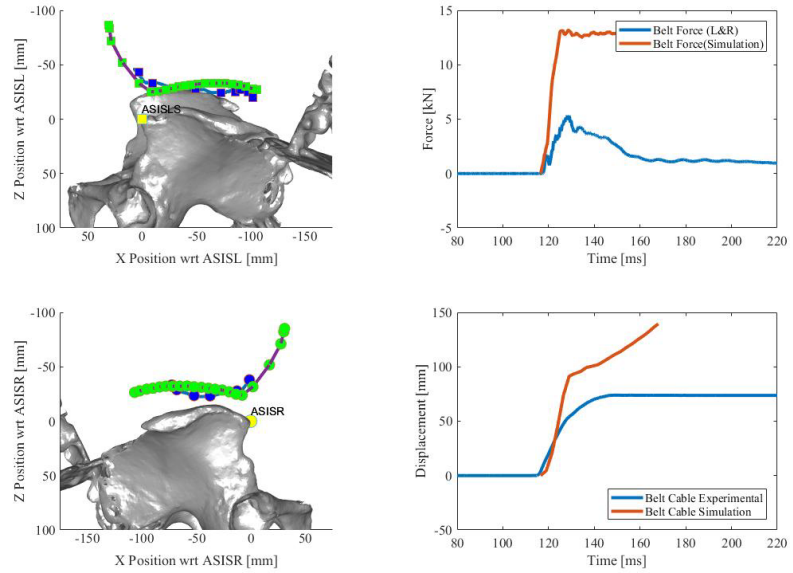

Figure 22. Three times baseline flat input simulation on simplified GHBMC obesity model with SPG formulation in updated Lagrangian kernel (kernel=2) with critical shear strain particle-to-particle bond failure criteria (critical shear strain=0.25 and critical stretch=1.25) #40

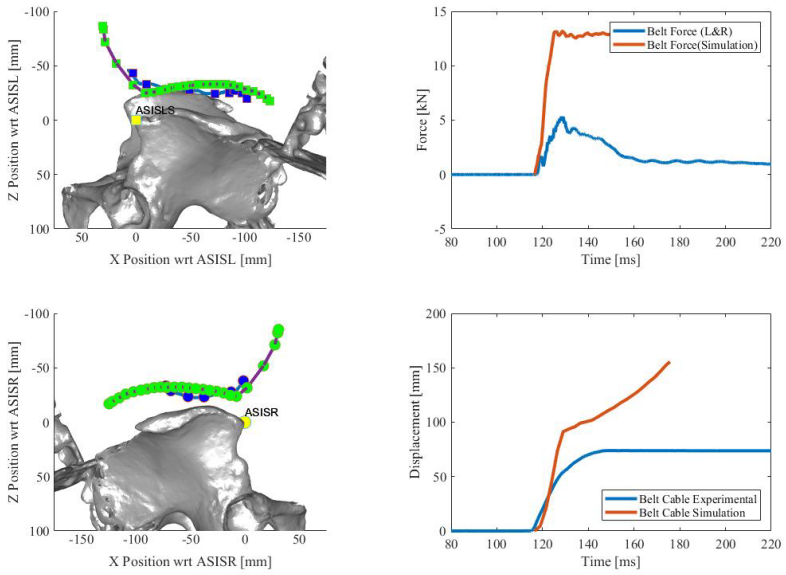

Figure 23. Three times baseline flat input simulation on simplified GHBMC obesity model with SPG formulation in updated Lagrangian kernel (kernel=2) with critical shear strain particle-to-particle bond failure criteria (critical shear strain=0.45 and critical stretch=1.45) #41

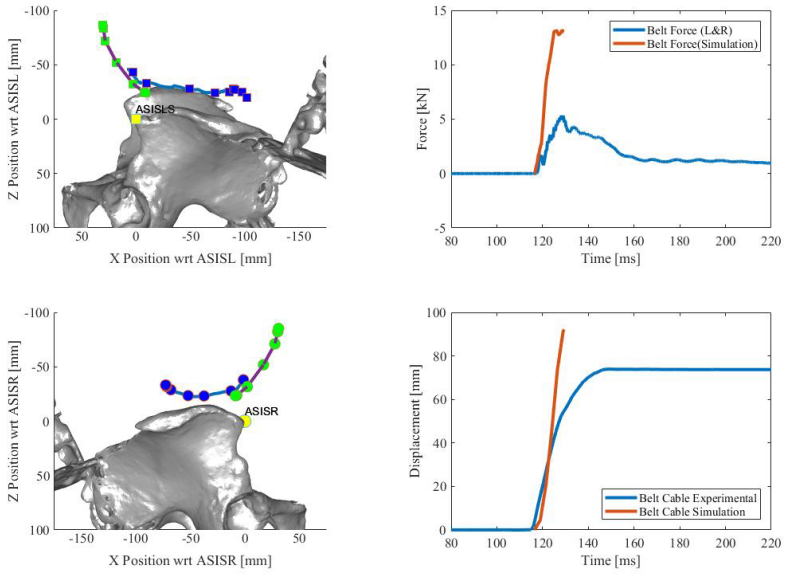

Figure 24. Three times baseline flat input simulation on simplified GHBMC obesity model with SPG formulation in updated Lagrangian kernel (kernel=2) with critical shear strain particle-to-particle bond failure criteria (critical shear strain=0.65 and critical stretch=1.65) #42

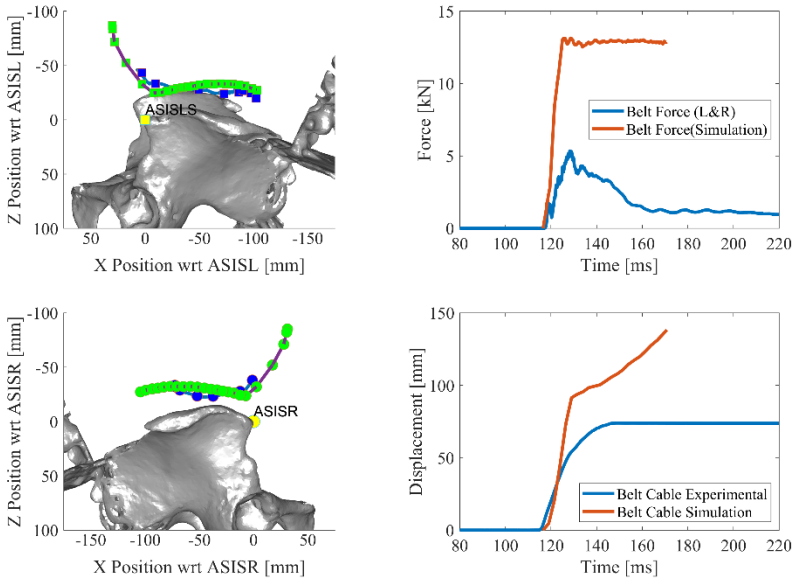

Figure 25. Three times baseline flat input simulation on simplified GHBMC obesity model with SPG formulation in updated Lagrangian kernel (kernel=2) with critical shear strain particle-to-particle bond failure criteria (critical shear strain=0.85 and critical stretch=1.85) #43

The above simulations showed that SPG has the potential to simulate large deformation controlled by a set of particle-to-particle failure parameters, which leads to model submarining in a test situation like the belt pull test. However, the objective of this simplified model remains a primary feasibility study of the SPG method. The boundary and input conditions could not be matched to the belt pull test perfectly. Therefore, we moved to the full model with implemented remesh.

Page intentionally left blank.

Type II Submarining

Twenty-two simulations were performed in Lagrangian elements (Table 3).

Table 3. Summary of all simulations for type II submarining

Full Remeshed Belt Pull Test Model in Lagrangian Elements			
Simulation #	Boundary Condition	Input	Mesh
1~10	Complete	Various	Remesh
11~12	Modified Pelvis	3 times baseline Flat	Remesh
13~18	Lower flesh stiffness	Baseline Flat	Remesh
19~22	Complete	Various	Split Hexa

For simplicity, Table 4 shows results from 10 simulations while the complete set of results can be found in the Appendix A under Type II Submarining Appendix.

Table 4. Simulation results from full remeshed belt pull test model in Lagrangian elements

Full Remeshed Belt Pull Test Model in Lagrangian Elements					
Simulation #	**Belt Pull Force**	**Boundary Conditions**	**Mesh**	**Results**	**Belt Displacement**
2	Baseline flat	Complete	Tetrahedral Remesh	Normal termination, no submarining	75 mm
3	sfo3 flat	Complete		Normal termination, submarining but pelvic wings fractured	125 mm
6	sfo5 flat	Complete		Error termination, negative volume on rectus muscle	140 mm
7	sfo5sfa5 flat	Complete		Error termination, submarining but pelvic wings fractured	160 mm
12	sfo3sfa3 flat	Turn off pelvic wing failure		Error termination, negative volume on rectus muscle	110 mm
18	Baseline flat	Material stiffness 0.001		Normal termination, not enough energy for submarining	95 mm
19	Baseline flat	Complete	Hexahedral split 1 time	Normal termination, no submarining	80 mm
20	sfo3sfa3 flat	Complete	Hexahedral split 1 time	Error termination, no submarining	100 mm
21	sfo3sfa3 flat	Complete	Hexahedral split 2 times	Normal termination, submarining but pelvic wings fractured	125 mm
22	sfo3sfa3 flat	Complete	Hexahedral split 3 times		135 mm

The baseline simulation with complete boundary conditions and the tetrahedral remesh showed similar kinematics to the model with the original mesh.

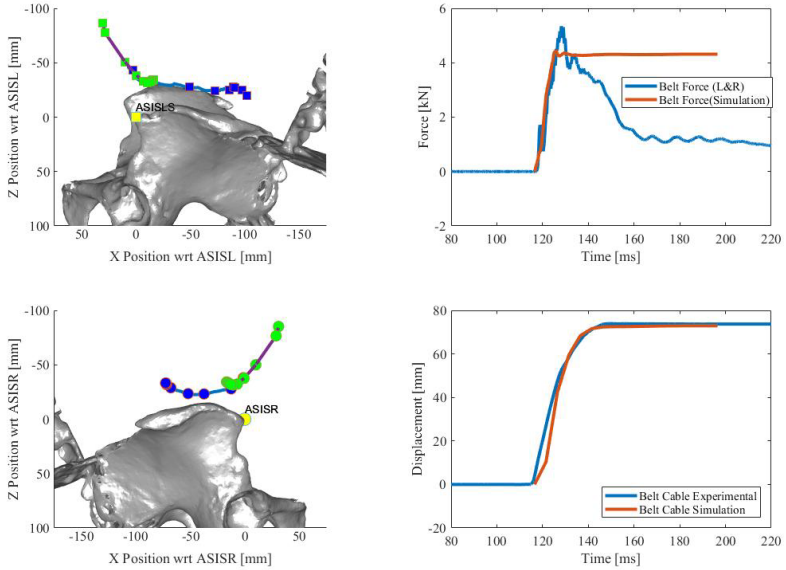

Figure 26. Baseline flat input simulation in Lagrangian formulation with complete boundary condition #2

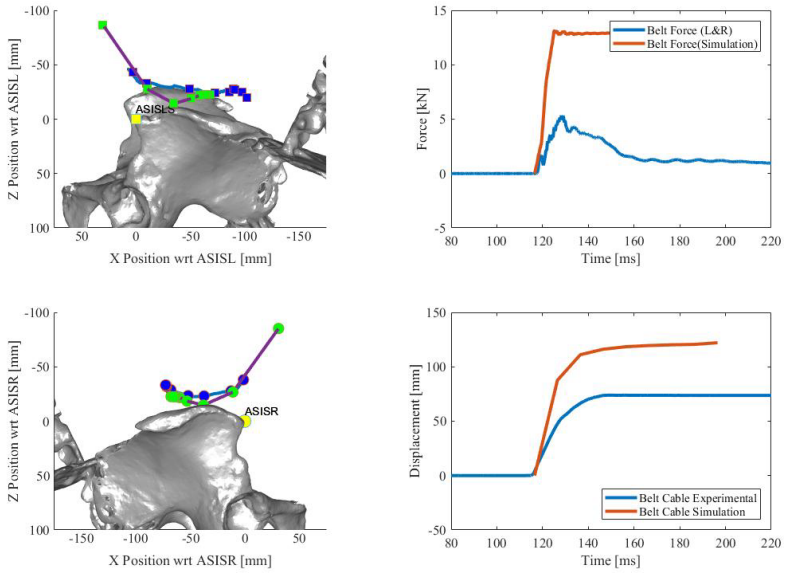

Figure 27. Three times peak force and rate flat input simulation in Lagrangian formulation with complete boundary condition #3

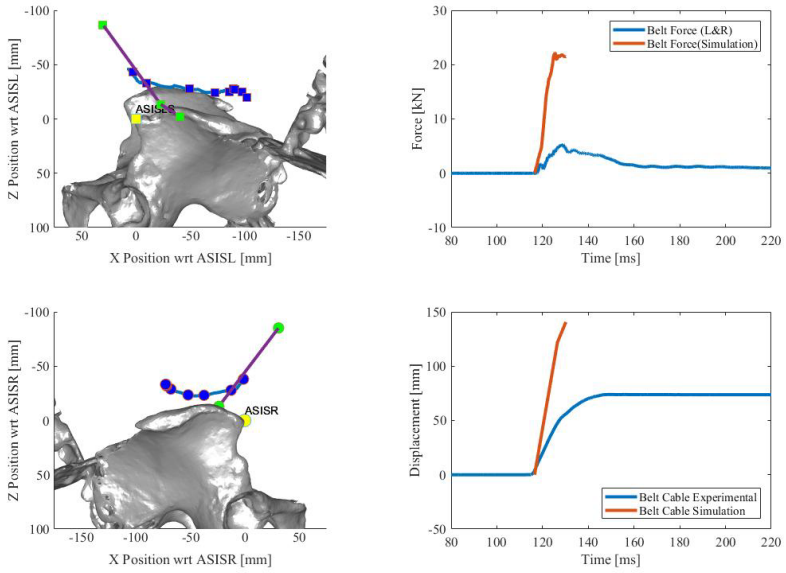

Figure 28. Five times peak force and rate flat input simulation in Lagrangian formulation with complete boundary condition #6

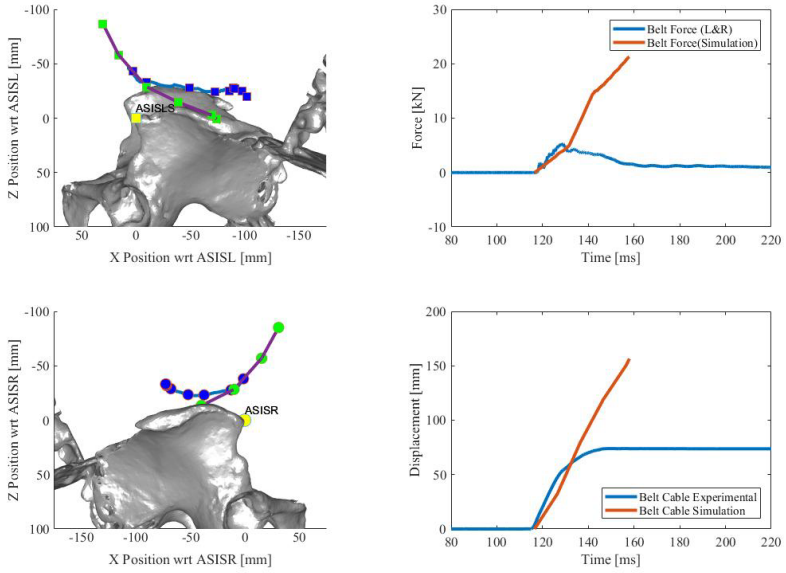

Figure 29. Five times peak force and baseline rate flat input simulation in Lagrangian formulation with complete boundary condition #7

Figure 26 to Figure 29 show the results obtained for the remeshed model with the original Lagrangian formulation. It was found that under baseline loading conditions, the model could not submarine due to lack of energy. With the increased input energy, the model was observed to submarine. On inspection it was discovered that the shearing motion of the flesh over the pelvis was facilitated through the failure of the iliac wing's cortical bone material, and consequently the release of the original boundary condition. It was also found that with higher input load, the model does not submarine. Instead, the belt goes straight towards the pelvic wings and results in negative volume problem. The observed belt motion was referred to as type II submarining and

identified as pseudo submarining, since it was achieved through the artificial release of predefined boundary condition.

Since the model response may be dependent on the mesh type used, and the tetrahedral elements have a tendency to become overly stiff for highly incompressible materials, the original GHBMC model was used to develop a hexahedral abdominal mesh with comparable mesh density to the evaluated tetrahedral model (Figure 30 to Figure 33).

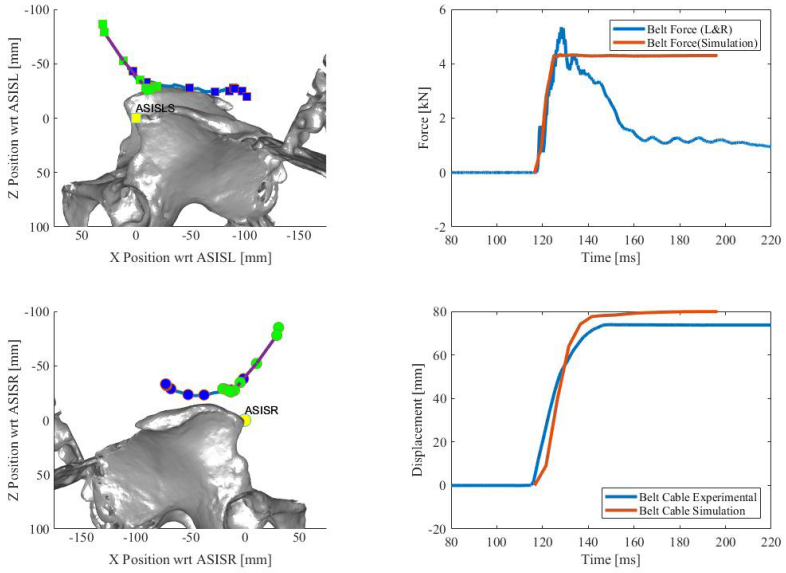

Figure 30. Baseline flat input simulation in Lagrangian formulation with complete boundary condition and an alternative hexahedral remesh created by splitting the original mesh once #19

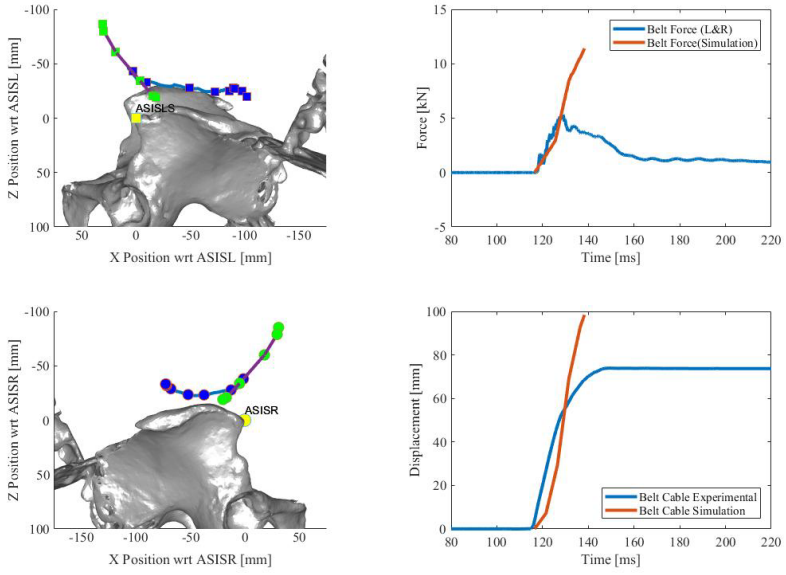

Figure 31. Three times baseline flat input simulation in Lagrangian formulation with complete boundary condition and an alternative hexahedral remesh created by splitting the original mesh once #20

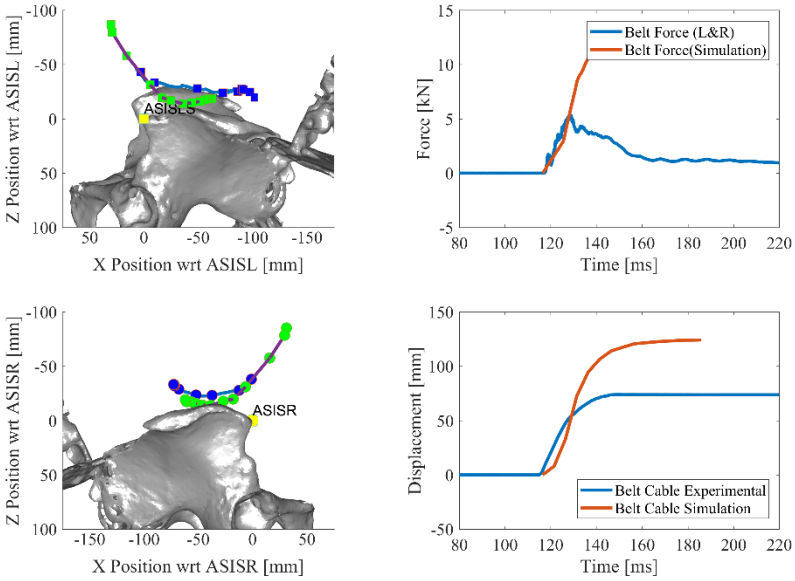

Figure 32. Three times baseline flat input simulation in Lagrangian formulation with complete boundary condition and an alternative hexahedral remesh created by splitting the original mesh two times #21

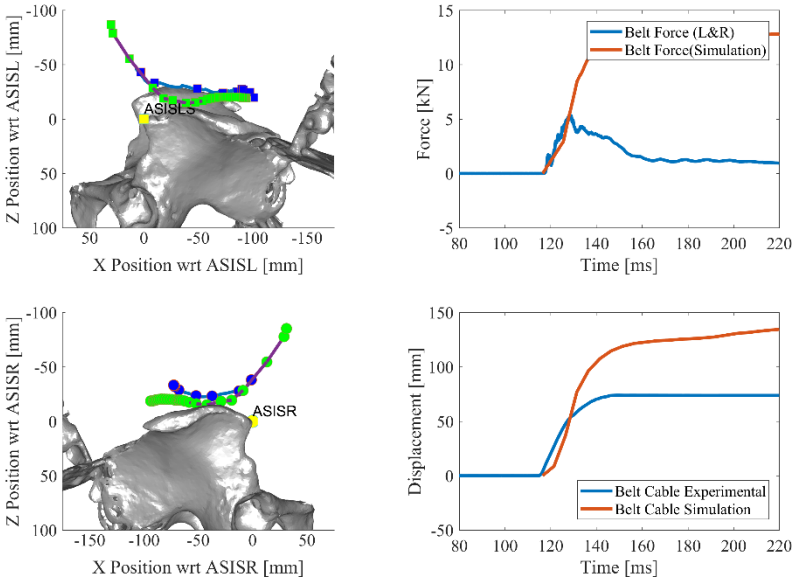

Figure 33. Three times baseline flat input simulation in Lagrangian formulation with complete boundary condition and an alternative hexahedral remesh created by splitting the original mesh three times #22

Comparing across all three scaling factor simulations, it can be clearly observed that as spatial resolution increased, global belt cable displacement also increased. However, the reason was consistent that boundary condition was broken due to failure of pelvic wings. We then concluded that the remeshed model could increase the element's ability in handling extreme deformation but not lead to submarining by enabling large shear deformation. In all remeshed models, pseudo submarining was still caused by yielding of the pelvic wings.

Since it was found that pseudo submarining is due to yielding of the pelvic wings, we could turn off the pelvic wing failure criteria. This can be achieved in two ways. The first method is to increase the yielding point to make it almost not reachable in the current simulation setting. The second method is to turn off the yielding criteria directly. Both methods gave the same response. Once the failure of the iliac wings was disabled, the model failed to replicate the submarining response (Figure 34).

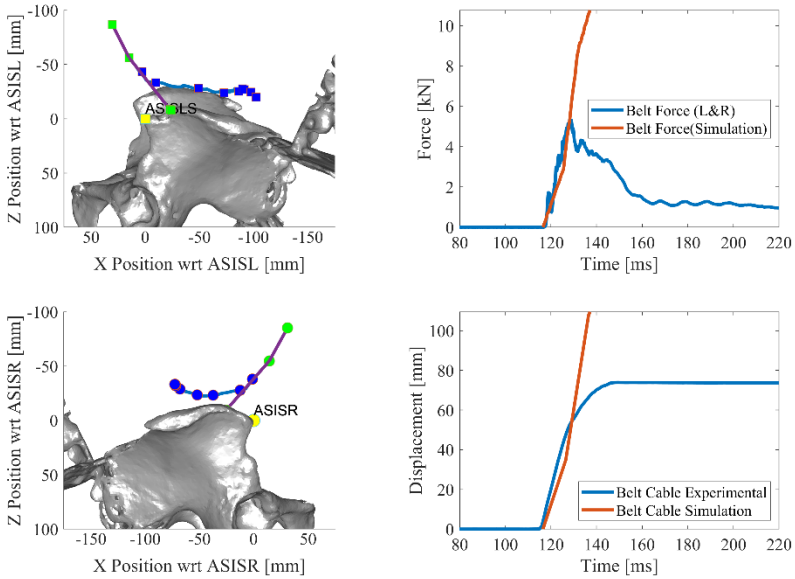

Figure 34. Three times peak force and rate flat input simulation in Lagrangian formulation with pelvis failure turned off #12

These results showed that effectively turning off failure criteria of pelvis resulted in negative volume in flesh—no submarining. Since we believed that submarining is due to the property of the abdominal flesh and the GHBMC flesh is too stiff, we started to investigate the effect of using a lower pulling force combined with a more compliant material model for the abdominal flesh.

We adjusted the flesh material stiffness by changing the scaling factor of the input stress-strain curve in the simplified rubber/foam material card in LS-DYNA. We started by using 75 percent of baseline stiffness and gradually decrease the stiffness to 0.1%. For brevity, the complete set of results can be found in Appendix A.

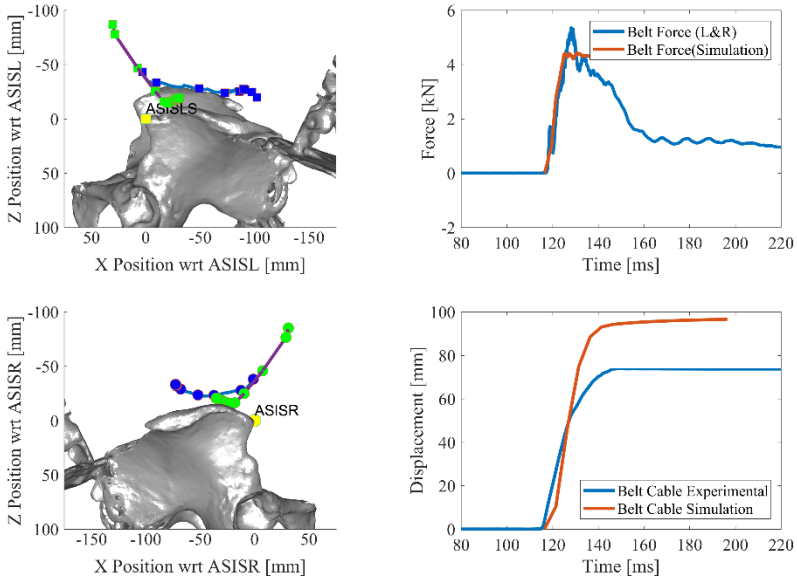

Figure 35. Baseline flat input simulation in Lagrangian formulation with complete boundary condition and abdominal flesh material stiffness turned downto 0.1% of its original #18

It was found that even the least stiff model could not replicate the belt kinematics observed in the experiments using only baseline input pulse. Overall kinematics had little sensitivity to modified material property of flesh. However, belt cable displacement increased as abdominal stiffness decreased. As described in Gepner et al. (2018), there are two distinctive phases of the belt motion observed in Kim et al. (2015). First the belt compresses the abdominal tissue, and after engaging the iliac wing the reaction force from the pelvis changes the direction of belt movement. Once the direction is changed, the belt moves into the abdomen loading the soft tissues instead of the bony pelvic wings. Models with the lowest stiffness (1or 0.1%), showed the belt midline passing the turning point, however in this case the belt motion was arrested by the remaining, unmodified tissues, such as, the internal organ block and other connective tissue.

Page intentionally left blank.

Type III Submarining

After investigating the response of the various models based on the Lagrangian formulation, we moved to SPG simulations to explore the benefits of this meshless method. The outer thoracic and abdominal flesh were turned into smoothed particles while the skin and inner flesh remained as Lagrangian shells. Note that we based the SPG model on the remeshed model with tetrahedral elements. SPG particles were generated at every nodal position of the remeshed model, replacing tetrahedral solid mesh. In this section, a total of 27 simulations were performed. The effects of input force and rate, boundary conditions and material properties of flesh were studied and presented in this section. For brevity, we would present all simulation results with the detailed parameters used to create them in Appendix A. Table 5 summarizes the results from the simulations presented in this section.

Table 5. Simulation result from complete remeshed (tetrahedral) belt pull test model in SPG

Complete Remeshed (Tetrahedral) Belt Pull Test Model in SPG				
Simulation #	**Boundary Condition**	**Input**	**SPG Parameters**	**Notes**
10	Complete	Baseline Flat	K=2; IDAM=3; fs=0.25;s=1.25	Normal termination, submarining trend showed no pelvic wing fracture
1	Complete	sfo3sfa3 Flat	K=2; IDAM=3; fs=0.25;s=1.25	Normal termination, submarining but pelvic wings fractured
2	Turn off pelvic wing failure	sfo3sfa3 Flat	K=2; IDAM=3; fs=0.25;s=1.25	Normal termination, submarining no pelvic wing fracture
5	Complete	sfo3sfa3 Flat	K=2; IDAM=3; fs=0.45;s=1.45	Normal termination, submarining but pelvic wings fractured
6	Turn off pelvic wing failure	sfo3sfa3 Flat	K=2; IDAM=3; fs=0.45;s=1.45	Normal termination, submarining no pelvic wing fracture
3	Turn off pelvic wing failure	sfo3sfa3 Flat	K=2; IDAM=3; fs=0.10;s=1.15	
4	Turn off pelvic wing failure	sfo3sfa3 Flat	K=2; IDAM=3; fs=0.25;s=2.0	
8	Turn off pelvic wing failure	sfo2sfa2 Flat	K=2; IDAM=3; fs=0.25;s=1.25	
13	Material stiffness 0.01; Turn off pelvic wing failure	sfo2sfa2 Flat	K=2; IDAM=3; fs=0.25;s=1.25	Error termination due to out-of-range forces on nodes on the SPG part
14	Material stiffness 0.01;Turn off pelvic wing failure	sfo2sfa2 Flat	K=2; IDAM=3; fs=0.15;s=1.15	Normal termination, submarining no pelvic wing fracture
15	Material stiffness 0.01;Turn off	sfo1.5sfa1.5 Flat	K=2; IDAM=3; fs=0.15;s=1.25	

Complete Remeshed (Tetrahedral) Belt Pull Test Model in SPG				
Cont.	pelvic wing failure			
17	Turn off pelvic wing failure	Displacement Control	K=2; IDAM=3; fs=0.25;s=1.25	
18	Turn off pelvic wing failure	Displacement Controlv2	K=2; IDAM=3; fs=0.25;s=1.25	

We first ran the simulation in SPG with the baseline input energy and no submarining was observed (Figure 36). This observation was consistent with the Lagrangian simulations.

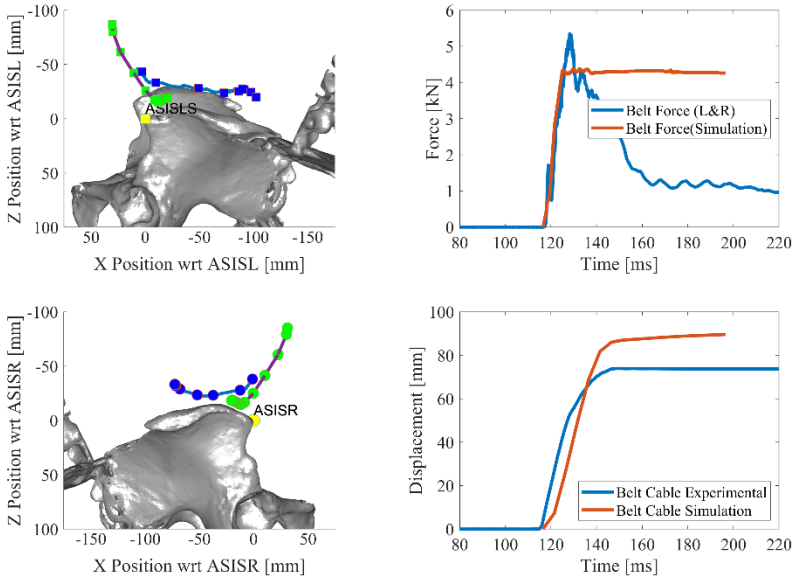

Figure 36. Baseline flat input simulation with complete boundary condition with SPG formulation in updated Lagrangian kernel (kernel=2) with critical shear strain particle-to-particle bond failure criteria (critical shear strain=0.25 and critical stretch=2.0) with pelvic wing yielding criteria on #10

Then, we scaled up the input energy to three times both with and without the pelvic wing failure criteria.

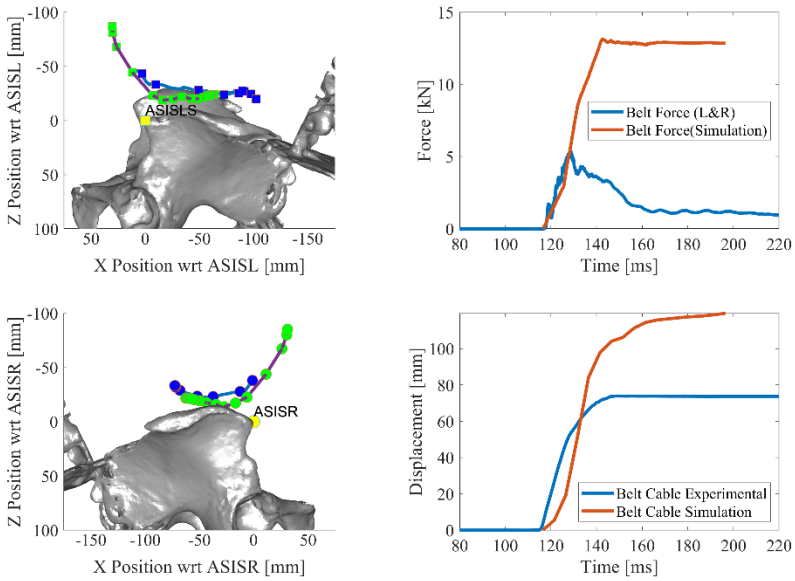

Figure 37. Three times peak force and baseline rate flat input simulation in SPG formulation with complete boundary condition #1

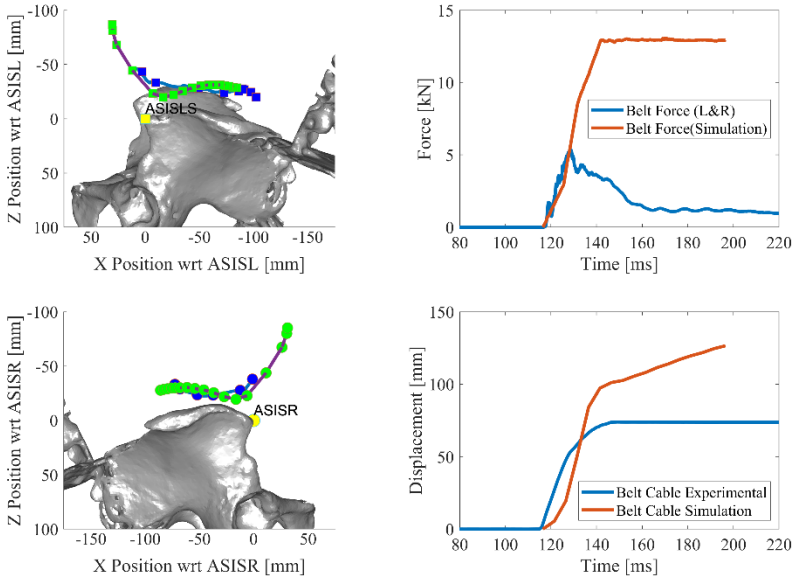

Figure 38. Three times peak force and baseline rate flat input simulation in SPG formulation with pelvis failure turned off #2

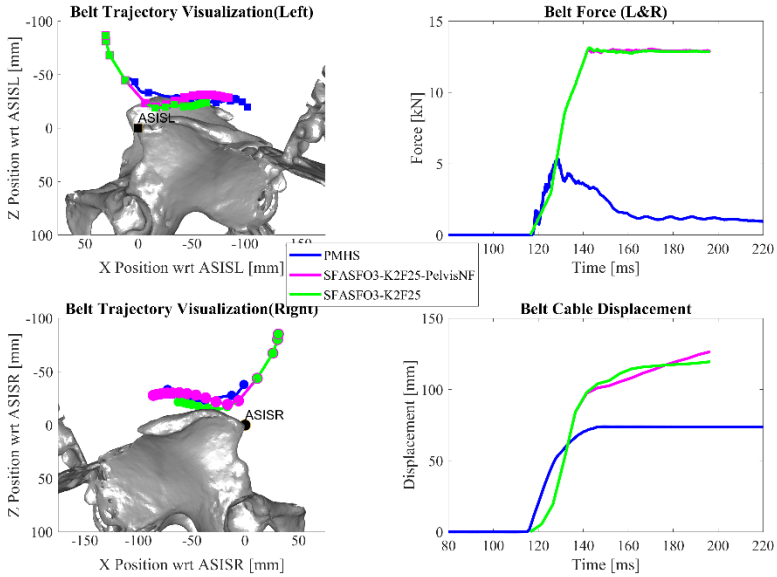

Figure 39. Comparison between both three times peak force and baseline rate flat input simulation in SPG formulation with (in green) or without pelvis failure (in pink)

We understood that the baseline energy input was not enough for submarining due to both difference in anthropometry between subjects and an over stiff flesh material model. Consequently, we started with the three times peak force and baseline rate flat input as the first SPG simulation. Like the remeshed model in Lagrangian, the model submarined but the pelvic wing was fractured (Figure 37) when the pelvis failure criteria was on. However, when turning off the pelvic failure criteria, the belt also managed to load the abdomen into large shear (Figure 38) without running into a negative volume problem as encountered in the Lagrangian models. A comparison revealed that the lap belt found a different path to load the abdomen, avoiding loading the pelvic wings to failure. Specifically, when turning off the failure criteria on the pelvis, the belt followed a path superior to the pelvic wings, avoiding dragging on flesh particles tied to the pelvic wings.

When the critical shear strain increased from 0.25 to 0.45, the model still demonstrated abdominal belt intrusion, but the amount of penetration was smaller. This trend is the same as predicted since the model with a higher failure strain is stiffer. Also, the effect of pelvic yielding criteria was found to be consistent in the case of a different bond-to-bond failure parameter. In the simulation with pelvic yielding criteria, submarining happened partially due to breaking of the boundary condition (Figure 40). In the simulation without pelvic yielding criteria, we still see similar kinematics, but the belt went through a trajectory more above the pelvis (Figure 41). A comparison of both belt trajectories was shown in Figure 42.

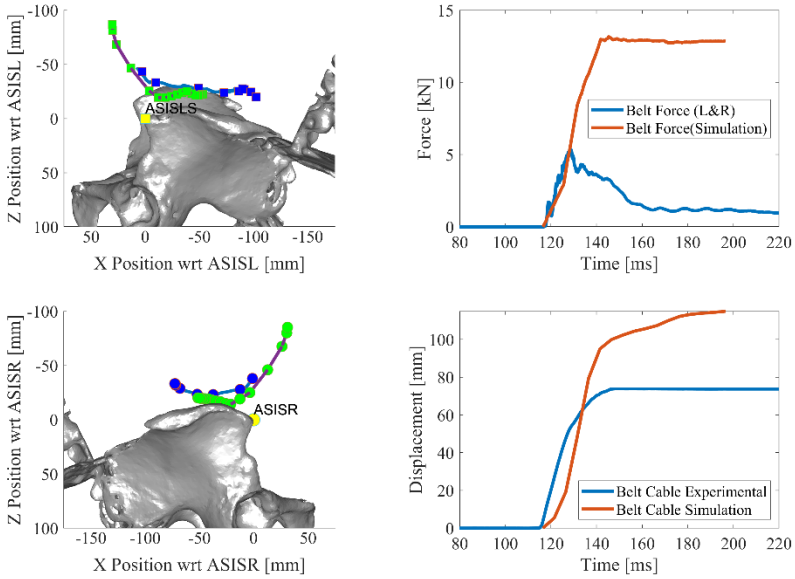

Figure 40. Three times baseline flat input simulation with complete boundary condition with SPG formulation in updated Lagrangian kernel (kernel=2) with critical shear strain particle-to-particle bond failure criteria (critical shear strain=0.45 and critical stretch=1.45) with pelvic wing yielding criteria on #5

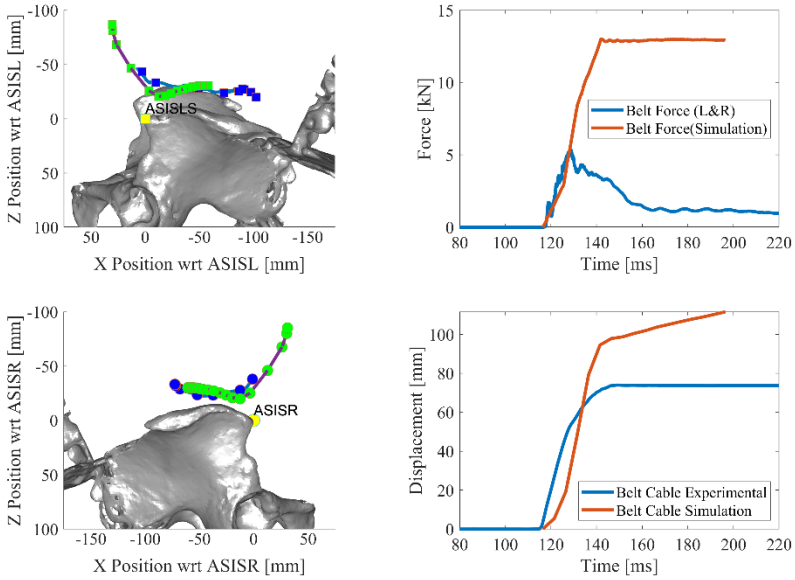

Figure 41. Three times baseline flat input simulation with complete boundary condition with SPG formulation in updated Lagrangian kernel (kernel=2) with critical shear strain particle-to-particle bond failure criteria (critical shear strain=0.45 and critical stretch=1.45) with pelvic wing yielding criteria off #6

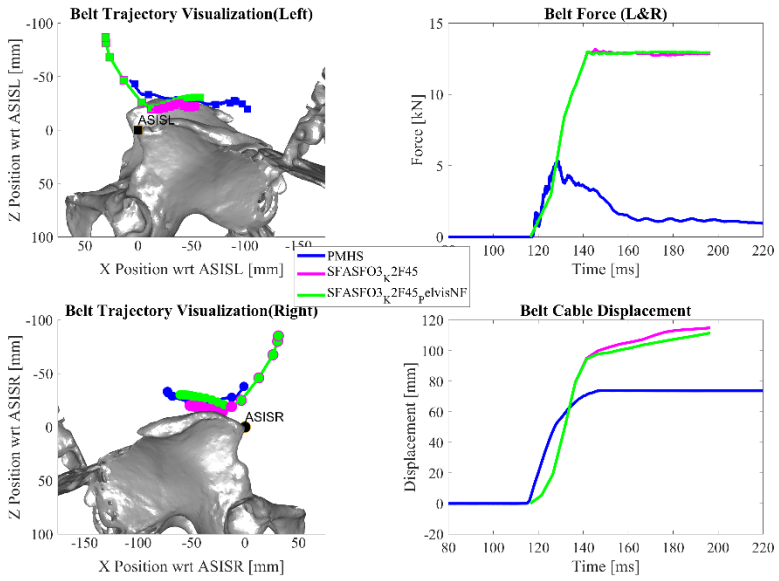

Figure 42. Comparison on belt trajectory with and without pelvic wing failure criteria

Effects of bond-to-bond failure criteria can be observed more clearly in Figure 43 and Figure 44. These two simulations use a critical shear strain of 0.1, critical stretch of 1.15 (Figure 43) and shear strain of 0.25, critical stretch of 2 (Figure 44), respectively. A set of harder-to-fail bond-to-bond failure parameters leads to reduced belt intrusion since the belt motion is controlled by the overall structural stiffness and martial flow (facilitated by bond failure) within the abdominal flesh (Figure 43 and Figure 44).

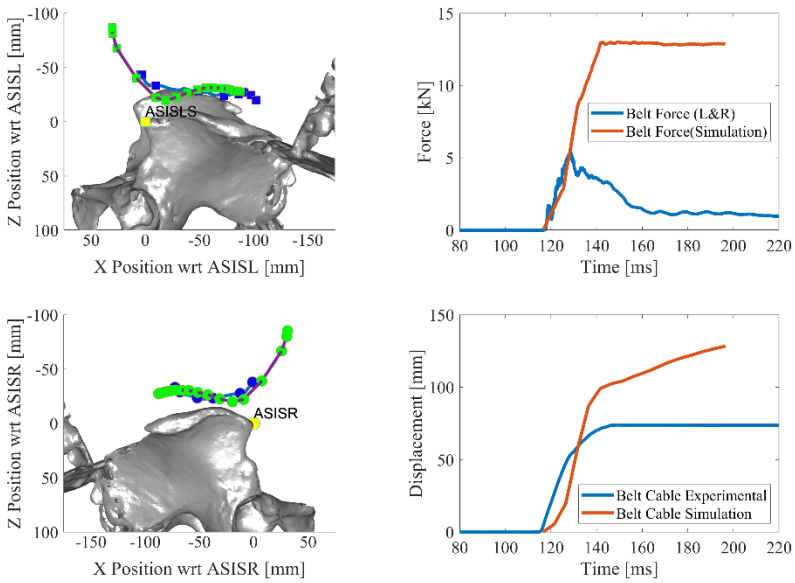

Figure 43. Three times baseline flat input simulation with complete boundary condition with SPG formulation in updated Lagrangian kernel (kernel=2) with critical shear strain particle-to-particle bond failure criteria (critical shear strain=0.1 and critical stretch=1.15) with pelvic wing yielding criteria off #3

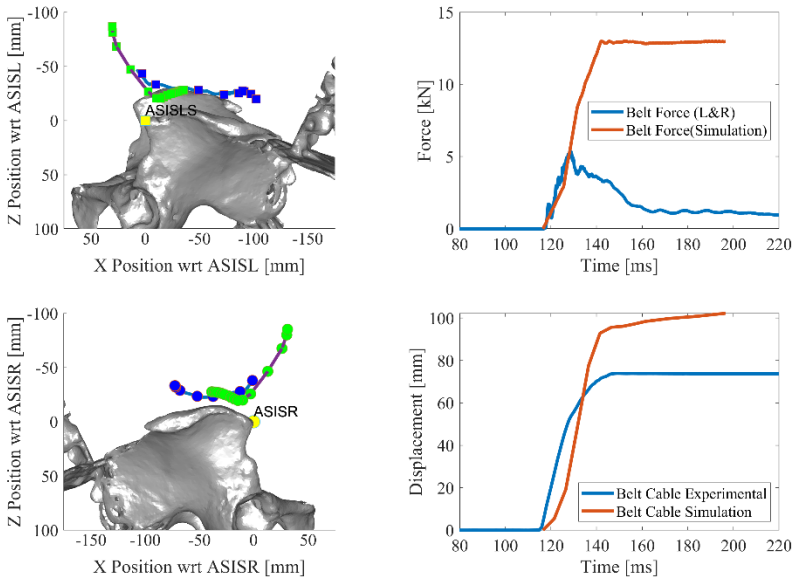

Figure 44. Three times baseline flat input simulation with complete boundary condition with SPG formulation in updated Lagrangian kernel (kernel=2) with critical shear strain particle-to-particle bond failure criteria (critical shear strain=0.25 and critical stretch=2.0) with pelvic wing yielding criteria off #4

The previous simulations using SPG domain discretization (Figure 36 and Figure 44) showed that SPG is capable of facilitating the submarining belt motion and allows for the belt to pass over the iliac wings into the abdomen. Since the original material model used in the GHBMC abdominal flesh was shown to be too stiff to be used for modeling the adipose tissue, we decided to investigate capabilities of the SPG method with the reduced force input and flesh material properties. As a first step, only the input energy was turned down to a level of two times the force of the experiment. The reduction of input energy reduced the extent of belt penetration (Figure 45).

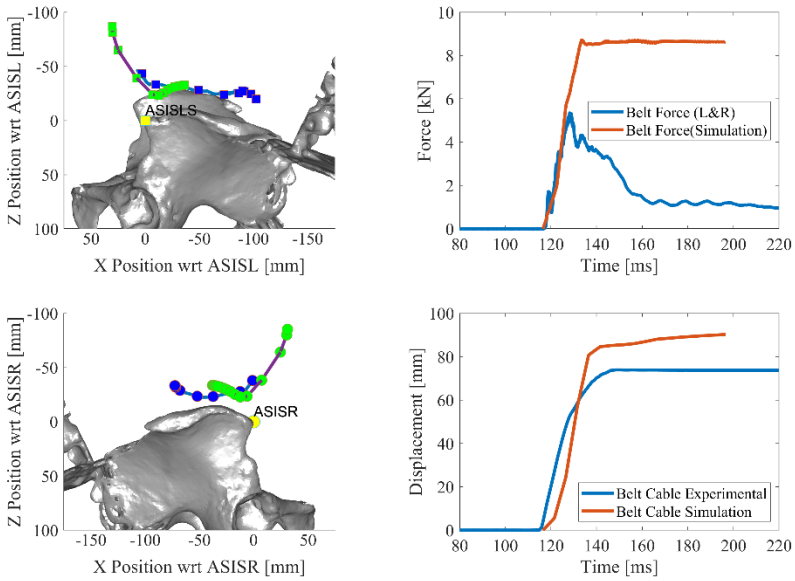

Figure 45. Two times baseline flat input simulation with complete boundary condition with SPG formulation in updated Lagrangian kernel (kernel=2) with critical shear strain particle-to-particle bond failure criteria (critical shear strain=0.25 and critical stretch=1.25) with pelvic wing yielding criteria off #8

To investigate the capabilities of SPG method of modeling adipose tissue material deformation with the reduced material properties (similar to the approach in Figure 35) we decided to proceed with the reduced force input shown in Figure 45. The first simulation used the reduced material properties (1% stiffness of the original model), and reduced force input (two times the force of the experiment) without any changes to other SPG parameters (Figure 46). This simulation terminated with error. With the reduced stiffness of the material model of adipose tissue the material failure parameters (shear strain and critical stretch) dominated the initial response of the tissue, leading to the compression failure during the initial belt pull without providing necessary support for the belt to transition over the iliac wings into the abdomen.

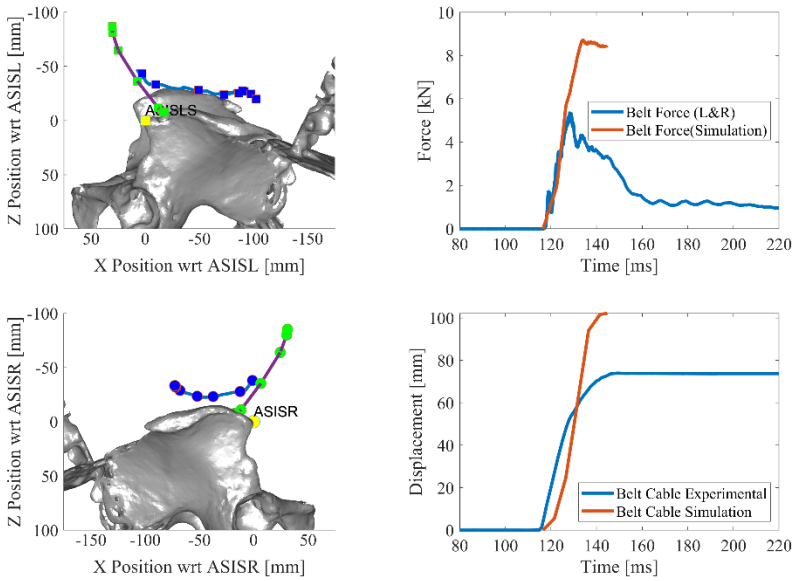

Figure 46. Two times baseline flat input simulation with complete boundary condition with SPG formulation in updated Lagrangian kernel (kernel=2) with critical shear strain particle-to-particle bond failure criteria (critical shear strain=0.25 and critical stretch=2.0) with pelvic wing yielding criteria off (material stiffness turned to 1% stiffness) #13

Adjustment of the failure parameters allowed the model to reach successful termination where submarining was observed (Figure 47). This showed that model submarining in SPG is highly sensitive to the combination of failure parameters and input energy. To verify this, we performed another simulation with a different combination (1.5 times baseline force with critical shear strain 0.15 and critical stretch of 1.25). Differences in kinematic response were shown, but nevertheless submarining trend could be observed (Figure 48). The belt passed the turning point, defined as the point where belt changed its direction of motion, and then moved into the abdomen. A series of simulation results showed that the distance the belt could travel after the turning point depended more on the input energy while the ability to pass the turning point depended on the combination of input energy, input rate and failure criteria implementation.

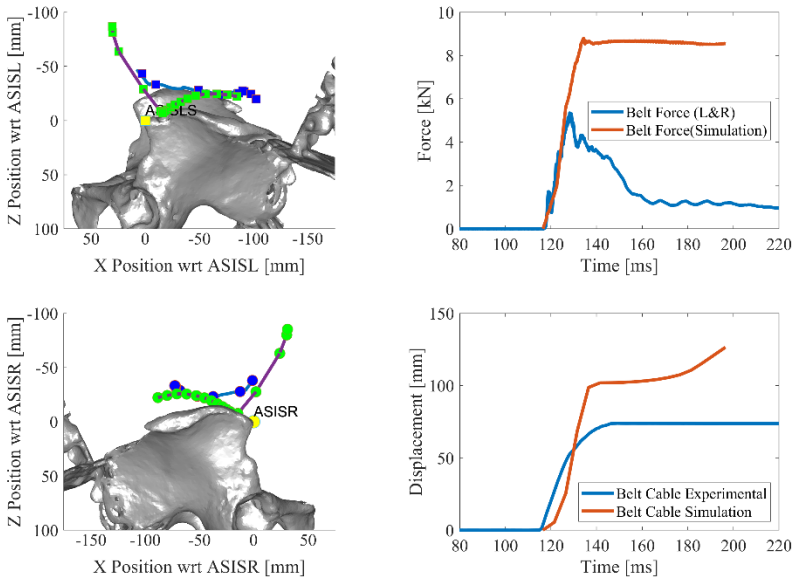

Figure 47. Two times baseline flat input simulation with complete boundary condition with SPG formulation in updated Lagrangian kernel (kernel=2) with critical shear strain particle-to-particle bond failure criteria (critical shear strain=0.25 and critical stretch=1.15) with pelvic wing yielding criteria off (material stiffness turned to 1% stiffness) #14

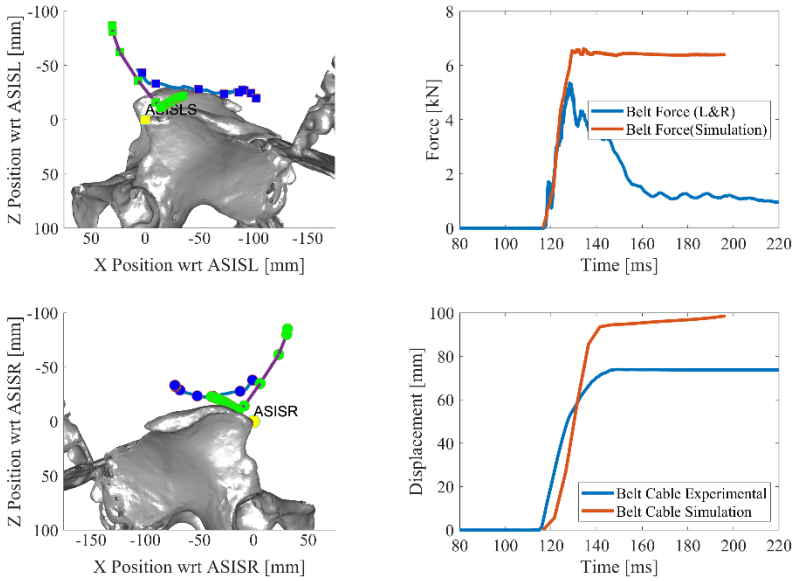

Figure 48. 1.5 times baseline flat input simulation with complete boundary condition with SPG formulation in updated Lagrangian kernel (kernel=2) with critical shear strain particle-to-particle bond failure criteria (critical shear strain=0.25 and critical stretch=1.25) with pelvic wing yielding criteria off (material stiffness turned to 1% stiffness) #15

Additional simulation with displacement-controlled input were performed to additionally evaluate the robustness and stiffness response of the proposed SPG formulation. Since the model differed in anthropometry with the PMHS used in the experiment, matching displacement time history resulted only in partial penetration of the belt into the abdomen (Figure 49). Additionally, the recorded force remained higher than the one observed in the PMHS experiment. To address

both discrepancies a higher belt displacement and a softer material was used, resulting in a higher abdominal penetration of the belt (Figure 50).

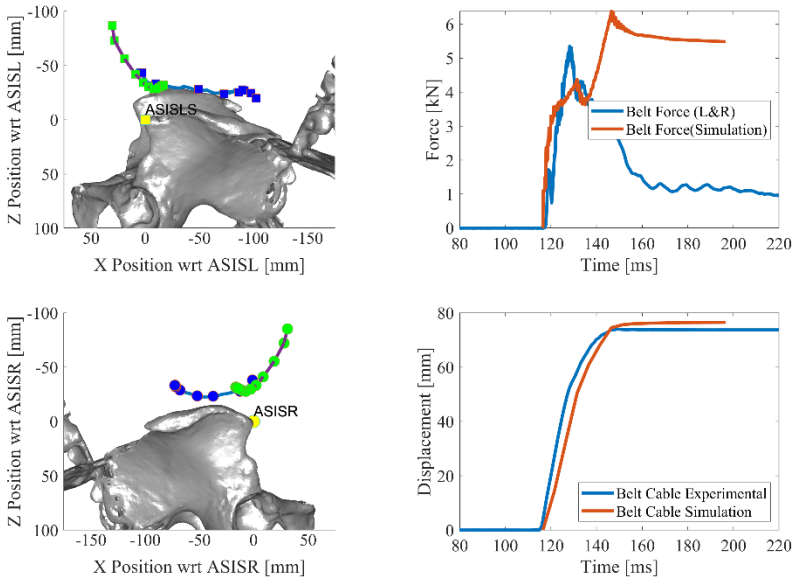

Figure 49. Displacement controlled simulation with complete boundary condition with SPG formulation in updated Lagrangian kernel (kernel=2) with critical shear strain particle-to-particle bond failure criteria (critical shear strain=0.25 and critical stretch=1.25) with pelvic wing yielding criteria #17

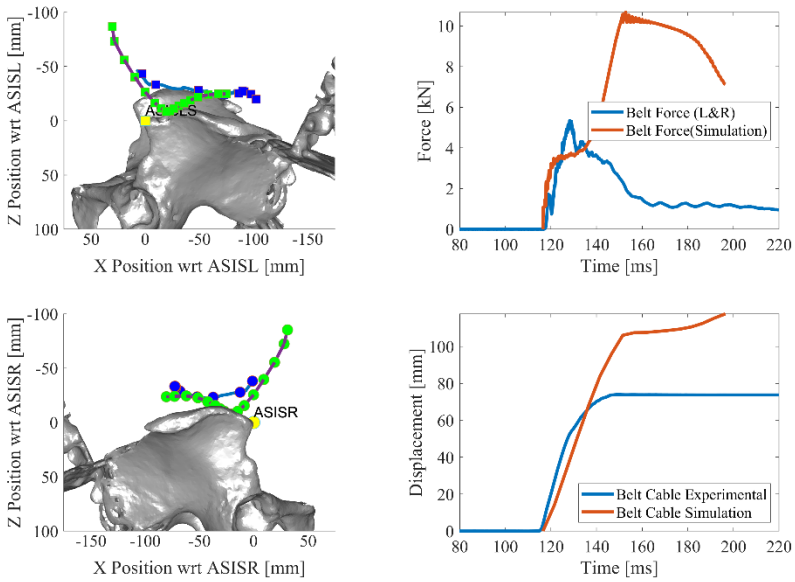

Figure 50. Displacement controlled simulation with complete boundary condition with SPG formulation in updated Lagrangian kernel (kernel=2) with critical shear strain particle-to-particle bond failure criteria (critical shear strain=0.25 and critical stretch=1.25) with pelvic wing yielding criteria off (material stiffness turned to 1% stiffness) #18

Page intentionally left blank.

SPG in Rear Seat Sled Test

In the belt pull test simulation, we remeshed the whole abdominal and thoracic flesh parts using constant density tetrahedral elements and converted the whole flesh into SPG. However, to expedite the remesh process for the models that were previously positioned in the rear seat sled environment, only the frontal part of the abdominal flesh was remeshed. The frontal part of the abdomen was remeshed by splitting elements along the primary axis of loading. In this way, we created 12 elements across the abdominal wall, and this yields more than 10 layers of particles in between the boundary layers (Figure 51). The subsequent sled simulations showed that the model was unable to progress to the stage where the lap belt fully engages with the HBM. This was due to out-of-range force problem within the SPG, likely associated with contact instabilities between the SPG particles and Lagrangian mesh. We found that using a full-scale sled simulation to debug these issues is not the optimal choice. Instead, we decided to focus on a well-established and controlled loading scenario that would allow us to evaluate the response of the abdomen to the direct, dynamic impact. For this purpose, we chose the abdominal bar impact (Hardy et al., 2001) which is included in the GHBMC certification suite.

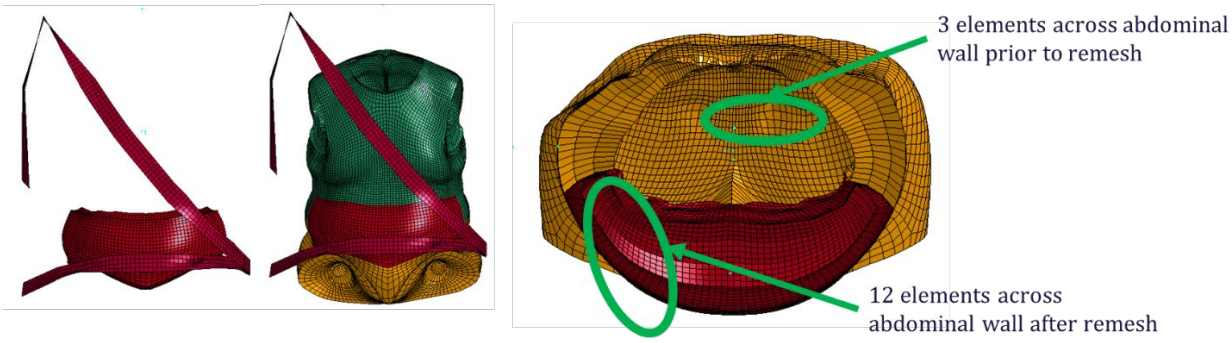

Figure 51. New part creation for running SPG in the rear seat sled test simulation

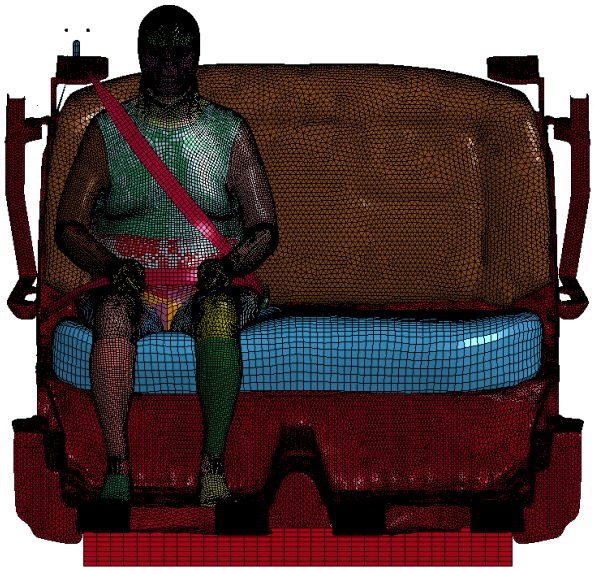

Figure 52. Setup of the modified SPG model in the rear seat sled test simulation

Page intentionally left blank.

Abdominal Bar Impact With SPG

Since we modified the GHBMC obesity models, it is essential to explore its accuracy and robustness by simulating it in the GHBMC certification simulations. We received a document along with the GHBMC obesity models, which provide an overview of the 12 morphed human models based on GHBMC M50-O v4.4 developed by UMTRI. We chose to compare the response of modified models (SPG) and the original GHBMC obesity model in the abdominal bar impact simulation. The force-deflection curves for the AM50 GHBMC and the obese models as per the abdominal impact test are shown in Figure 53.

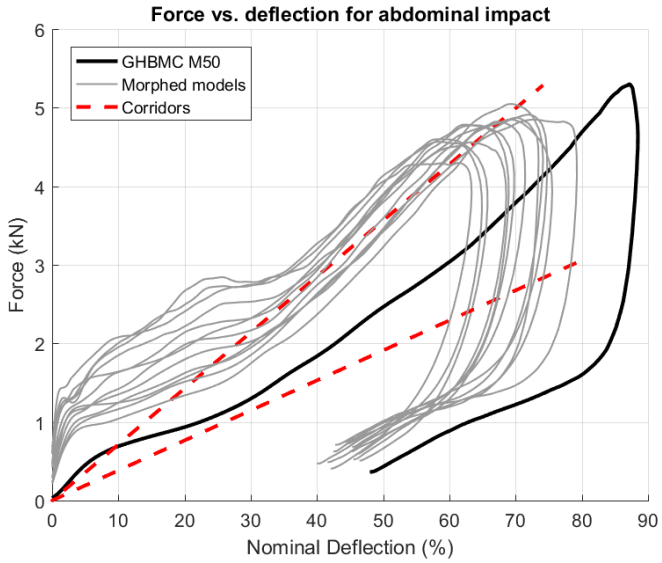

Figure 53. Force versus deflection for abdominal impact from UMTRI

It was mentioned that the abdominal impact tests were conducted according to the test set up from Hardy et al. (2001) paper. The data are shown in Figure 54.

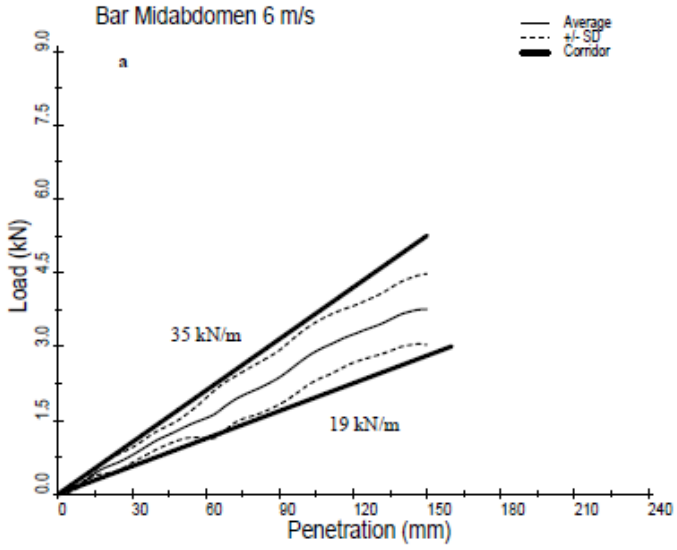

Figure 54. Force versus deflection for abdominal impact from Hardy et al. (2001)

Several tests were run in Hardy et al. (2001) with fixed back and free back configurations. The corridors mentioned by UMTRI matched with the mid-abdomen impact with free back and an impact velocity of 6 m/s. To make comparisons, we scaled the normalized deflection to the absolute penetration data.

The positioned GHBMC obesity model used in the belt pull test were simulated with the mid-abdomen bar impact with free back and 6 m/s of impact velocity from Hardy et al. (2001). The set-up of the model is shown in Figure 55. The abdominal bar was only allowed to move along the impact direction. Both thoracic and abdominal flesh of the GHBMC obesity model were modelled in SPG with an Ogden rubber material model. Particle-to-particle failure criteria was implemented with a critical shear strain of 0.45. The force vs deflection curve is shown below in Figure 56.

Figure 55. Set up of the abdominal bar impact with the GHBMC obesity model used in the belt pull tests

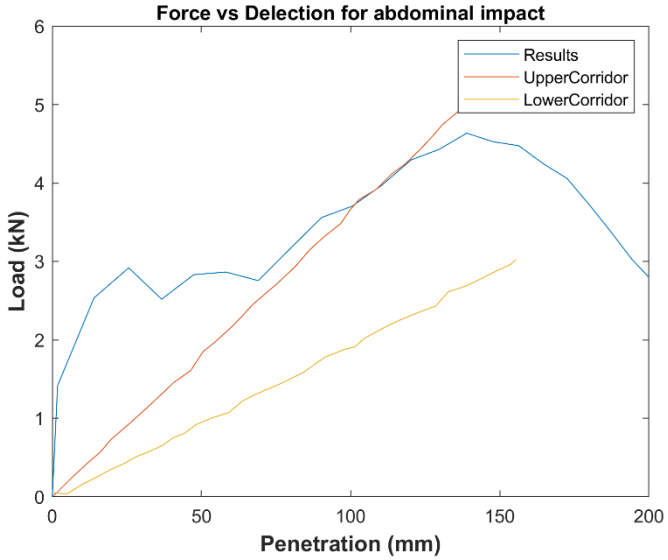

Figure 56. Force versus deflection curve from the belt pull model with SPG formulation in updated Lagrangian kernel (kernel=2) with critical shear strain particle-to-particle bond failure criteria (critical shear strain=0.45 and critical stretch=1.45)

The positioned GHBMC obesity model used in the rear seat sled test were also simulated with same conditions. The setup of the model is shown in Figure 57. The newly created abdominal flesh part of the GHBMC obesity model were modelled in SPG with an Ogden rubber material model. Specifically, we implemented a non-failure criteria SPG simulation along with the 0.45 critical shear strain particle-to-particle failure criteria implemented simulation. The force vs deflection curve is shown below in Figure 58 and Figure 59. The results further showed that by implementing the particle-to-particle failure criteria in the SPG part, the structural stiffness of the model can be controlled.

Figure 57. Set up of the abdominal bar impact with the GHBMC obesity model used in the rear seat sled tests

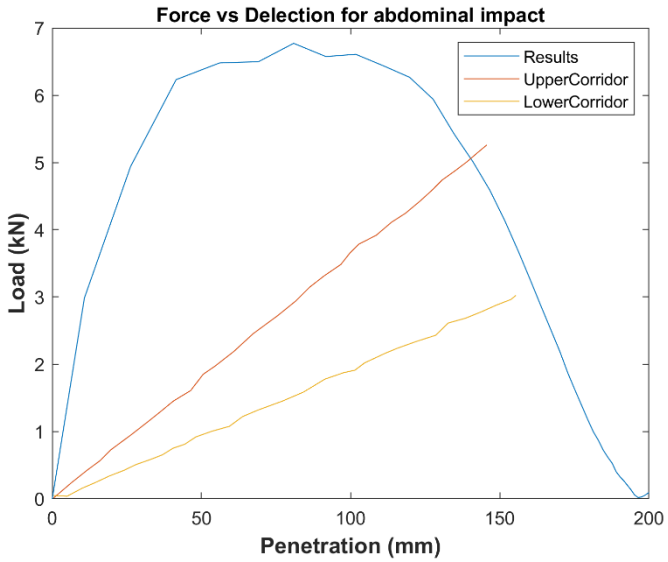

Figure 58. Force versus deflection curve from the belt pull model with Ogden rubber model and SPG formulation in updated Lagrangian kernel (kernel=2) with no particle bond failure criteria implemented

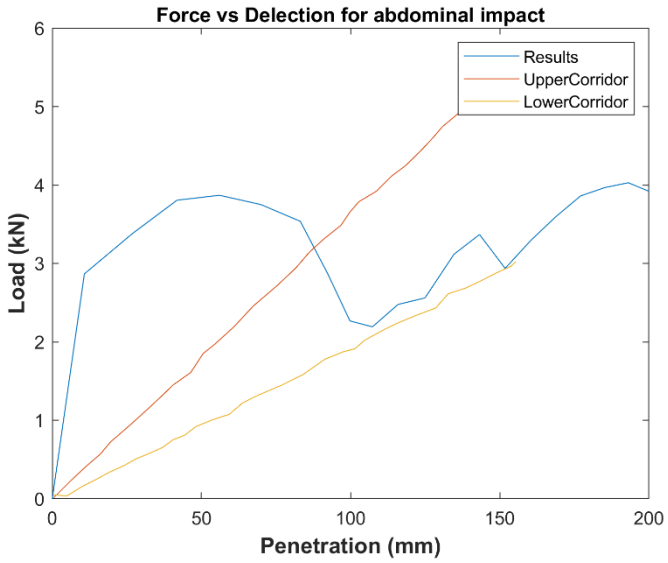

Figure 59. Force versus deflection curve from the belt pull model with Ogden rubber model and SPG formulation in updated Lagrangian kernel (kernel=2) with critical shear strain particle-to-particle bond failure criteria (critical shear strain=0.45 and critical stretch=1.45)

References

Forman, J., Lin, H., Gepner, B., Wu, T., & Panzer, M. (2018) Occupant safety in automated vehicles: Effect of seatback recline on occupant restraint. *International Journal of Automotive Engineering*, *10*(2), 139–143. https://www.researchgate.net/publication/339581175_Occupant_Safety_in_Automated_Vehicles_-_Effect_of_Seatback_Recline_on_Occupant_Restraint_-

Forman, J., Lopez-Valdes, F. J., Lessley, D., Kindig, M., Kent, R., & Bostrom, O. (2009). The effect of obesity on the restraint of automobile occupants. *Annals of Advances in Automotive Medicine*, *53*, p. 25.

Gepner, B. D., Joodaki, H., Sun, Z., Jayathirtha, M., Kim, T., Forman, J. L., & Kerrigan, J. R. (2018, September 12-14). *Performance of the obese GHBMC models in the sled and belt pull test conditions* (Paper No. IRC-18-60). IRCOBI Conference 2018, Athens, Greece. www.ircobi.org/wordpress/downloads/irc18/pdf-files/60.pdf

Hardy, W. N,, Schneider, L. W., & Rouhana, S. W. (2001, November). Abdominal impact response to rigid-bar, seatbelt, and airbag loading. *Stapp Car Crash Journal,* (45)1-32. doi: 10.4271/2001-22-0001 PMID: 17458738

Hu, J., Fanta, A., Neal, M. O., Reed, M. P., & Wang, T.-Y. (2016, June 15-17). *Vehicle crash simulations with morphed GHBMC human models of different stature, BMI, and age* 4th International Digital Human Modeling Conference, Montreal, Canada.

Jehle, D., Gemme, S., & Jehle, C. (2012). Influence of obesity on mortality of drivers in severe motor vehicle crashes. *The American Journal of Emergency Medicine*, *30*(1), 191–195.

Kent, R. W., Forman, J. L., & Bostrom, O. (2010). Is there really a "cushion effect"?: A biomechanical investigation of crash injury mechanisms in the obese. *Obesity*, *18*(4), 749–753.

Kim, T., Park, G., Montesinos, S., Subit, D., Bolton, J., Overby, B., Forman, J., Crandall, J., & Kim, H. (2015, June 8-11). *Abdominal characterization test under lap belt loading* [Paper presented]. 24th International Technical Conference on the Enhanced Safety of Vehicles (ESV), Gothenburg, Switzerland.

Kitagawa, Y., Hayashi, S. & Yasuki, T. (2017, September 13-15). *Comparison of impact kinematics between non-obese and obese occupants in frontal and lateral impacts* (Paper IRC-17-19). IRCOBI Conference 2017, Antwerp, Belgium. www.ircobi.org/wordpress/downloads/irc17/pdf-files/19.pdf

Libersky, L. D., Petschek, A. G., Carney, T. C., Hipp, J. R., & Allahdadi, F. A. (1993). High strain Lagrangian hydrodynamics: A three-dimensional SPH code for dynamic material response. *Journal of Computational Physics*, *109*(1), 67–75.

Li, S., & Liu, W. K. (2002). Meshfree and particle methods and their applications. *Applied Mechanics Reviews*, *55*(1), 1–34.

Lin, H., Gepner, B., Wu, T., Forman, J., & Panzer, M. (2017, September 12-14). *Effect of seatback recline on occupant model response in frontal crashes* (Paper IRC-18-64). IRCOBI Conference 2018, Athens, Greece. www.ircobi.org/wordpress/downloads/irc18/pdf-files/64.pdf

Mock, C. N., Grossman, D. C., Kaufman, R. P., Mack, C. D., & Rivara, F. P. (2002). The relationship between body weight and risk of death and serious injury in motor vehicle crashes. *Accident Analysis & Prevention*, *34*(2), 221–228.

Reed, M. P., Ebert-Hamilton, S. M., & Rupp, J. D. (2012). Effects of obesity on seat belt fit. *Traffic Injury Prevention*, *13*(4), 364–372.

Shi, X., Cao, L., Reed, M. P., Rupp, J. D., & Hu, J. (2015). Effects of obesity on occupant responses in frontal crashes: a simulation analysis using human body models. *Computer Methods in Biomechanics and Biomedical Engineering*, *18*(12), 1280–1292.

Sommer, G., Eder, M., Kovacs, L., Pathak, H., Bonitz, L., Mueller, C., Regitnig, P., & Holzapfel, G. A. (2013). Multiaxial mechanical properties and constitutive modeling of human adipose tissue: A basis for preoperative simulations in plastic and reconstructive surgery. *Acta Biomaterialia*, *9*(11), 9036–9048.

Viano, D. C., Parenteau, C. S., & Edwards, M. L. (2008). Crash injury risks for obese occupants using a matched-pair analysis. *Traffic Injury Prevention*, *9*(1), 59–64.

Wang, Y., Bai, Z., Cao, L., Reed, M. P., Fischer, K., Adler, A., & Hu, J. (2015). A simulation study on the efficacy of advanced belt restraints to mitigate the effects of obesity for rear-seat occupant protection in frontal crashes. *Traffic Injury Prevention*, *16*(Sup1), S75–S83.

Wu, C. T., Guo, Y., & Hu, W. (2014). *An introduction to the LS-DYNA Smoothed Particle Galerkin method for severe deformation and failure analyses in solids* [Paper presented]. 13th International LS-DYNA Users Conference, Detroit, MI. https://lsdyna.ansys.com/wp-content/uploads/attachments/an-introduction-to-the-ls-dyna-r-smoothed-particle-galerkin-method-for-severe-deformation-and-failure-analyses-in-solids.pdf

Zhu, S., Layde, P. M., Guse, C. E., Laud, P. W., Pintar, F., Nirula, R., & Hargarten, S. (2006). Obesity and risk for death due to motor vehicle crashes. *American Journal of Public Health*, *96*(4), 734–739.

Appendix A.

Obese GHBMC Model Simplification and Remesh

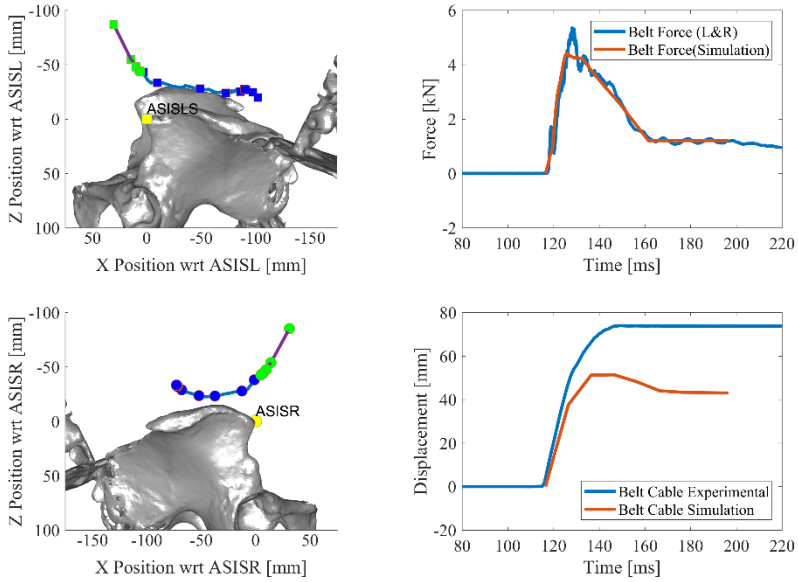

Figure A-1. Baseline fit input simulation on simplified GHBMC obesity model with Lagrangian elements #1

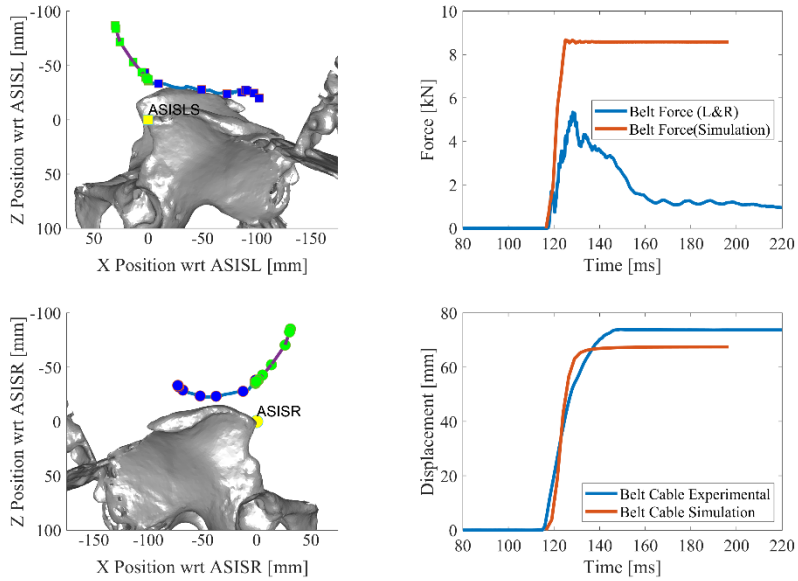

Figure A-2. Two times baseline flat input simulation on simplified GHBMC obesity model with Lagrangian elements #3

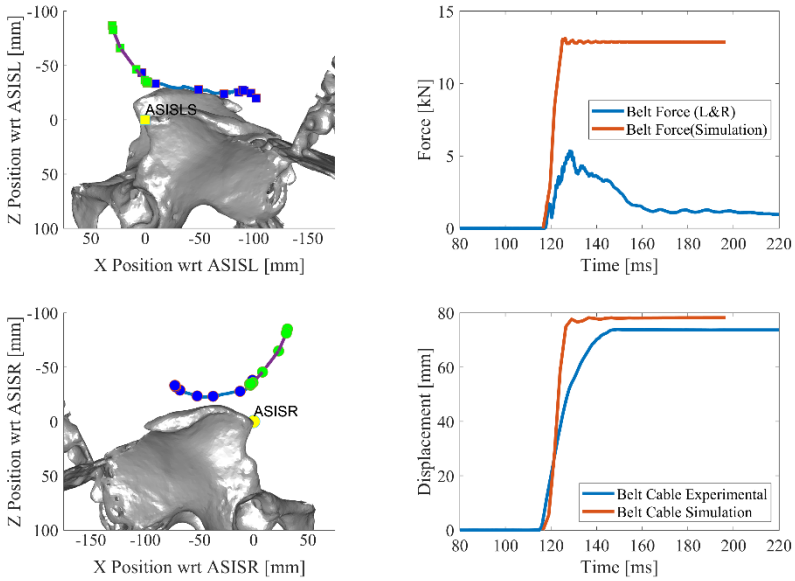

Figure A-3. Three times baseline flat input simulation on simplified GHBMC obesity model with Lagrangian elements #4

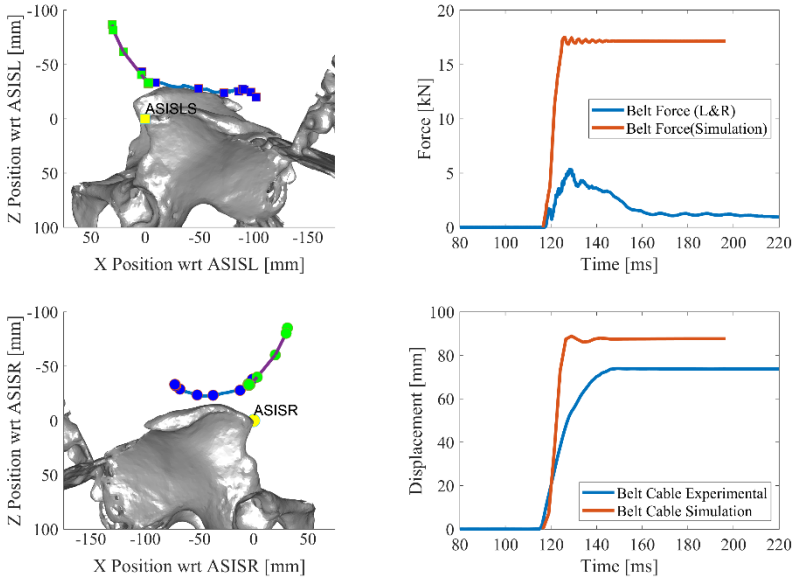

Figure A-4. Four times baseline flat input simulation on simplified GHBMC obesity model with Lagrangian elements #5

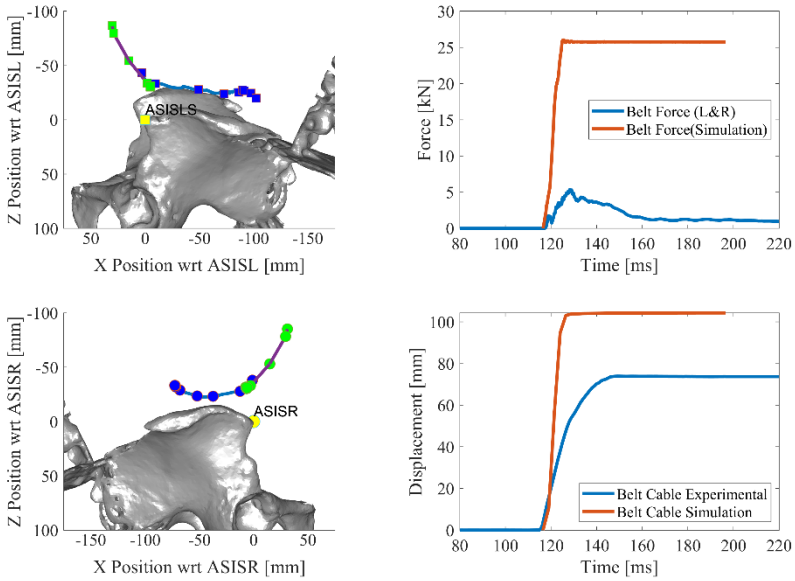

Figure A-5. Six times baseline flat input simulation on simplified GHBMC obesity model with Lagrangian elements #6

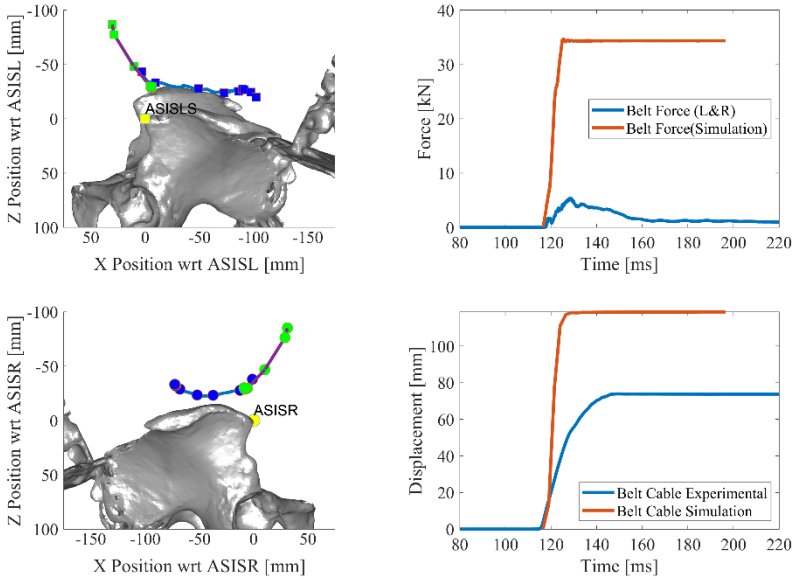

Figure A-6. Eight times baseline flat input simulation on simplified GHBMC obesity model with Lagrangian elements #7

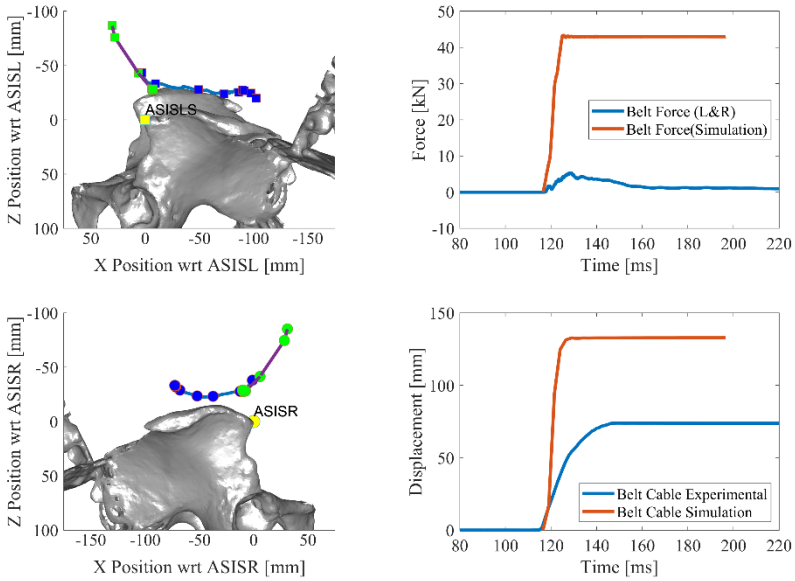

Figure A-7. Ten times baseline flat input simulation on simplified GHBMC obesity model with Lagrangian elements #8

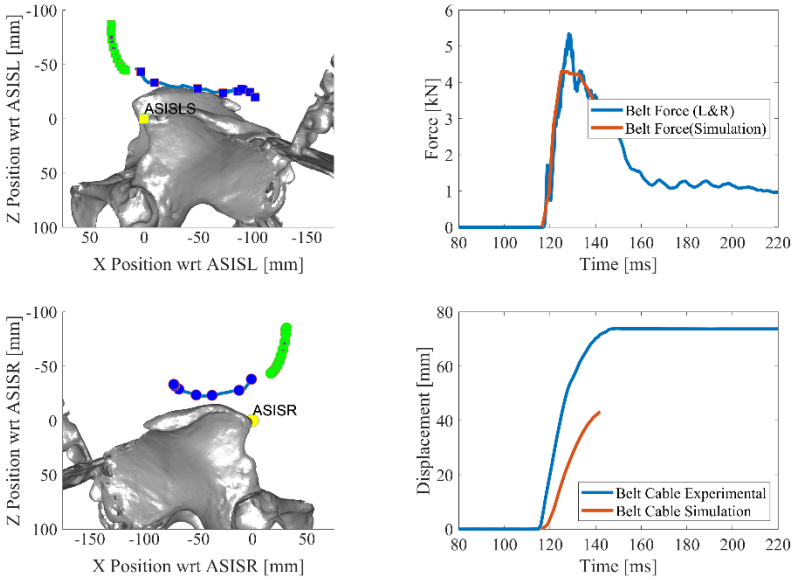

Figure A-8. Baseline fit input simulation on simplified GHBMC obesity model with SPG formulation in updated Lagrangian kernel (kernel=2) with critical shear strain particle-to-particle bond failure criteria (critical shear strain=0.85 and critical stretch=1.2) #10

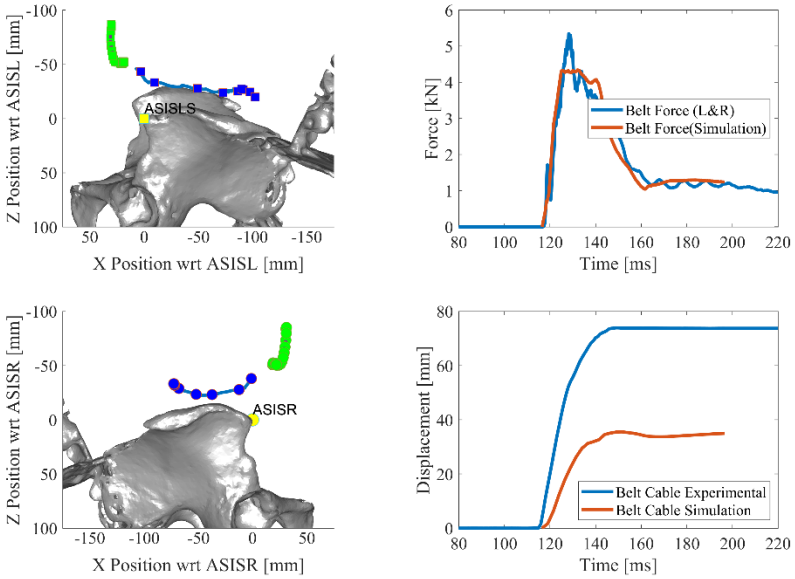

Figure A-9. Baseline fit input simulation on simplified GHBMC obesity model with SPG formulation in Lagrangian kernel (kernel=0) with critical shear strain particle-to-particle bond failure criteria (critical shear strain=0.85 and critical stretch=1.2) #11

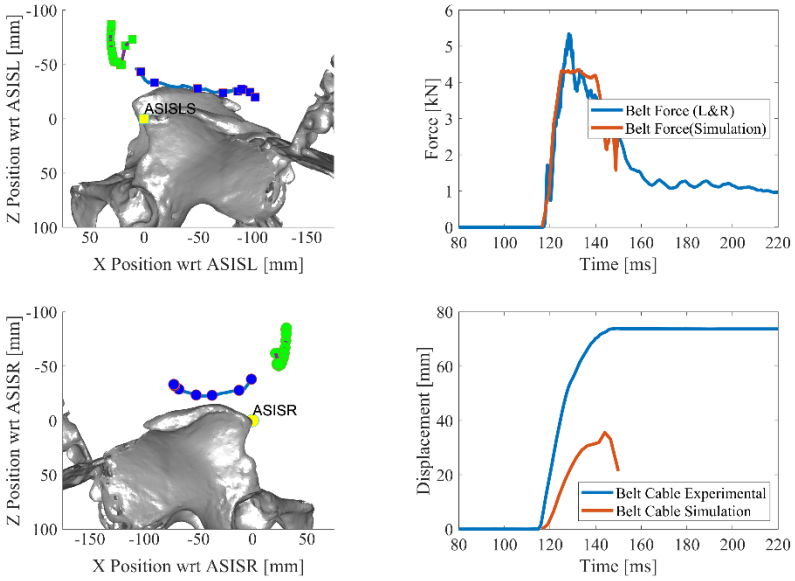

Figure A-10. Baseline fit input simulation on simplified GHBMC obesity model with SPG formulation in Lagrangian kernel (kernel=0) with no particle-to-particle bond failure criteria implemented #12

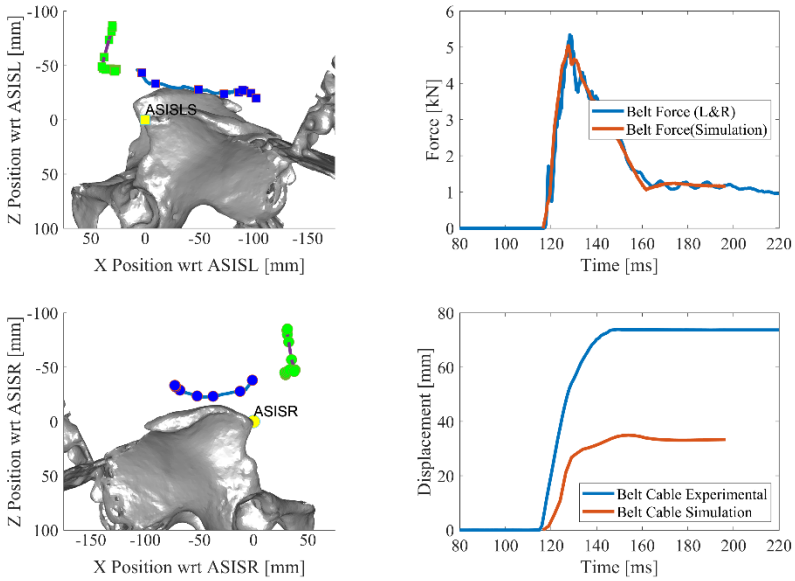

Figure A-11. Baseline fit input simulation on simplified GHBMC obesity model with SPG formulation in Eulerian kernel (kernel=1) with no particle-to-particle bond failure criteria implemented #13

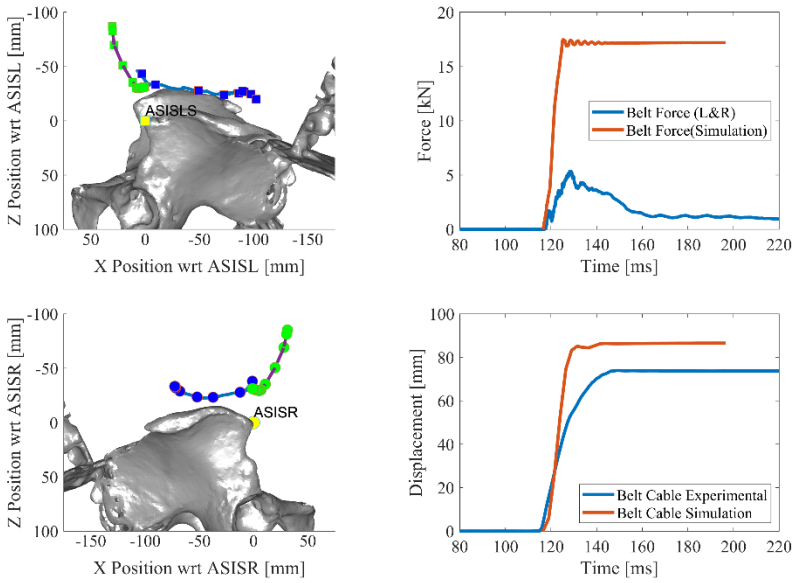

Figure A-12. Four times baseline flat input simulation on simplified GHBMC obesity model with SPG formulation in updated Lagrangian kernel (kernel=2) with critical shear strain particle-to-particle bond failure criteria (critical shear strain=0.85 and critical stretch=1.5) #15

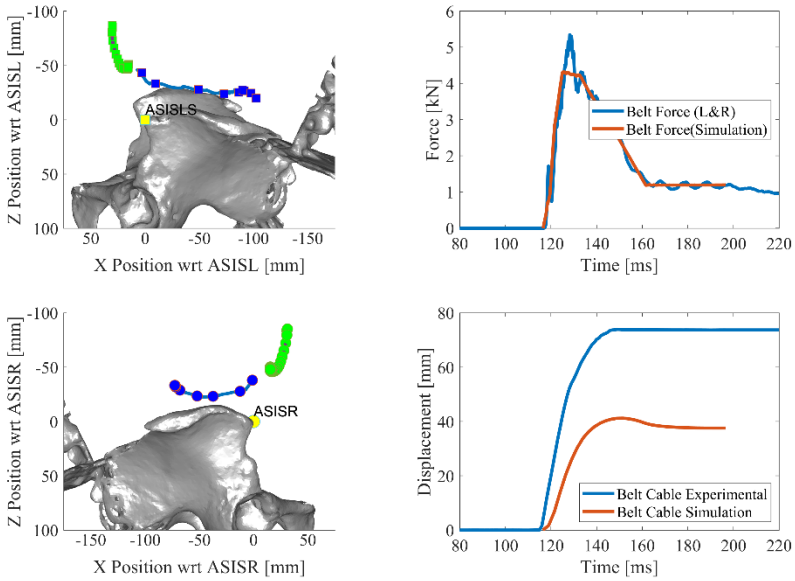

Figure A-13. Baseline fit input simulation on simplified GHBMC obesity model with SPG formulation in updated Lagrangian kernel (kernel=2) with critical shear strain particle-to-particle bond failure criteria (critical shear strain=0.85 and critical stretch=1.5) #16

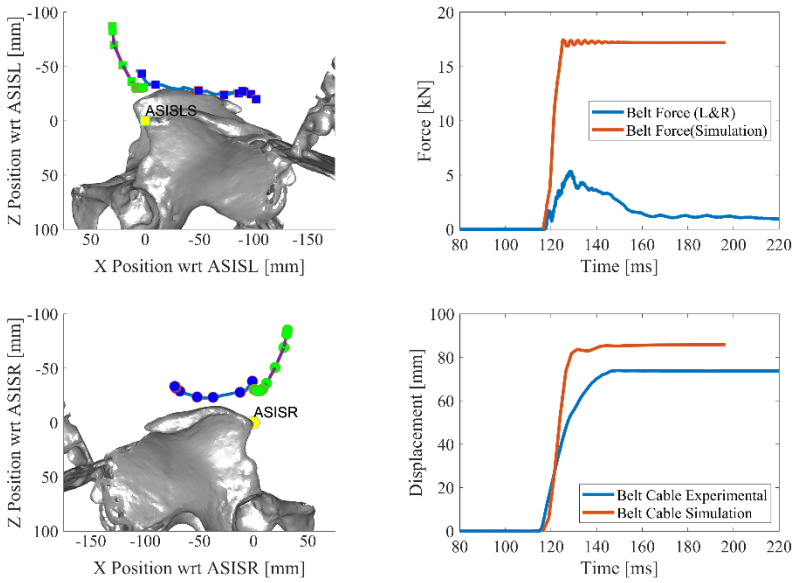

Figure A-14. Four times baseline flat input simulation on simplified GHBMC obesity model with SPG formulation in updated Lagrangian kernel (kernel=2) with critical shear strain particle-to-particle bond failure criteria (critical shear strain=1 and critical stretch=2) #17

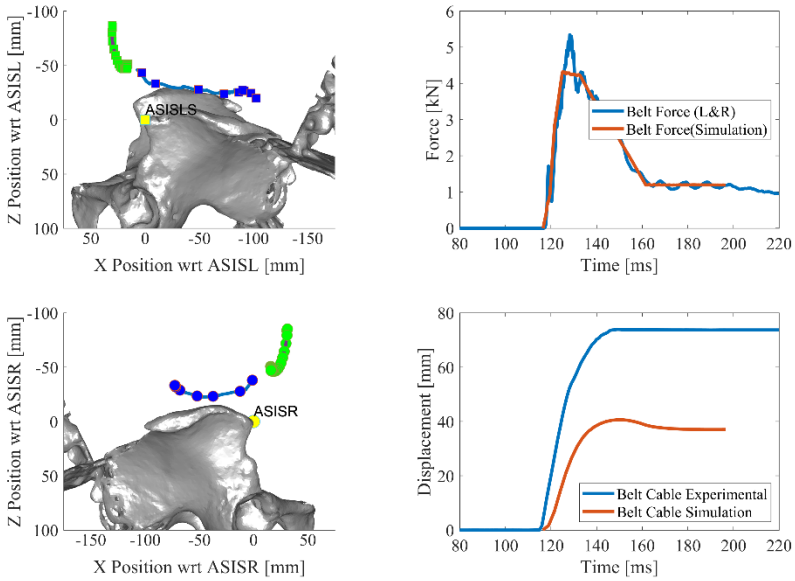

Figure A-15. Baseline fit input simulation on simplified GHBMC obesity model with SPG formulation in updated Lagrangian kernel (kernel=2) with no particle-to-particle bond failure criteria #18

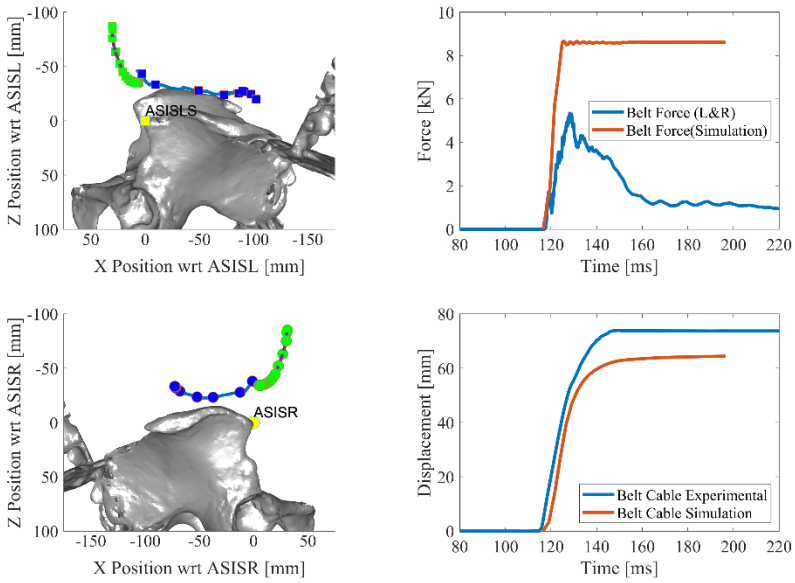

Figure A-16. Two times baseline flat input simulation on simplified GHBMC obesity model with SPG formulation in updated Lagrangian kernel (kernel=2) with no particle bond failure criteria #19

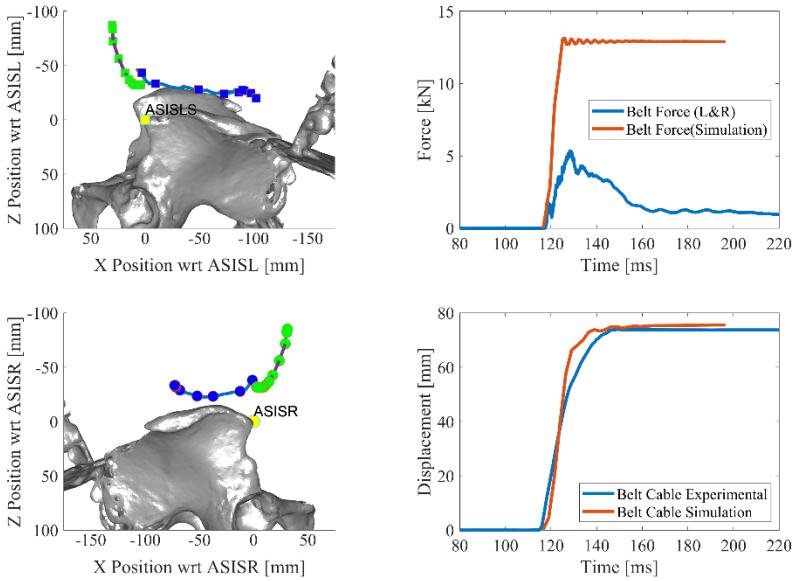

Figure A-17. Three times baseline flat input simulation on simplified GHBMC obesity model with SPG formulation in updated Lagrangian kernel (kernel=2) with no particle bond failure criteria #20

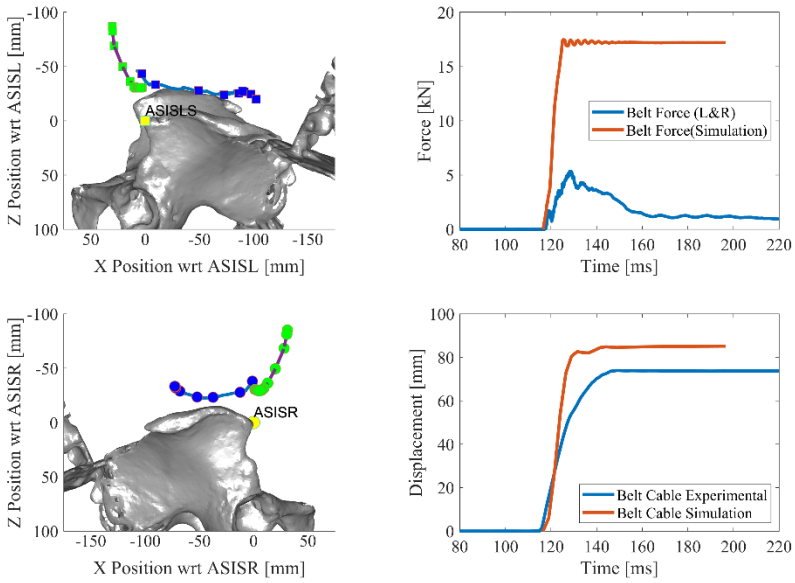

Figure A-18. Four times baseline flat input simulation on simplified GHBMC obesity model with SPG formulation in updated Lagrangian kernel (kernel=2) with no particle bond failure criteria #21

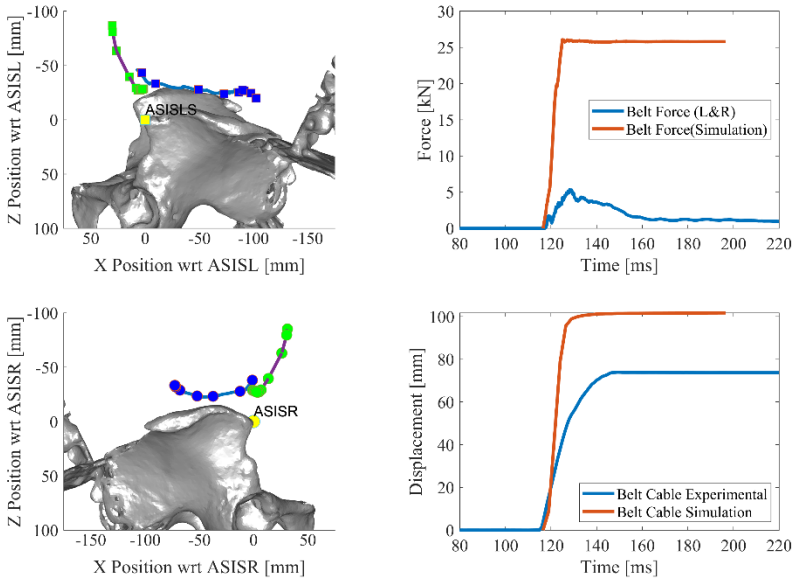

Figure A-19. Six times baseline flat input simulation on simplified GHBMC obesity model with SPG formulation in updated Lagrangian kernel (kernel=2) with no particle bond failure criteria #22

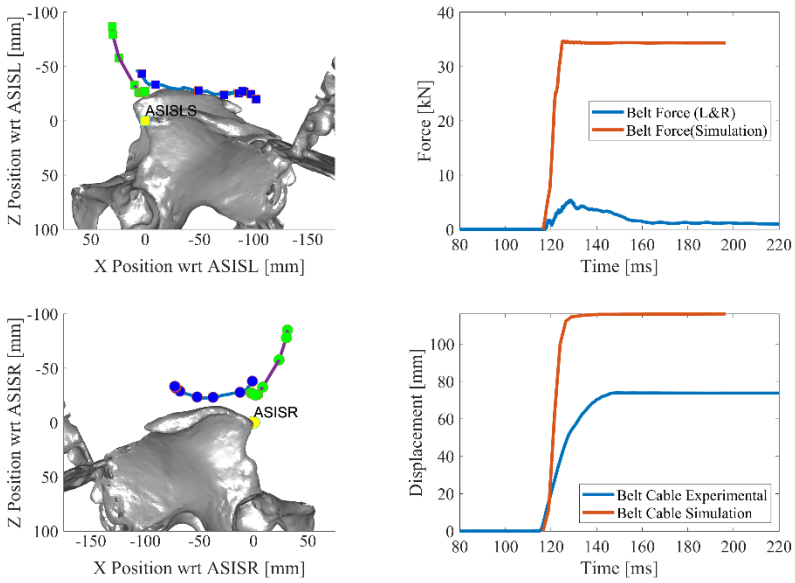

Figure A-20. Eight times baseline flat input simulation on simplified GHBMC obesity model with SPG formulation in updated Lagrangian kernel (kernel=2) with no particle bond failure criteria #23

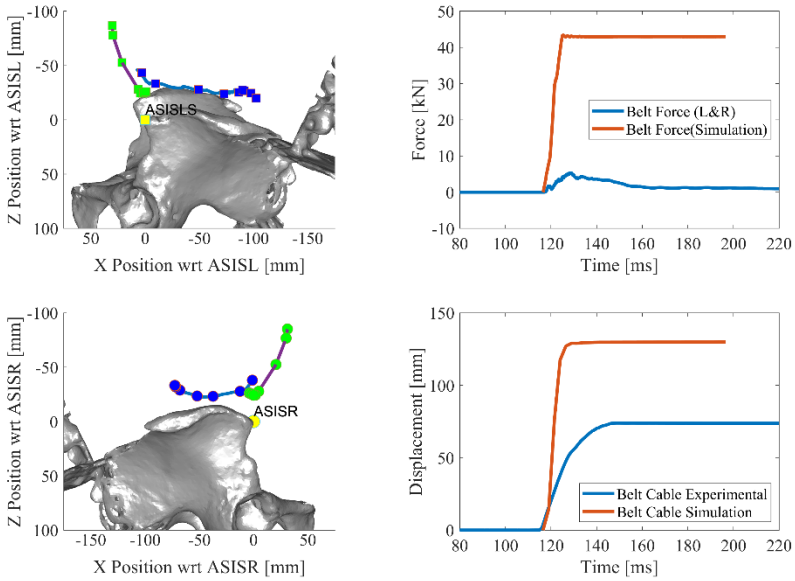

Figure A-21. Ten times baseline flat input simulation on simplified GHBMC obesity model with SPG formulation in updated Lagrangian kernel (kernel=2) with no particle bond failure criteria #24

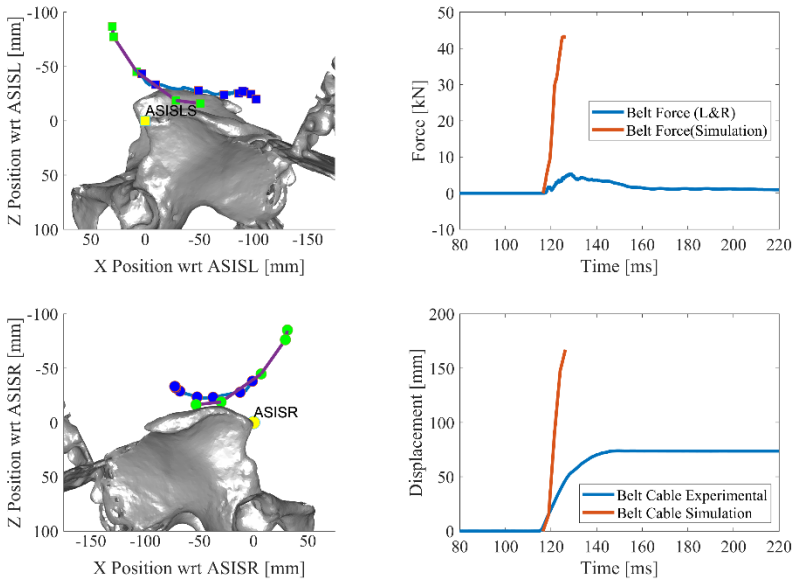

Figure A-22. Ten times baseline flat input simulation on simplified GHBMC obesity model with Lagrangian elements #29

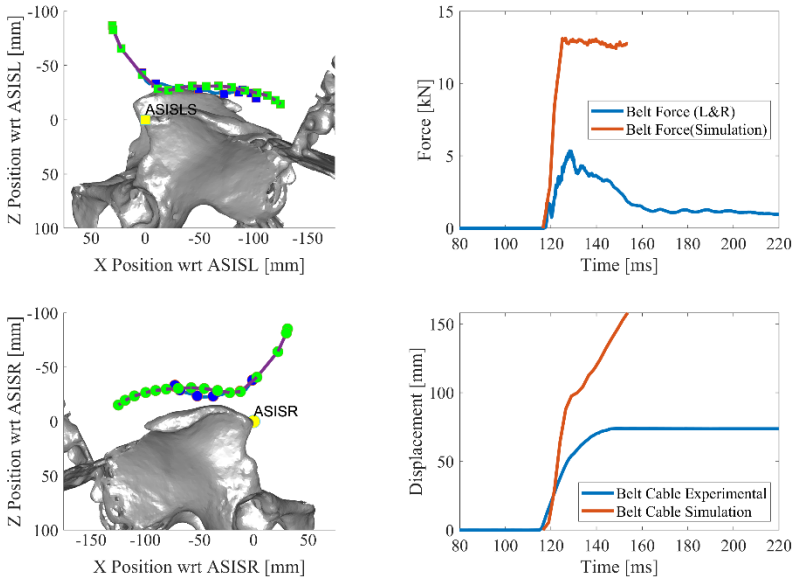

Figure A-23. Three times baseline flat input simulation on simplified GHBMC obesity model with Lagrangian elements #31

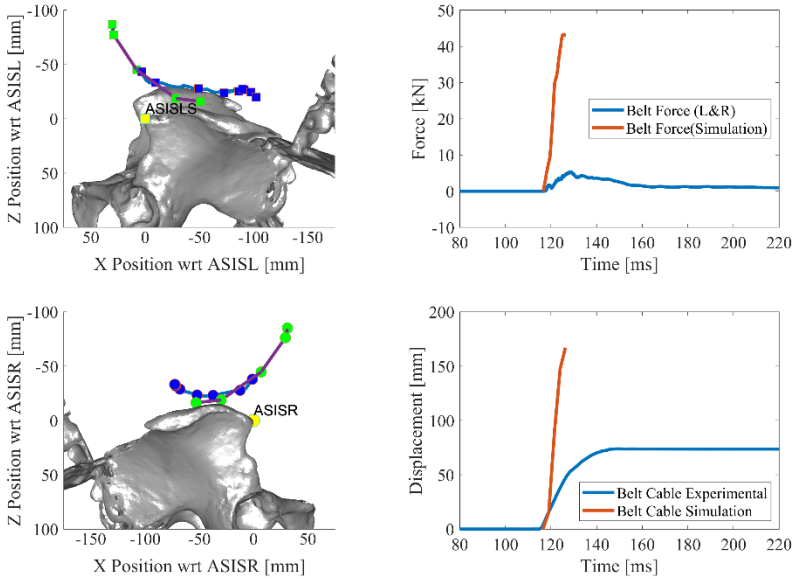

Figure A-24. Ten times baseline flat input simulation on simplified GHBMC obesity model with Lagrangian elements #32

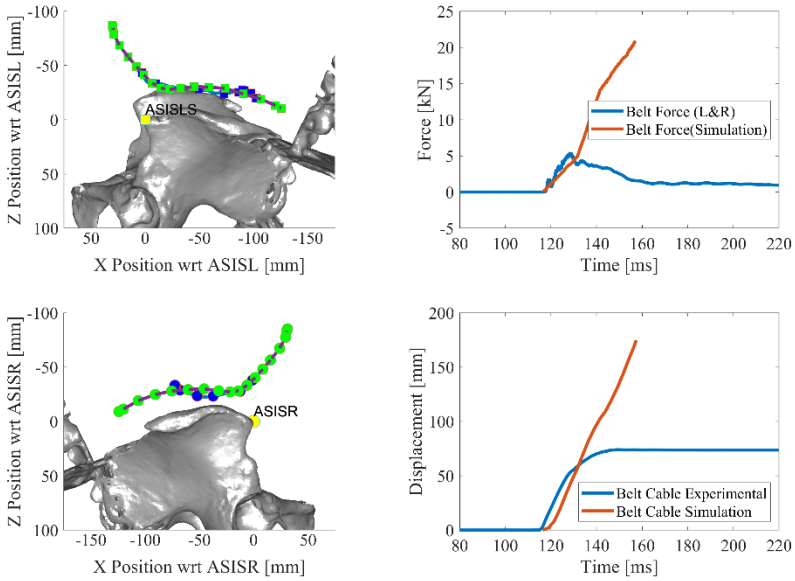

Figure A-25. Five times peak force and rate flat input simulation on simplified GHBMC obesity model in Lagrangian formulation #34

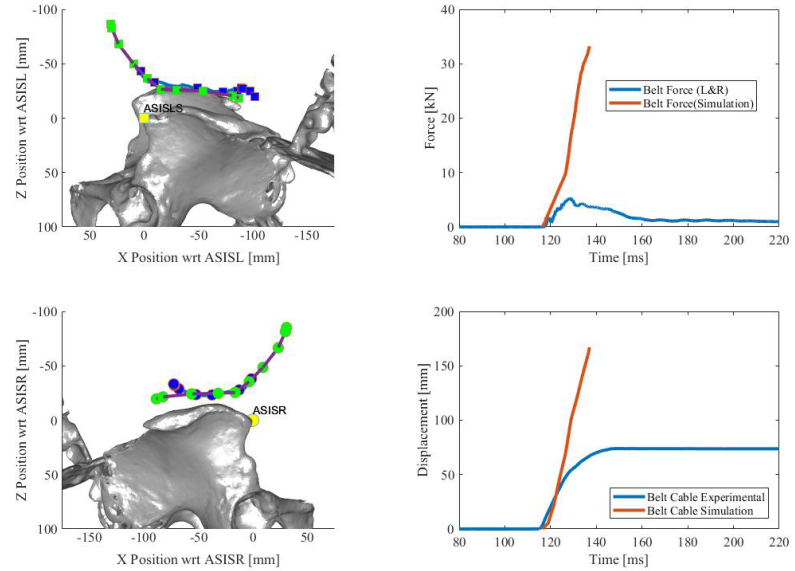

Figure A-26. Ten times peak force and three times rate flat input simulation on simplified GHBMC obesity model in Lagrangian formulation #35

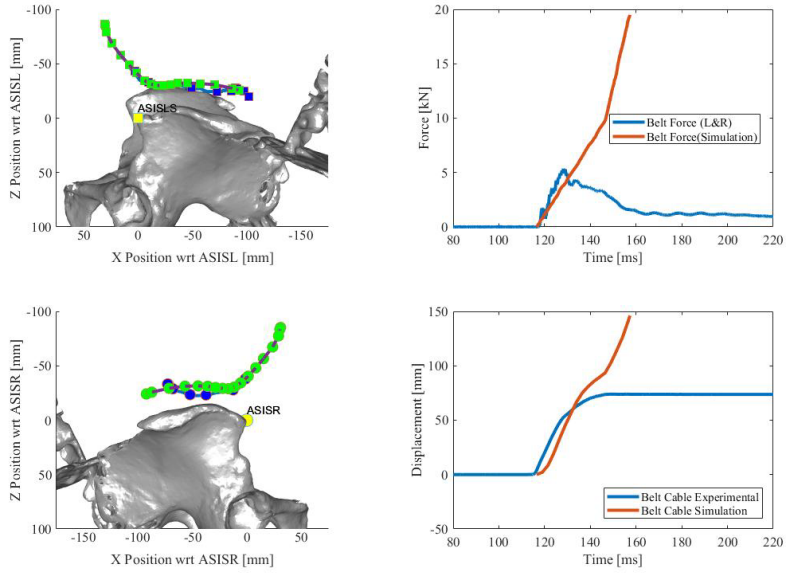

Figure A-27. Ten times peak force and rate flat input simulation on simplified GHBMC obesity model in Lagrangian formulation #36

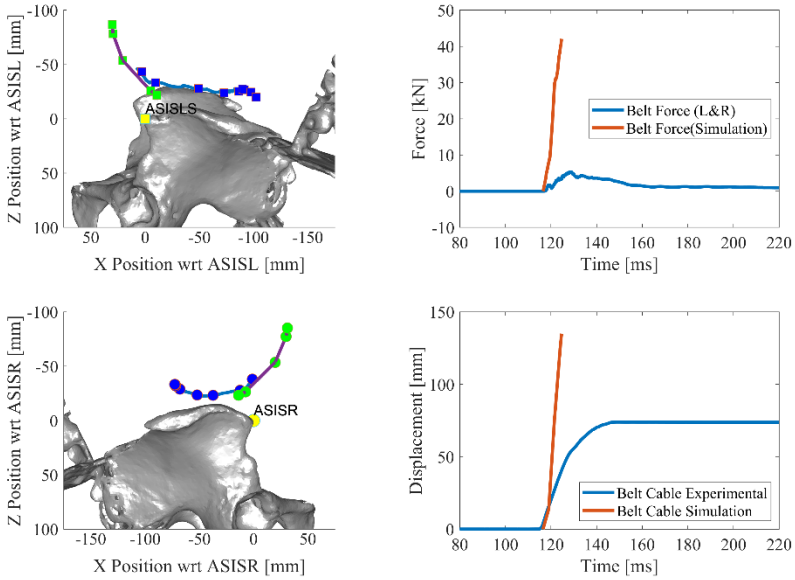

Figure A-28. Ten times baseline flat input simulation on simplified GHBMC obesity model with SPG formulation in Lagrangian kernel (kernel=0) with no particle bond failure criteria #44

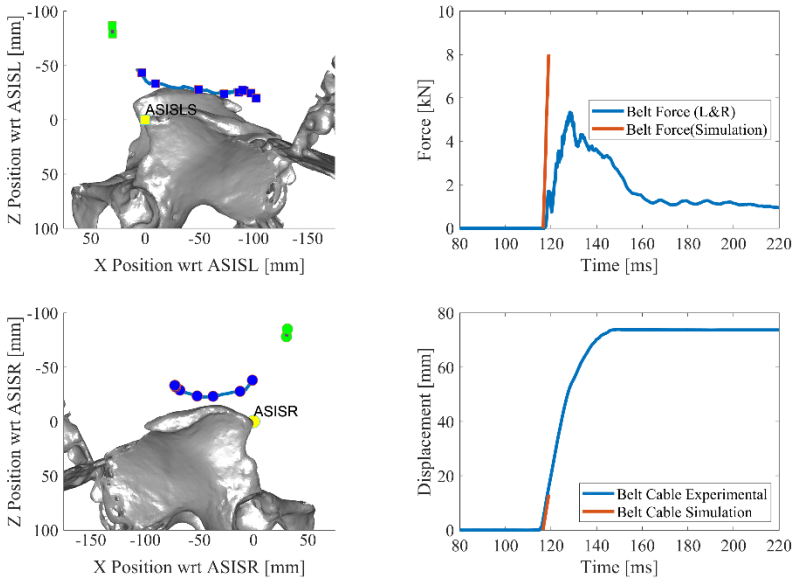

Figure A-29. Ten times baseline flat input simulation on simplified GHBMC obesity model with SPG formulation in Eulerian kernel (kernel=1) with no particle bond failure criteria #45

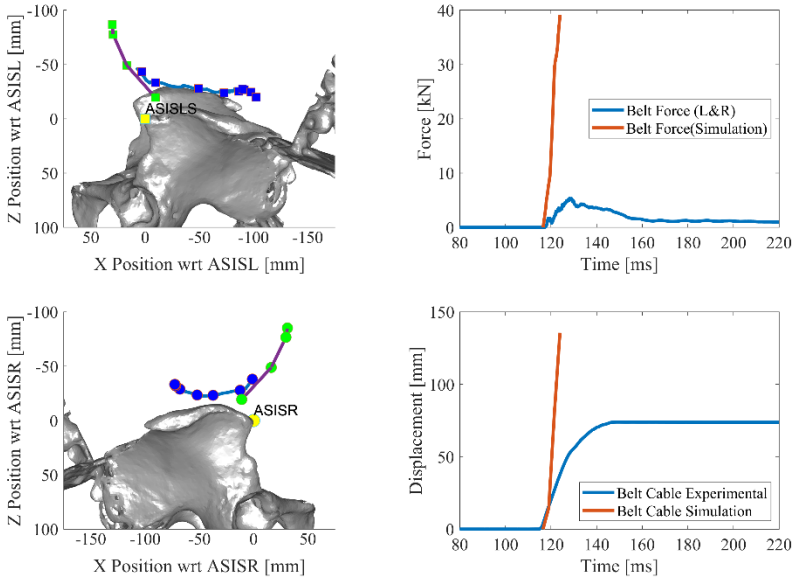

Figure A-30. Ten times baseline flat input simulation on simplified GHBMC obesity model with SPG formulation in updated Lagrangian kernel (kernel=2) with no particle bond failure criteria #46

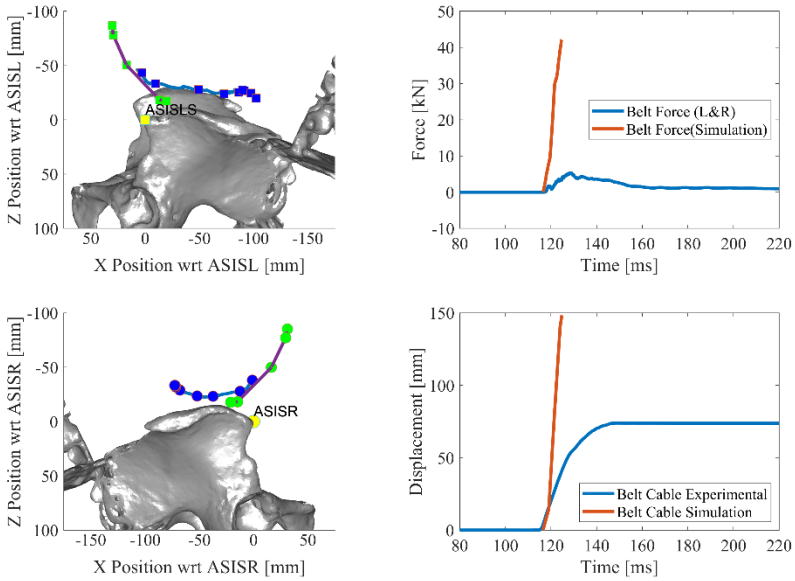

Figure A-31. Ten times baseline flat input simulation on simplified GHBMC obesity model with SPG formulation in updated Lagrangian kernel (kernel=2) with critical shear strain particle-to-particle bond failure criteria (critical shear strain=0.45 and critical stretch=1.45) #47

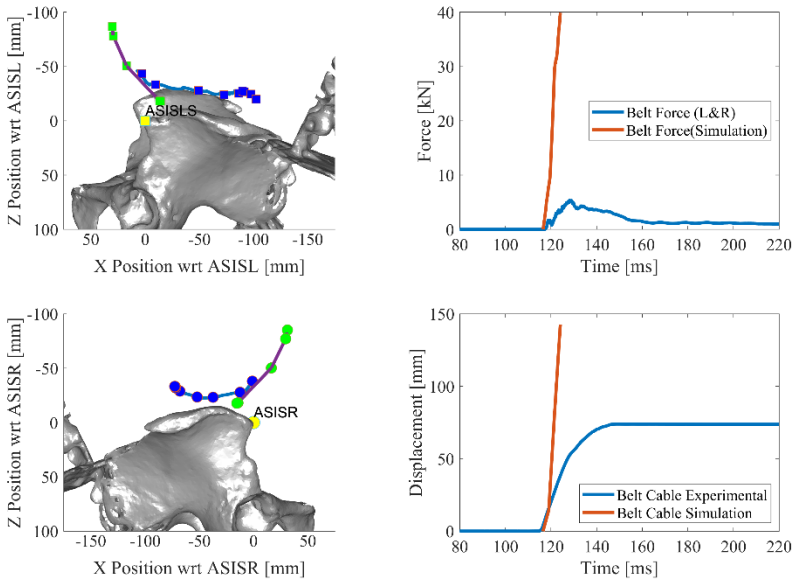

Figure A-32. Ten times baseline flat input simulation on simplified GHBMC obesity model with SPG formulation in updated Lagrangian kernel (kernel=2) with critical shear strain particle-to-particle bond failure criteria (critical shear strain=0.85 and critical stretch=1.85) #48

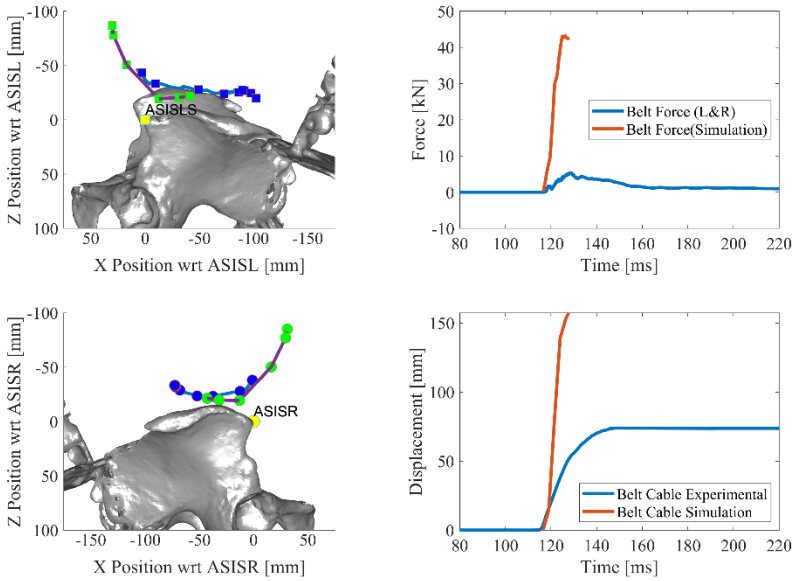

Figure A-33. Ten times baseline flat input simulation on simplified GHBMC obesity model with SPG formulation in updated Lagrangian kernel (kernel=2) with critical shear strain particle-to-particle bond failure criteria (critical shear strain=1 and critical stretch=2) #49

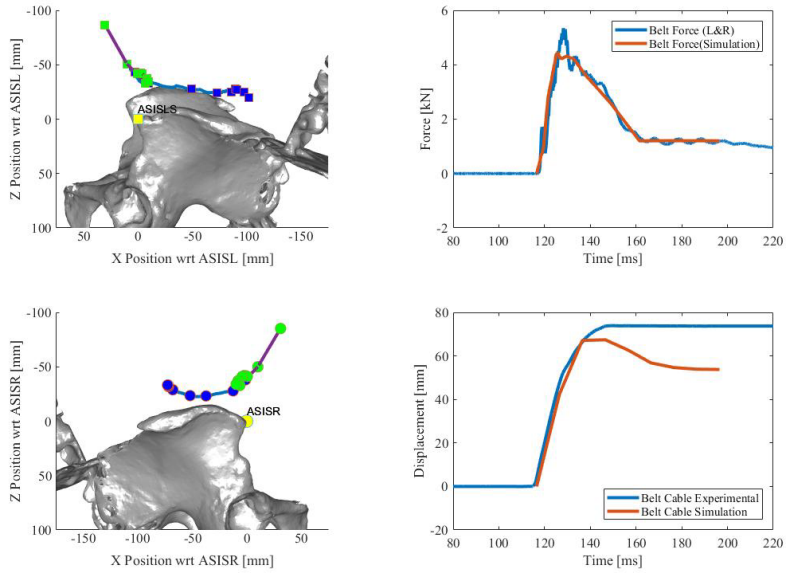

Figure A-34. Baseline fit input simulation in Lagrangian formulation with complete boundary condition #1

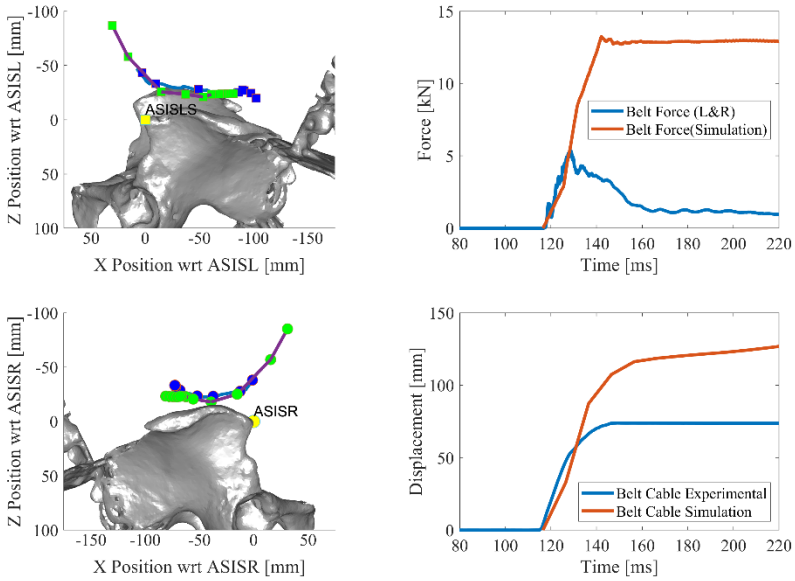

Figure A-35. Three times of both peak force and rate flat input simulation in Lagrangian formulation with complete boundary condition #4

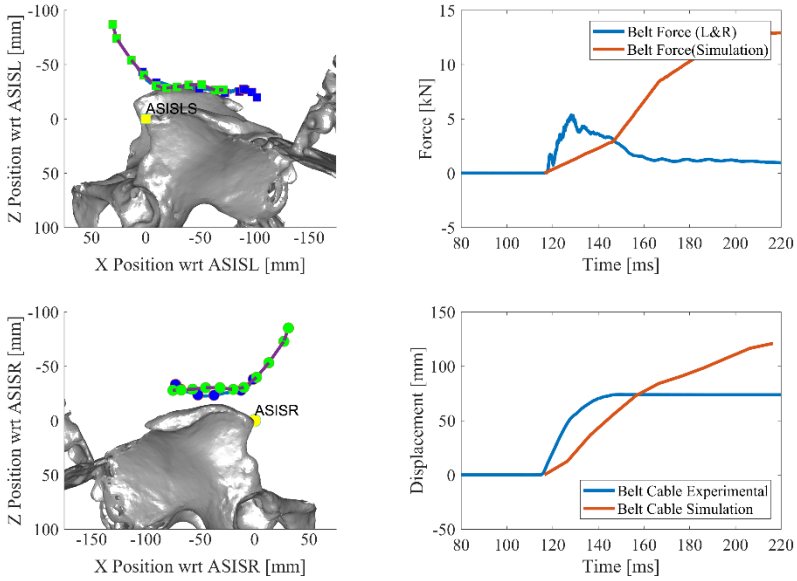

Figure A-36. Three times baseline slow simulation in Lagrangian formulation with complete boundary condition #5

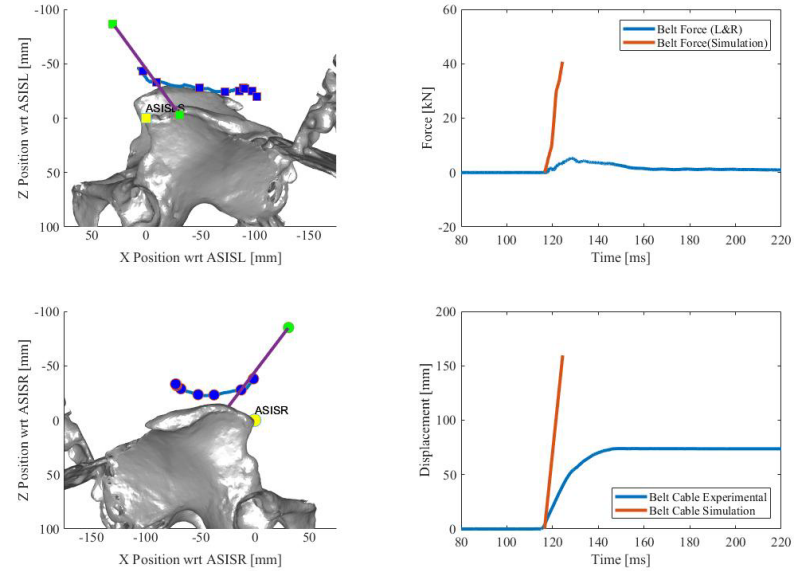

Figure A-37. Ten times baseline simulation in Lagrangian formulation with complete boundary condition #8

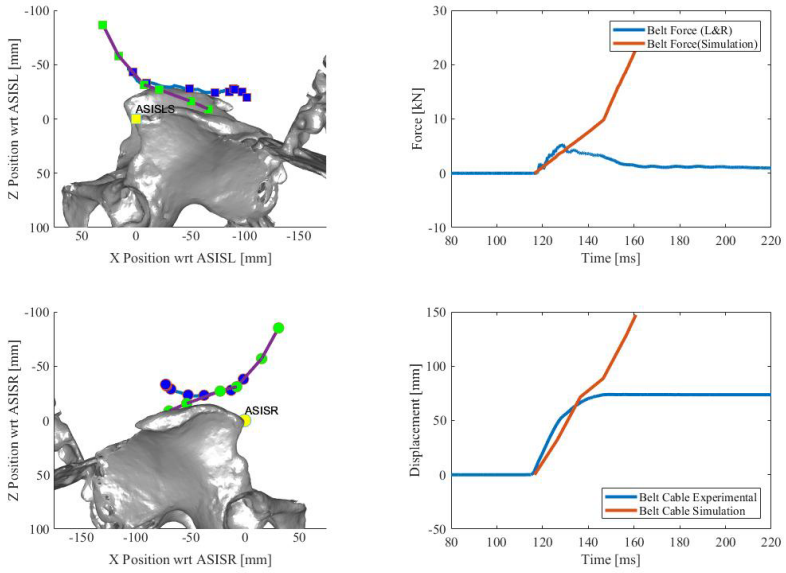

Figure A-38. Three times baseline slow simulation in Lagrangian formulation with complete boundary condition #9

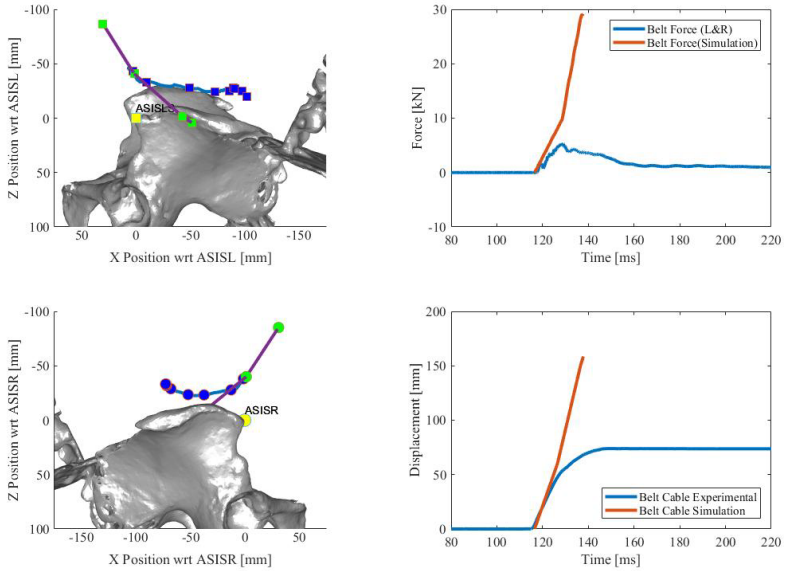

Figure A-39. 2.5 times baseline slow simulation in Lagrangian formulation with complete boundary condition #10

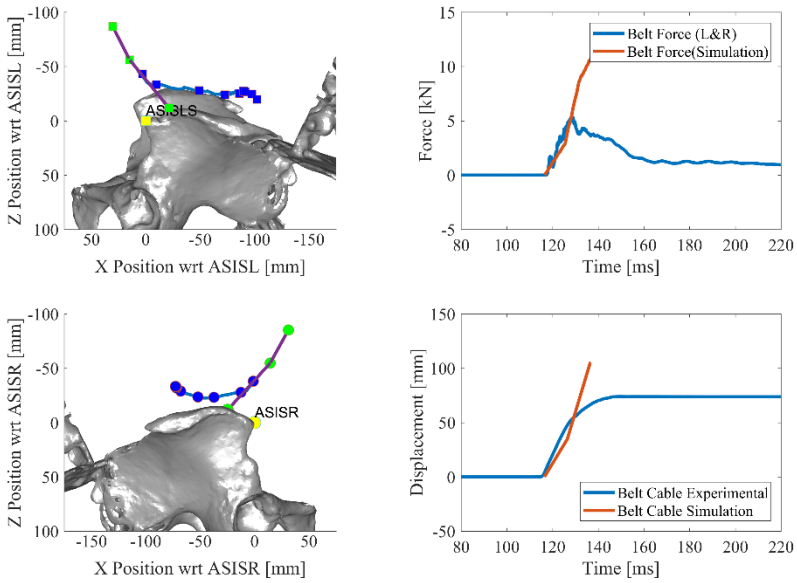

Figure A-40. Three times peak force and rate flat input simulation in Lagrangian formulation with high pelvis yielding point #11

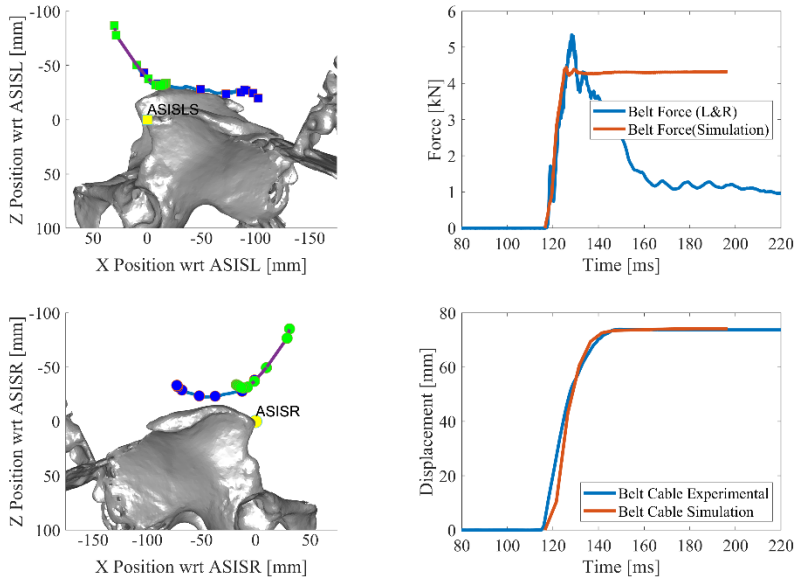

Figure A-41. Baseline flat simulation in Lagrangian formulation with complete boundary condition with turned down material stiffness of the abdomen (75 percent baseline) #13

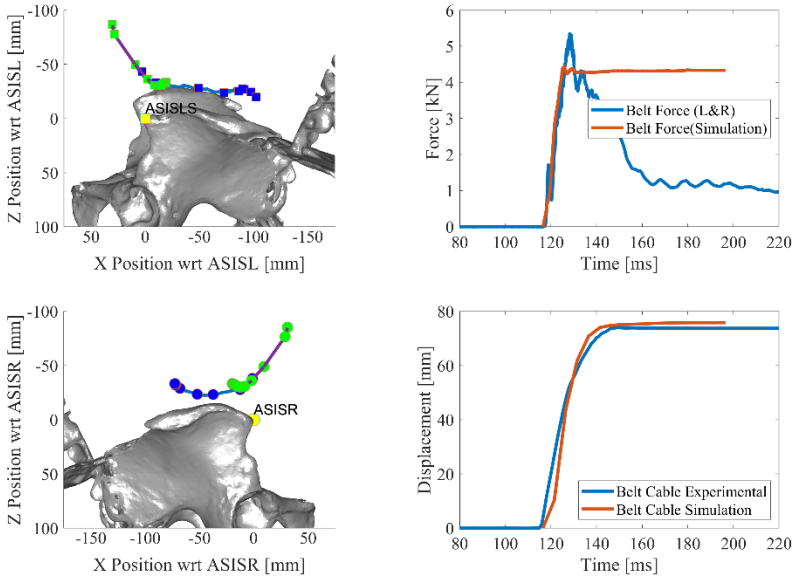

Figure A-42. Baseline flat simulation in Lagrangian formulation with complete boundary condition with turned down material stiffness of the abdomen (50 percent baseline) #14

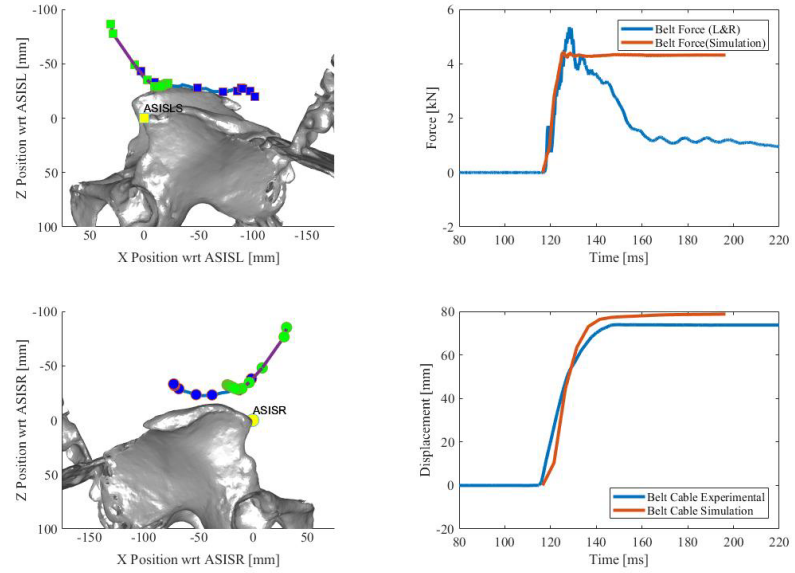

Figure A-43. Baseline flat simulation in Lagrangian formulation with complete boundary condition with turned down material stiffness of the abdomen (25 percent baseline) #15

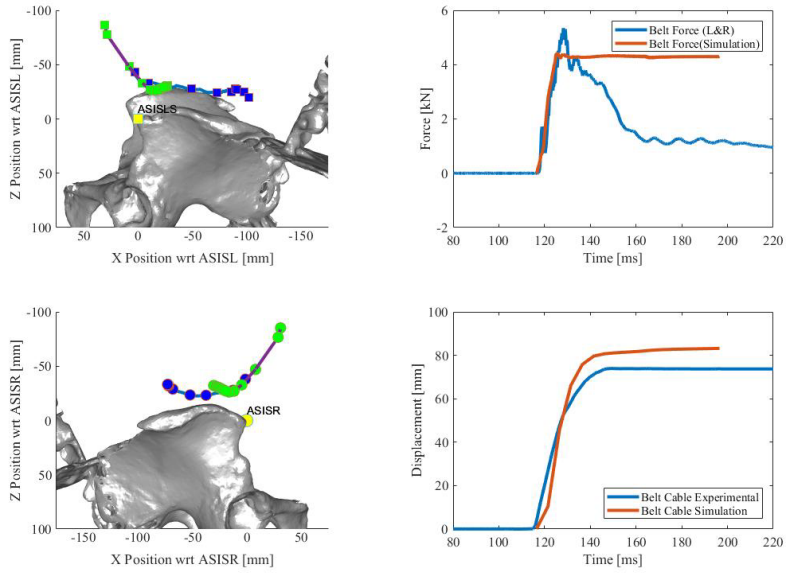

Figure A-44. Baseline flat simulation in Lagrangian formulation with complete boundary condition with turned down material stiffness of the abdomen (10 percent baseline) #16

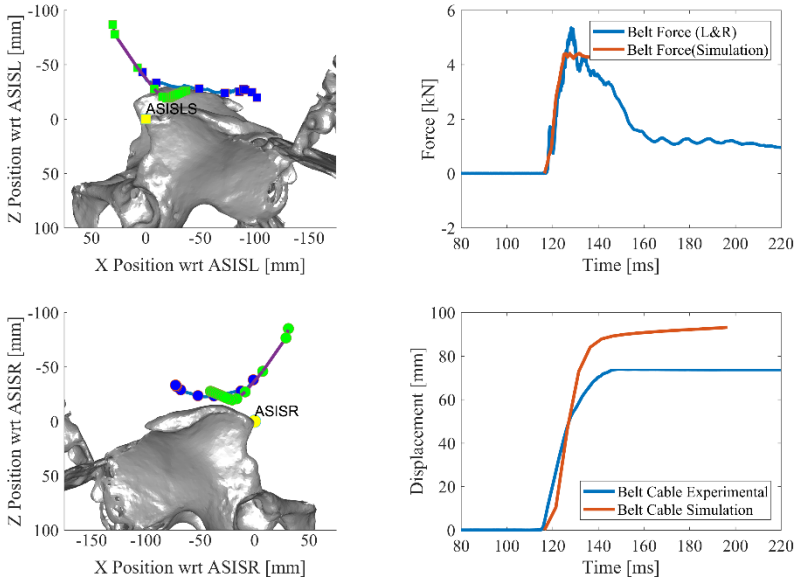

Figure A-45. Baseline flat simulation in Lagrangian formulation with complete boundary condition with turned down material stiffness of the abdomen (1% baseline) #17

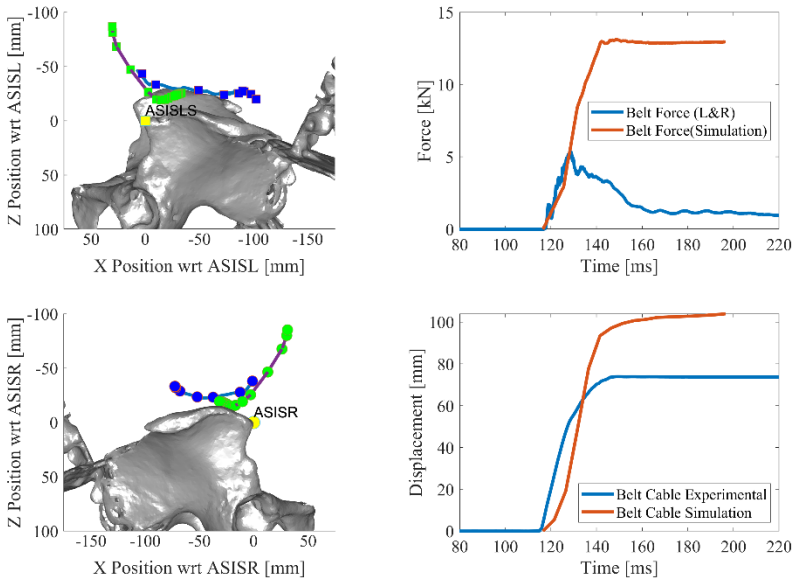

Figure A-46. Three times baseline flat input simulation with complete boundary condition with SPG formulation in updated Lagrangian kernel (kernel=2) with critical shear strain particle-to-particle bond failure criteria (critical shear strain=0.85 and critical stretch=1.85) with pelvic wing yielding criteria on #7

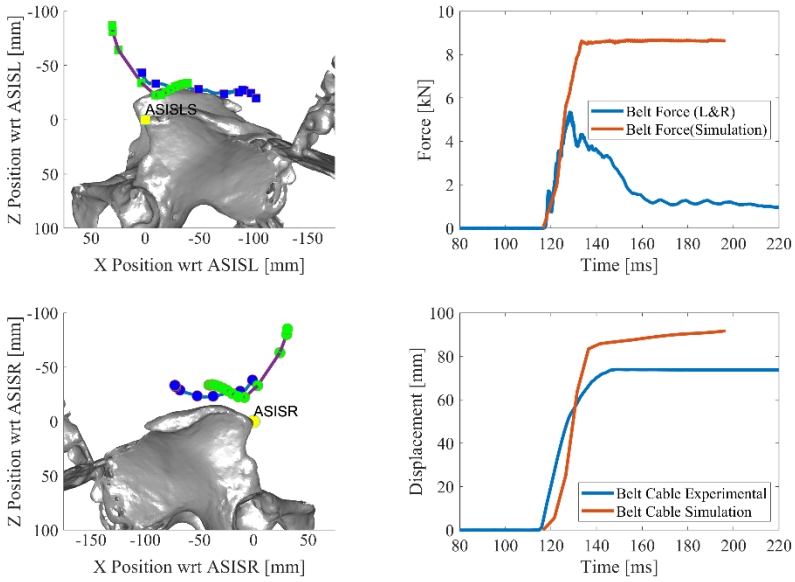

Figure A-47. Two times baseline flat input simulation with complete boundary condition with SPG formulation in updated Lagrangian kernel (kernel=2) with critical shear strain particle-to-particle bond failure criteria (critical shear strain=0.15 and critical stretch=1.15) with pelvic wing yielding criteria off #9

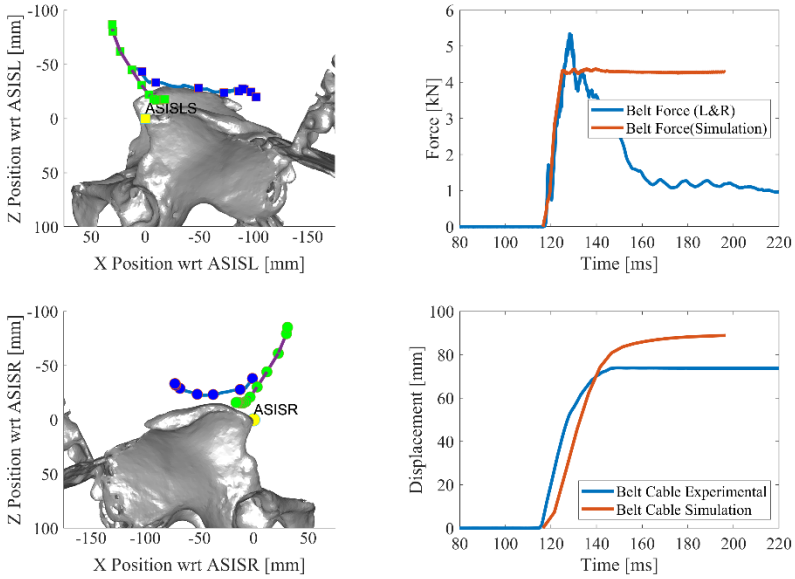

Figure A-48. Baseline flat input simulation with complete boundary condition with SPG formulation in updated Lagrangian kernel (kernel=2) with critical shear strain particle-to-particle bond failure criteria (critical shear strain=0.45 and critical stretch=1.45) with pelvic wing yielding criteria on #11

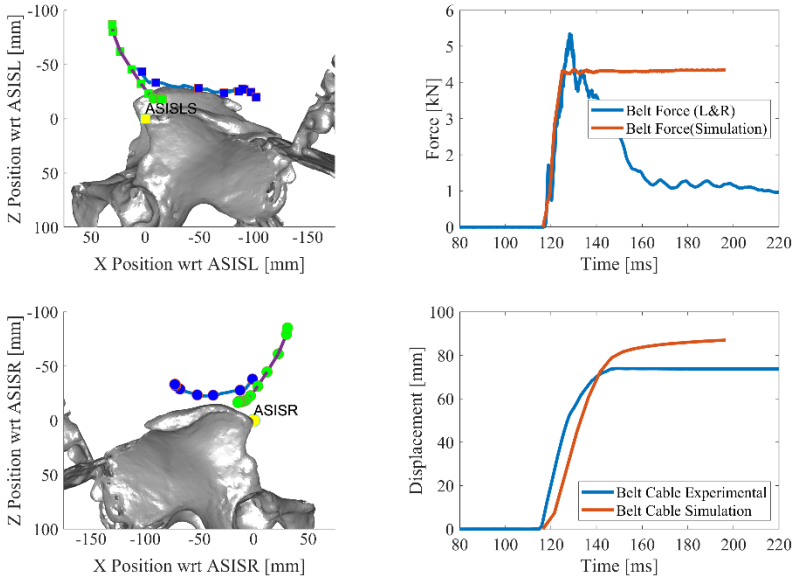

Figure A-49. Baseline flat input simulation with complete boundary condition with SPG formulation in updated Lagrangian kernel (kernel=2) with critical shear strain particle-to-particle bond failure criteria (critical shear strain=0.85 and critical stretch=1.85) with pelvic wing yielding criteria on #12

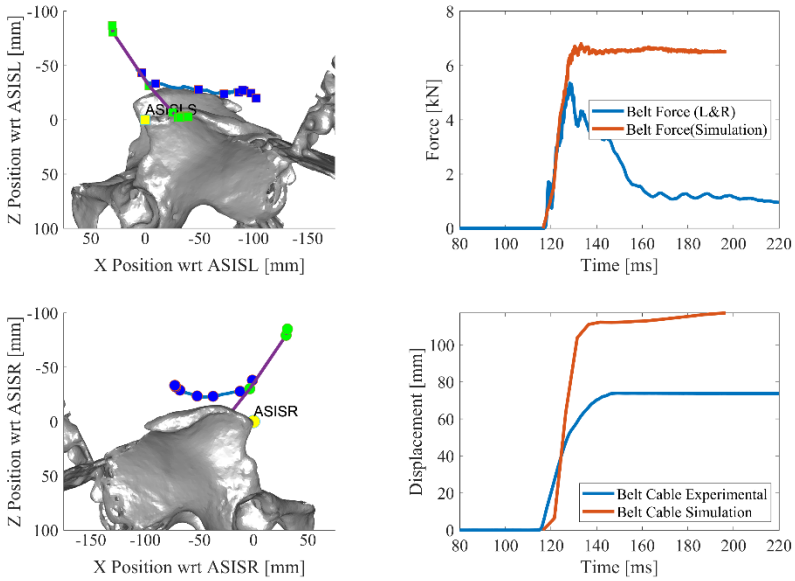

Figure A-50. 1.5 times baseline flat input simulation with complete boundary condition with SPG formulation in updated Lagrangian kernel (kernel=2) with critical shear strain particle-to-particle bond failure criteria (critical shear strain=0.15 and critical stretch=1.15) with pelvic wing yielding criteria off (material stiffness turned to 1% stiffness) #16

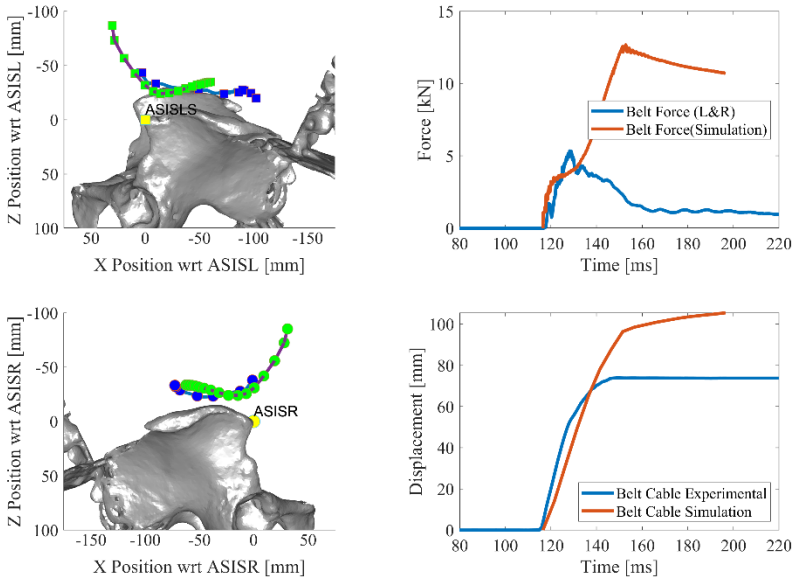

Figure A-51. Displacement controlled simulation with complete boundary condition with SPG formulation in updated Lagrangian kernel (kernel=2) with no particle-to-particle bond failure criteria (critical shear strain=0.25 and critical stretch=1.25) with pelvic wing yielding criteria off #19

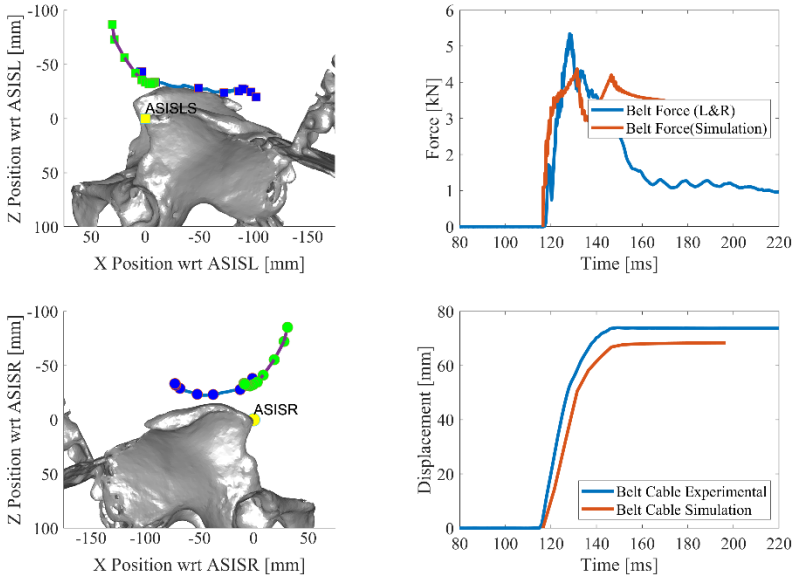

Figure A-52. Displacement controlled simulation with complete boundary condition with SPG formulation in updated Lagrangian kernel (kernel=2) with no particle-to-particle bond failure criteria (critical shear strain=0.25 and critical stretch=1.25) with pelvic wing yielding criteria off #21

Now all simulations with the GHBMC original material card has been introduced. Next, we investigated those with alternative material models.

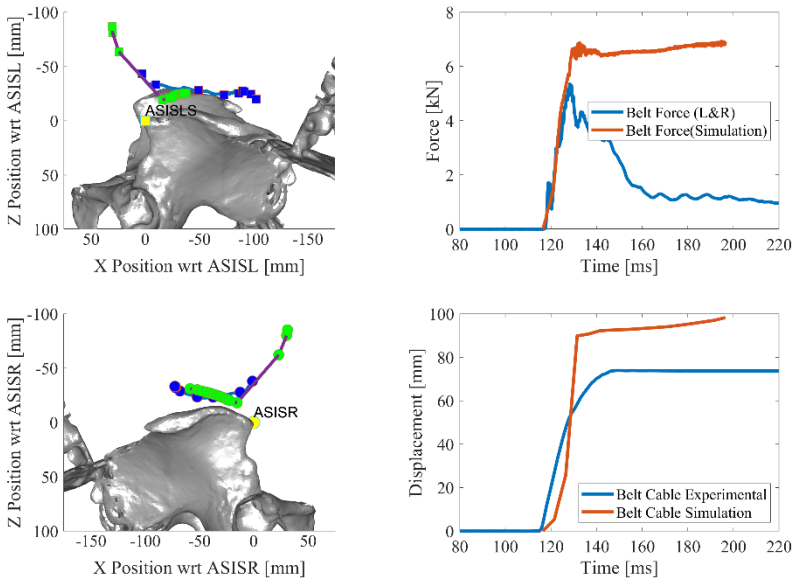

Figure A-53. 1.5 times baseline flat input simulation with complete boundary condition and Ogden rubber material with SPG formulation in updated Lagrangian kernel (kernel=2) with critical shear strain particle-to-particle bond failure criteria (critical shear strain=0.25 and critical stretch=1.25) with pelvic wing yielding criteria off #22

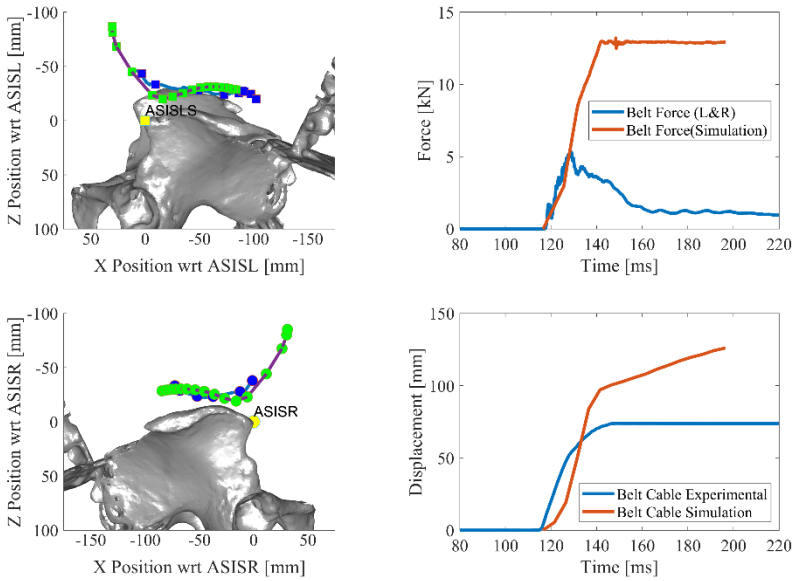

Figure A-54. Three times baseline flat input simulation with complete boundary condition and Ogden rubber material with SPG formulation in updated Lagrangian kernel (kernel=2) with critical shear strain particle-to-particle bond failure criteria (critical shear strain=0.25 and critical stretch=1.25) with pelvic wing yielding criteria off #23

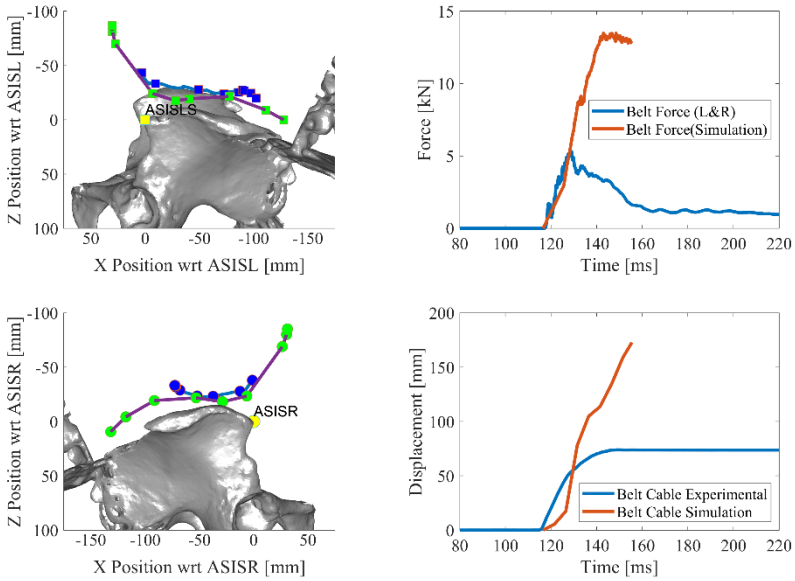

Figure A-55. Three times baseline flat input simulation with complete boundary condition and Ogden rubber material (v2) with SPG formulation in updated Lagrangian kernel (kernel=2) with critical shear strain particle-to-particle bond failure criteria (critical shear strain=0.25 and critical stretch=1.25) with pelvic wing yielding criteria off #24

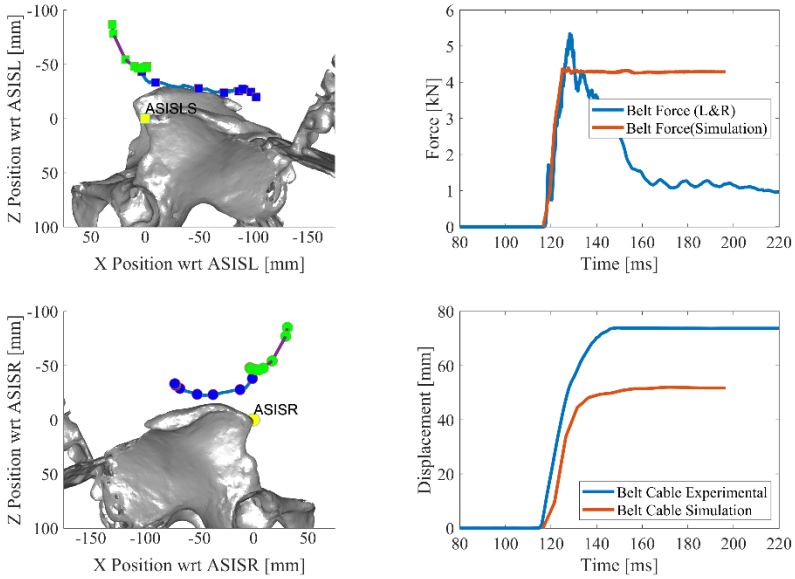

Figure A-56. Baseline flat input simulation with complete boundary condition and Ogden rubber material (v Engle6) with SPG formulation in updated Lagrangian kernel (kernel=2) with no particle-to-particle bond failure criteria #25

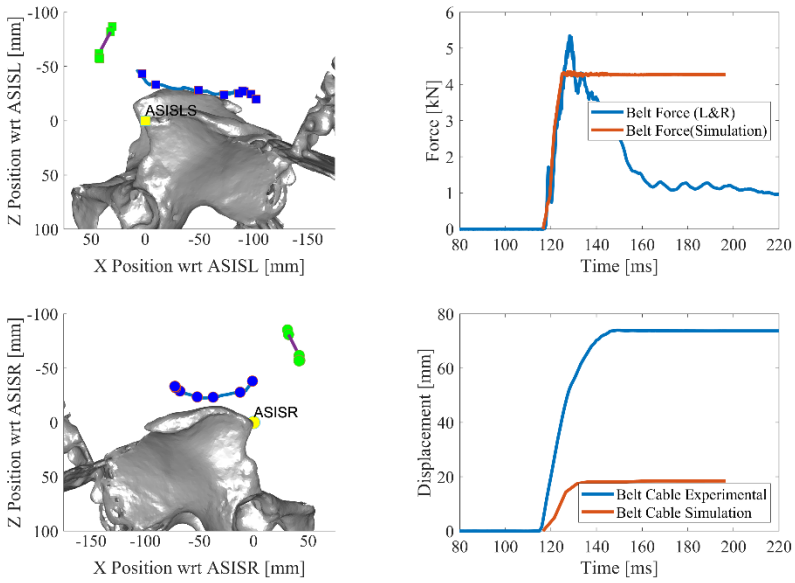

Figure A-57. Baseline flat input simulation with complete boundary condition and incompressible material (Poisson ratio=0.499, stiffness is 1% baseline) with SPG formulation in updated Lagrangian kernel (kernel=2) with no particle-to-particle bond failure criteria #26

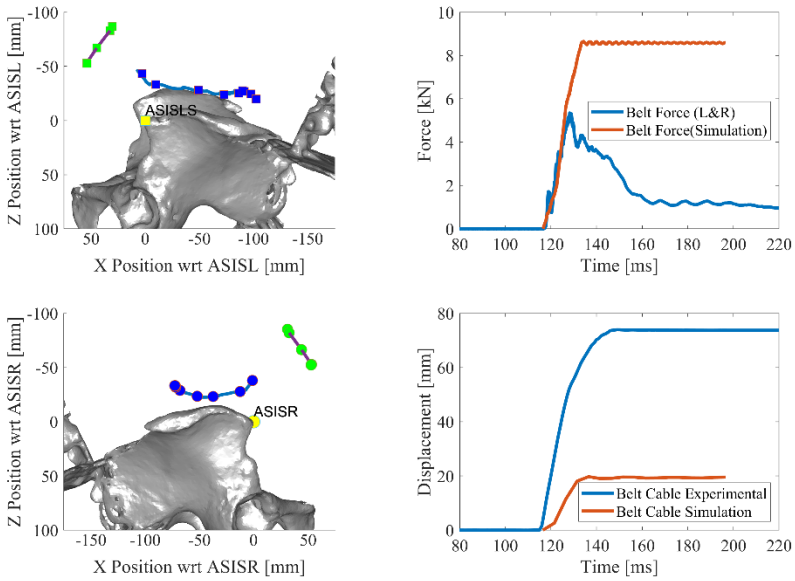

Figure A-58. Baseline flat input simulation with complete boundary condition and incompressible material (Poisson ratio=0.499, stiffness is 1% baseline) with SPG formulation in updated Lagrangian kernel (kernel=2) with critical shear strain particle-to-particle bond failure criteria (critical shear strain=0.15 and critical stretch=1.15) #27

Figure A-57 and Figure A-58 show that we could not change the Poisson's ratio of the simplified rubber/foam material model without changing other relevant parameters.

DOT HS 813 540d
May 2024

U.S. Department
of Transportation

**National Highway
Traffic Safety
Administration**

16164d-050324-v3